Optimisation and Control of Distributed Energy Resources for Power and Voltage Regulation in Distribution Networks

Wilhiam Cesar de Carvalho

A thesis submitted for the degree of
Doctor of Philosophy at
The Australian National University

February 2024

Except where otherwise indicated, this thesis is my own original work.

Wilhiam Cesar de Carvalho
24 February 2024

“But nature is always more subtle, more intricate, more elegant than what we are able to imagine.” - Carl Sagan, The Demon-Haunted World: Science as a Candle in the Dark.

To Mom, who showed me the wonders of nature

Acknowledgments

First and foremost I would like to thank, in alphabetical order, Dr. Elizabeth Ratnam and Prof. Hemanshu Pota, for their patience, understanding and guidance during my PhD journey.

Thanks to, in alphabetical order, Prof. Alexandra von Meier and Prof. Lachlan Blackhall for their insightful comments which greatly contributed to my work.

Thanks to all academics and students whom I have worked with as a tutor, for the invaluable teaching and learning experience.

Big thanks to all officemates and colleagues I have met at the ANU, for the helpful conversations and also enjoyable moments.

And last but not least, I would like to thank my family and friends, including my dog, Theo, who have always been my source of support, kindness and love.

Publications

- de Carvalho, W. C.; Ratnam, E. L.; Blackhall, L.; von Meier, A.; and Murray, A., 2020. Over-voltage disconnection of DER inverters: Assessing customer savings. *IFAC-PapersOnLine*, 53, 2 (2020), 13230–13235. 21th IFAC World Congress, Berlin, Germany.

- de Carvalho, W. C.; Ratnam, E. L.; Blackhall, L.; and von Meier, A., 2023. Optimization-based operation of distribution grids with residential battery storage: Assessing utility and customer benefits. *IEEE Transactions on Power Systems*, 38, 1 (2023), 218–228.

- de Carvalho, W.; Attarha, A.; and Pota, H. R., 2022. Local volt-var-watt control for voltage regulation in distribution networks. In *2022 IEEE PES 14th Asia-Pacific Power and Energy Engineering Conference (APPEEC)*, 1–6. 14th IEEE APPEEC, Melbourne, Australia.

- de Carvalho, W.; Attarha, A.; and Pota, H. R., 2024. Optimization-based proportional control for voltage regulation with DERs in distribution networks. 1–10. Manuscript in Preparation.

Other Publications

- Barra, P. H. A.; de Carvalho, W. C.; Menezes, T. S.; Fernandes, R. A. S.; and Coury, D. V., 2021. A review on wind power smoothing using high-power energy storage systems. *Renewable and Sustainable Energy Reviews*, Volume 137, (2021), 110455, ISSN 1364-0321.

- Bhardwaj, A.; de Carvalho, W.; Nimalsiri, N.; Ratnam, E.; and Rin, N., 2022. Communication-censored-ADMM for electric vehicle charging in unbalanced distribution grids. In *11th Bulk Power Systems Dynamics and Control Symposium (IREP 2022)*, July 25-30, (2022), pp. 1-14. 11th IREP, Banff, Canada.

- de Carvalho, W.; Bataglioli, R. P.; Fernandes, R. A. S.; Coury, D. V., 2020. Fuzzy-based approach for power smoothing of a full-converter wind turbine generator using a supercapacitor energy storage. *Electric Power Systems Research*, Volume 184, (2020), 106287, ISSN 0378-7796.

Abstract

Increasing levels of distributed energy resources (DERs) have created significant technical challenges in today's distribution networks. Small-scale DERs such as rooftop solar photovoltaic, battery storage and electric vehicles, when not coordinated, can cause undesirable voltage deviations, peak power demand and power losses on the network. When properly optimised and controlled, the same DERs are the key elements in effectively overcoming such challenges and benefiting all energy users.

In this thesis, original optimisation and control approaches are proposed to control real and reactive power of DERs for grid power and voltage regulation. This thesis proposes local approaches that act autonomously to grid demand and voltage variations based only on local measurements. A two-layer central-local control is also proposed, where fast-acting local controllers receive updated parameters from a system-wide optimisation at a slower timescale. These optimisation and control approaches are presented along four main chapters in this thesis: from the third to sixth chapter.

In the third chapter, a local optimisation-based control is proposed to charge and discharge residential battery storage to prevent excessive grid voltage deviation. The proposed approach, formulated as a quadratic program (QP), is compared with other QP approaches. As DER owners experience financial losses due to over-voltage disconnection of inverters, the benefits for both the grid operation and financial savings for customers are quantified. To reduce complexity in this first part, only real power (charge/discharge) of batteries is controlled.

In the fourth chapter, an original optimisation-based control is proposed to actuate both real and reactive power of battery storage. The approach aims to regulate grid voltages and reduce power losses, while providing economic benefits for DER owners. The network model is also included in the control to capture the sensitivity of real and reactive power for voltage feedback regulation. When providing voltage feedback control with hundreds of DERs across the network, it is critical to design parameters to achieve system stability and prevent voltage oscillations in distribution networks.

In the fifth chapter, the condition for system stability is analytically obtained and assessed. Leveraging on the stability condition, a local volt-var-watt (VVW) proportional control is proposed to effectively regulate voltages while reducing grid power losses. The design of control parameters is based

on the stability criterion and an original local optimisation problem to weight real and reactive power actuation considering the grid impedance characteristic. This optimisation problem can be solved locally and analytically.

The sixth chapter proposes a central optimisation with system-wide information to design parameters of local VVW proportional control. In this two-layer central-local approach, autonomous VVW controllers act on a millisecond timescale for voltage regulation and have their gain (slope) coefficients updated regularly by the central optimisation problem at a minute timescale. The optimisation is similar to an optimal power flow (OPF) and formulated as a convex multi-period problem solved in a receding-horizon manner.

Numerical simulations are run with real-world customer data and distribution test feeders. We test and compare the optimisation and control proposed in this thesis with suitable benchmark approaches from the literature. In general, proposed approaches provide significant improvement in grid operation, particularly regarding voltage regulation, grid power losses and peak power demand. With fewer technical challenges, the proposed approaches allow for greater integration of low-carbon DERs and contribute to the sustainable electricity grid of the future.

List of Acronyms

13NF	IEEE 13-node test feeder
123NF	IEEE 123-node test feeder
8NF	8-node test feeder
42NF	42-node test feeder
ACT	Australian Capital Territory
ANU	Australian National University
AB-QP	alternate-balanced quadratic program
B-QP	balanced quadratic program
CIM	current injection method
CF-QP	customer-focused quadratic program
DER	distributed energy resource
ESS	energy storage system
EV	electric vehicle
GF-QP	grid-focused quadratic program
IEC	International Electrotechnical Commission
IFAC	International Federation of Automatic Control
L-QP	local quadratic program
LV	low-voltage
LP	linear program
LRVR	loss reduction per voltage regulated
LHS	left-hand side
MV	medium-voltage

MPPT	maximum power point tracking
MPC	model predictive control
NREL	National Renewable Energy Laboratory
OPF	optimal power flow
OPF-PC	optimal-power-flow-based proportional control
PMU	phasor measurement unit
PCC	point of common coupling
PF	power flow
PV	photovoltaic
QP	quadratic program
QCQP	quadratically constrained quadratic program
RHO	receding-horizon optimisation
RHS	right-hand side
SOC	state of charge
TOU	time-of-use
VVW	volt-var-watt
VB-VVW	voltage-based volt-var-watt

Contents

Chapter 1

Introduction

The ever-decreasing costs of renewable sources of electricity, in conjunction with advances in technology and government incentives, have led to a massive uptake of renewable energy worldwide [Annaswamy et al., 2023]. As a result, many countries are now experiencing periods of times in which a significant share of the total power generation comes from variable renewable sources such as wind and solar photovoltaic (PV) [AEMO, 2019]. Australia is one that has reached one of the highest levels of distributed (rooftop) PV generation in the world. In fact, some regions have already experienced periods of time in which 64% of the demand is supplied by distributed PV alone, and predictions say it can get as high as 85% by 2025 [AEMO, 2020b].

Distributed PV generation has the obvious benefits of being clean and a local source of electricity. However, high levels of PV generation in distribution networks offers significant technical challenges for grid operators, specially when it coincides with low demand, which is often the case of residential areas [Marra et al., 2014; Jayasekara et al., 2014]. Solar PV potentially creates large reverse power flows and, as a consequence, provokes voltage rise and congestion on the network [AEMO, 2020a; Ranaweera and Midtgard, 2016]. Excessive voltage rise, in turn, prompt over-voltage disconnection of the solar PV itself and other distributed energy resources (DERs), resulting in financial losses for customers and power quality concerns for distributors [Collins and Ward, 2015; EPRI, 2016; de Carvalho et al., 2020].

The electric vehicle (EV) is another emerging DER that impacts the operation of distribution networks [Annaswamy et al., 2023]. EVs are generally plugged-in for charging during periods of peak demand where the grid is already under stress. EV charging can then intensify power flows and voltage drop on the grid, potentially creating congestion and pushing the grid to its operating limits [ENEA et al., 2020; Callaway and Hiskens, 2011; Murray et al., 2021].

Distribution networks are already experiencing problems due to high levels of distributed PV and plugged-in EVs. With the intrinsically variable

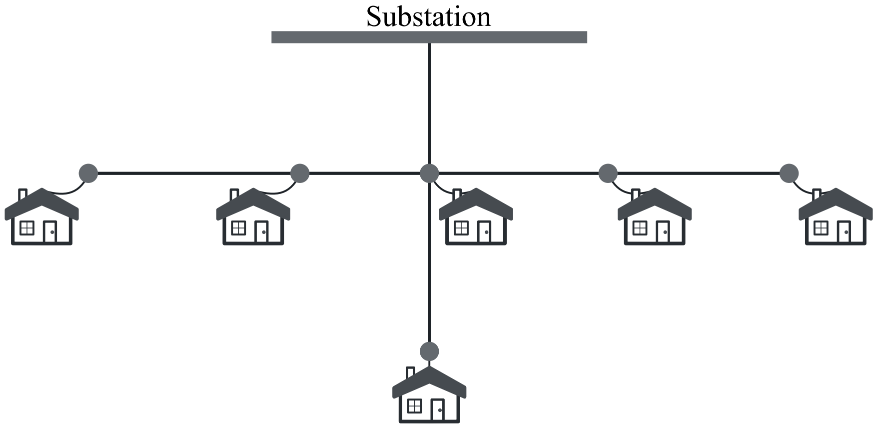

Figure 1.1: Example of a traditional electric power distribution network with one-way power flow. Customers only consume electricity and therefore power flows from substation to nodes. Voltage drop is expected. Variations are slow and predictable along the day and uncertainty is small.

nature of PV generation and uncertain time of EV charging, these two rarely match together and simply having both PV and EVs on the grid is not enough to solve those problems [AEMO, 2020a; ENEA et al., 2020]. Obvious solutions include curtailment of solar PV generation, restriction of EV charging power, and reinforcement of the network infrastructure, such as replacing transformers and conductors by others of larger gauge. These solutions are generally not desirable and they not only impact financial savings of customers, but also result in excessive costs for distributors [Jahangiri and Aliprantis, 2013].

An alternative and increasingly attractive way of mitigating the challenges caused by variable renewable generation and electrification of the transportation sector is the battery energy storage. Fast decreasing costs and progressing technology have made battery storage a promising asset to enable greater penetration of DERs and to postpone (or even avoid) network upgrades [Porteous et al., 2018; Marra et al., 2014; NREL, 2019a]. Battery storage can absorb the excess of PV generation during daylight and discharge during periods of peak demand, positively contributing to voltage levels and power flows in the network [Wang et al., 2016]. But again, as the number of battery storage or any other DER increases in distribution grids, they may end up producing their own technical difficulties if not properly controlled [Murray et al., 2021; AEMO, 2020a].

In summary, all this variety of DERs expected to multiply in distribution networks may pose major technical challenges, but they also create many promising opportunities. Such DERs and other demand response assets can be harmonised not only to solve the aforementioned issues but also to provide other important grid services [Arnold et al., 2018; Shahsavari et al., 2016;

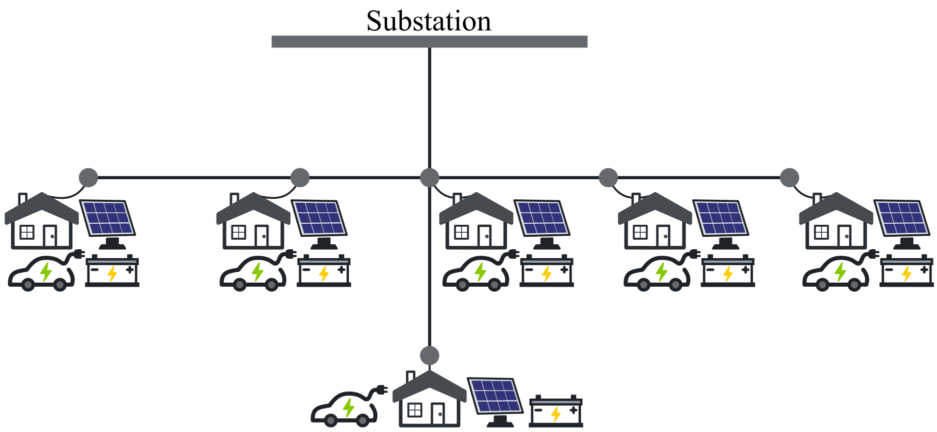

Figure 1.2: Example of a future electric power distribution network with two-way power flow. Customers consume and generate electricity and thus power can flow either way in each line segment. Both voltage drop and voltage rise are expected. Variations are quick and less predictable and uncertainty is higher.

de Carvalho, 2019]. In order to account for the variable and heterogeneous DERs, above all, *more elaborate approaches to control the increasing number of these resources are needed* [Annaswamy et al., 2023; von Meier et al., 2020].

Fig. 1.1 and Fig. 1.2 illustrate and summarise the challenges and transformation undergoing in today's electricity distribution networks. More elaborate and effective control tools are needed to operate a distribution grid with a large number of DERs as in Fig. 1.2.

In the sequel, a brief overview on control approaches is presented, followed by the main research question and original contributions of this thesis. Finally, at the end of this chapter, the organisation of this document is presented.

1.1 Controlling DERs in Distribution Networks

There are a number of approaches in the literature for controlling DERs in distribution networks. Approaches essentially fall into three main categories, depending on their communication requirements: Centralised, distributed and local/autonomous (see Fig. 1.3). A combination of two of more of these categories is also possible [Mahmud and Zahedi, 2016].

Centralised approaches require that every DER or customer, everywhere on the network, communicates all relevant information to a central coordinator. This central agent, with all grid measurements and data, computes the setpoints of all DERs, usually via a large optimisation problem, and sends back to customers. DERs then actuate on the provided setpoints; only the cen-

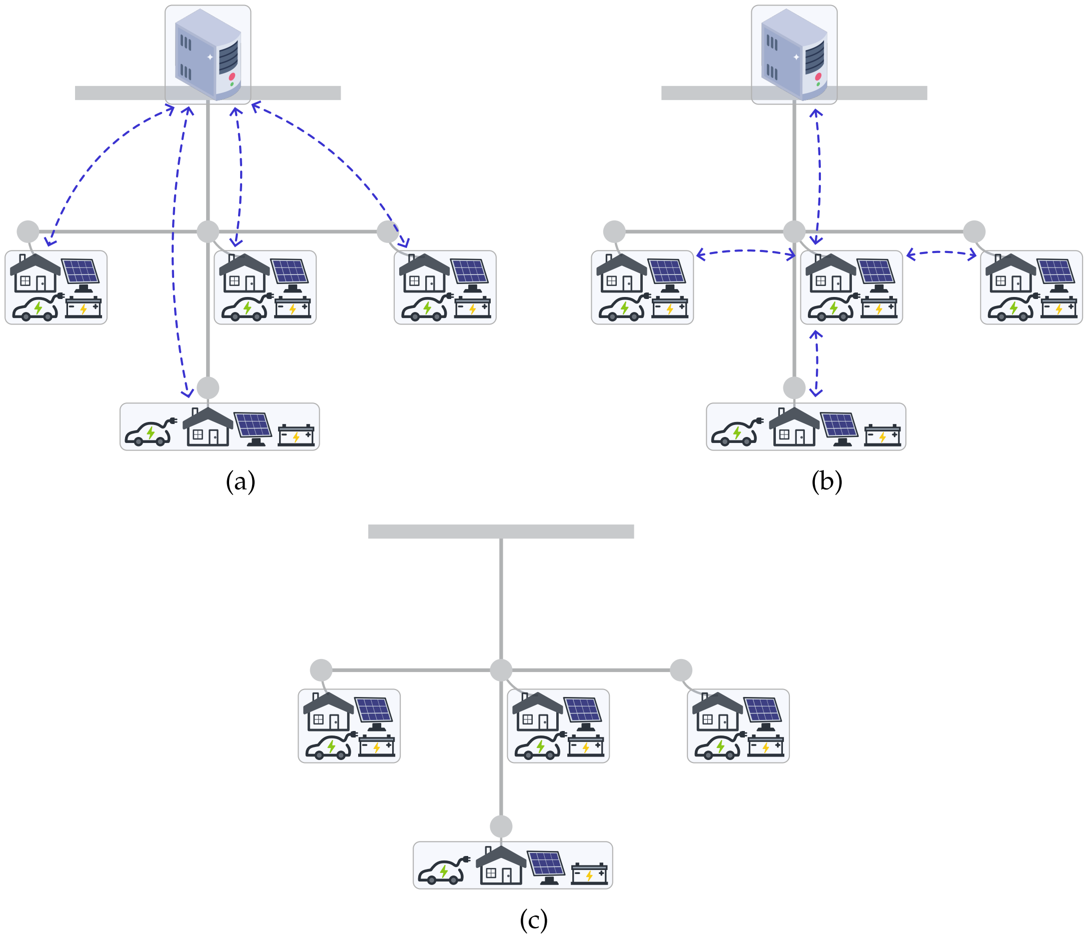

Figure 1.3: DER control in distribution networks based on communication requirements: (a) Centralised control; (b) Distributed control; and (c) Local/autonomous control. Remote communication and central coordinator are not required in local control. Dashed arrows indicate communication flows.

tral coordinator can start another cycle to update control actions [Antoniadou-Plytaria et al., 2017].

Distributed approaches aim at decomposing the large global optimisation problem into smaller problems that customers can solve separately. Customers across the network solve their own smaller optimisation problem and share part of their solution and some limited information with other customers. This process is then repeated multiple times, in a iterative manner, until a convergence is reached. When the convergence criterion is satisfied, then DERs actuate on the converged final setpoints [Attarha, 2022].

Local approaches, also called autonomous or fully decentralised approaches, do not require remote communication with a central coordinator or other customers. As the name suggests, DERs actuate autonomously based on local measurements and locally stored information [Murray et al., 2021]. The combination of local control with another system-wide approach is completely possible and provides great opportunity for enhancing grid operation [NREL, 2019b; Maharjan et al., 2021; Annaswamy et al., 2023].

Both centralised and distributed approaches can achieve global (system-wide) objectives in the distribution network, while keeping the network operating point within the bounds [Cavraro and Carli, 2018; Arnold et al., 2016]. However, the high communication and computational costs, along with convergence challenges, make these approaches complex and insufficiently fast to respond to quick network demand and voltage variations. Also, many distribution networks do not possess ubiquitous measuring devices and a reliable and secure communication infrastructure to support centralised and distributed approaches [Singhal et al., 2019].

Local approaches might not achieve globally optimal solutions but have shown surprising performance potential when compared to system-wide approaches [Turitsyn et al., 2010b]. With minimal or no communication, local approaches are privacy strengthening, robust to communication failures, autonomous and respond quickly to sudden demand or voltage variations – thus more applicable in practice [Antoniadou-Plytaria et al., 2017].

Local approaches provide promising opportunities for controlling DERs in distribution networks; and there are still many important aspects that the literature lacks within such a scope. We now outline a few relevant subjects with ample space for investigations and original contributions to the literature.

- Optimisation-based local control. Rather than purely time-based or rule-based control, optimisation problems can be cast either to formulate local control as a model predictive control (MPC) or to optimise parameters of local controllers;

- Incorporating the physics (models) of the grid and grid measurements in a local control setting. As opposed to other network-agnostic control, such as purely financial-based approaches, network-cognisant control unlocks greater potential for effective operation of DERs;

- Assessing system stability of local control. With hundreds of DERs acting independently in many locations across the grid, it is crucial to properly design control parameters to prevent sustained voltage oscillations and interactions between inverters;

- Two-layer central-local control. Algorithms that combine local controllers with global optimisation problems provide the opportunity to enhance overall system performance; and

- Financial impact of significant grid voltage deviation. Investigation of the impact of over-voltage disconnection of inverters on the financial savings of DER owners.

These points are motivated and discussed in more detail in the following chapters that focus in one of more of these subjects. The following section presents the general research question and original contributions of this PhD thesis.

1.2 Research Question and Contributions

The PhD program focused on developing original optimisation and control approaches of DERs considering chiefly local measurements, that is, measurements available behind-the-meter of an energy user. This thesis seeks to give answers to the following research question:

How to enhance distribution network operation with optimisation and local control of DERs?

More specifically, we aim to enhance distribution network operation by reducing: grid voltage deviations; peak power demand; resistive grid power losses; and impact on financial savings of DER owners. We propose original optimisation problems and control formulations to locally control real and reactive power of residential battery storage across the grid to mitigate such problems.

The proposed optimisation and control are presented along four main chapters: Chapter 3, 4, 5 and 6. Each one of these chapters is looking into one or more sides of the research question. As such, each one contains its own literature review, research gap and contributions specific to the context and part of the research question that is being investigated. As a whole, the contributions of this PhD thesis are summarised as follows:

- Formulation of original optimisation-based control approaches considering only variables measured locally;

- Formulation of original equations with valid approximations to locally describe voltage deviations and grid power losses in a local control setup;

- A new formulation for the proportional volt-var-watt control for voltage regulation which intrinsically includes the impedance characteristic of the network and local power measurements to reduce impact on grid power losses;

- Formulation of an original local optimisation problem to design parameters of local controllers with the optimal ratio of real to reactive power for voltage regulation;
- Formulation of new system-wide optimisation problem to design parameters of local controllers for voltage regulation that minimises grid power losses, preserves system stability, and incorporates DER power and energy limits within parameters; and
- An algorithm that combines a central approach with local controllers to provide globally optimal parameters that are regularly updated in a receding-horizon fashion.

Again, we refer readers to Chapter 3, 4, 5 and 6 for the specific original contributions of each part of this PhD thesis. Each one of these chapters is associated to a paper published in/submitted to a relevant journal or conference in the area. Thus each of these chapters are adaptations of the respective paper.

Chapter 3 is an adaptation of the paper published in the 21st International Federation of Automatic Control (IFAC) World Congress, in Berlin, Germany [de Carvalho et al., 2020]. Chapter 4 is related to the paper published in the IEEE Transactions on Power Systems [de Carvalho et al., 2023]. Chapter 5 is associated with the paper published in the IEEE PES Asia-Pacific Power and Energy Engineering Conference, in Melbourne, Australia [de Carvalho et al., 2022]. And finally, Chapter 6 is an adaptation of the paper in preparation [de Carvalho et al., 2024].

1.3 Thesis Outline

The remainder of this doctoral thesis is divided in a background chapter, the four main chapters, and finally the chapter with overall conclusions and future research. In more detail, the following chapters are organised as follows:

- **Chapter 2** describes the background content of this thesis. It starts with a broad literature review on optimisation-based approaches for controlling DERs, followed by a brief mathematical description of the main optimisation problems surrounding this thesis. The chapter ends describing the software, data and all relevant information for running numerical simulations and testing the proposed approaches.

- **Chapter 3** proposes a straightforward yet effective optimisation-based control for scheduling the charge and discharge of residential battery storage. We compare the approach with other similar ones and quantify their impact on reducing over-voltage disconnection of inverters and customer financial savings. The chapter finishes with several numerical simulations, then conclusions and final remarks.

- **Chapter 4** presents the well-known linear network model for distribution networks, the LinDistFlow, in which much of this thesis is based. The proposed formulation and approximations for grid voltage deviations and power losses are then given. These equations culminate in a new local optimisation-based approach for controlling real and reactive power of residential battery storage. Extensive numerical simulations, conclusions and final remarks finalise the chapter.

- **Chapter 5** gives a stability criterion in which voltage-based local controllers have to satisfy to provide convergence to steady-state voltages. Here, we propose an original formulation for the proportional volt-var-watt control and introduces a local optimisation problem to provide locally optimal parameters. Numerical simulations test and compare the new approach with benchmark approaches from the literature. Conclusions and final remarks are presented at the end of the chapter.

- **Chapter 6** introduces a combined central-local approach to control DERs in distribution networks. Local controllers follow the fast volt-var-watt proportional control law. Whereas a system-wide central optimisation problem is solved at a slower timescale to provide globally optimal parameters for local controllers. Numerical simulations quantify benefits for the grid operation and assess computational effort of the central-local approach. The chapter finishes with conclusions and some final remarks.

- **Chapter 7** concludes this thesis as a whole, presenting final remarks, the main takeaways of this doctoral research, and options for future works.

Chapter 2

Background

Voltage and power flow regulation in distribution networks is not new. Grid operators have been managing voltage and power variability in distribution networks for decades with the use of, for example, tap-changing transformers and shunt capacitor banks. The new challenge is the higher variability, intensity and uncertainty posed by DERs. With greater challenges also come promising opportunities to use DERs for grid services.

This chapter presents a closer look into optimisation and control approaches from the literature to manage the challenges introduced by solar PV and other DERs. This chapter is organised as follows. Section 2.1 presents the literature review on control of DERs for voltage and power flow regulation in distribution networks. Although Section 2.1 focuses on optimisation-based approaches, it also considers some of the most relevant studies using other approaches. Advantages and disadvantages of each approach are also discussed.

Section 2.2 mathematically describes the main optimisation formulations that are relevant for the proposed optimisation and control approaches in this thesis. Section 2.3 ends the chapter describing the software, data and all background content for testing the optimisation and control approaches. We describe the power flow (PF) calculation method, as well as the test feeders and real-world load and generation dataset for numerical simulations.

2.1 Literature Review

In this section, we describe and discuss the work available in the literature and contrast their work with the proposed work in this thesis. It is worth mentioning that a broad literature review is presented here, whereas Chapters 3 – 6 present a narrower and shorter literature review specific to the problem under investigation in the respective chapter.

Many studies have investigated different approaches to control DERs in distribution networks. Since DERs are commonly owned by customers, several authors have also included an analysis on the financial benefits for customers when proposing control approaches of DER.

von Appen et al. [2014] compared several voltage rise mitigating approaches using distributed solar PV and battery storage systems. The authors chiefly investigated rule-based approaches, including ones with PV curtailment. They also considered financial savings for DER owners, needed to promote the interest of customers to purchase a battery or curtail PV generation. A simple rule-based control investigated in the paper is: If there is export of power (i.e. PV generation is greater than local load) and battery is not fully charged, then charge battery with the export amount.

Ratnam et al. [2015a,b, 2016]; Ratnam and Weller [2018] have focused on optimisation-based approaches to schedule the charging/discharging of residential batteries. The optimisation problems are formulated to balance two main goals: (i) financial savings accrued by customers with battery storage co-located with solar PV, and (ii) the grid benefits of voltage and power regulation. Savings are calculated based on the battery operation and the different energy prices over the day, i.e. the time-of-use (TOU) tariff. Here, optimisation problems are multi-period, where future time steps are considered to ensure present control decisions are not short-sighted. For example, multi-period optimisation problems, as MPC, ensure the battery will not be fully charged in the future if forecast says there will be a peak PV generation where battery will be essential to soak up the excess.

In [Ranaweera and Midtgard, 2016] the economic part is not only modelled in terms of energy savings, but also in terms of battery degradation costs. The non-linear non-convex optimisation problem, formulated to improve savings and voltage rise issues on the grid, is solved with the dynamic programming method. Jayasekara et al. [2014] have gone even further in terms of modelling battery costs. Apart from degradation costs the authors in [Jayasekara et al., 2014] have included capital and replacement costs of the battery in the optimisation problem.

Although modelling detailed battery costs potentially extend the lifespan of the device, it may also limit benefits that batteries could provide to the grid and to customers in terms of operational energy savings. Another aspect of including excessive model details of DERs is that it often turns the optimisation into a non-convex problem and more complex and time-consuming to solve. The formulation of convex and compact models with fewer integer binary variables (ideally none) is well-known to increase solving efficiency of optimisation problems [Chen et al., 2023].

Non-convex optimisation problems presents poor scalability and solving efficiency and cannot guarantee the global minimiser. Particularly in control applications, it is highly desirable that optimisation problems are simple and convex. Convex problems are computed efficiently and reliably for real-time applications, and solutions will minimise (or maximise) the objectives [Borrelli et al., 2017; Boyd and Vandenberghe, 2004; Turitsyn et al., 2010b].

An optimisation problem to minimise a single variable 'alpha', that represents the percentage of PV power that should be limited to keep the grid voltage under 1.10 p.u., is proposed in [Marra et al., 2014]. Battery storage is then used to charge only when PV exceeds the threshold, which may result in the underutilisation of the storage asset. Kabir et al. [2014] proposes a combined rule- and droop-based approach that charges/discharges the battery only when the voltage on the grid exceeds thresholds, which can also result in underutilisation.

In terms of communication requirements, we see authors proposing control approaches in every category. A combined central-local optimisation-based approach is presented in [Ranaweera et al., 2017]. The local optimisation objective is selected by the battery owner, while the central one modifies the locally-scheduled setpoints if over-voltage is detected on critical nodes of the network.

A distributed control approach based on multi-agent systems to control batteries has been proposed in [Zhang et al., 2020]. A detailed literature review on distributed and decentralised approaches for voltage regulation in distribution networks is given in [Antoniadou-Plytaria et al., 2017]. Another literature review on optimisation and voltage control approaches with both centralised and decentralised control structures is presented in [Murray et al., 2021]. A table comparing many papers and their control strategies is presented in [Alonso et al., 2022].

Central approaches are known for requiring extensive communication infrastructure, but they can also achieve globally optimal results on the monitoring area and explicitly integrate grid constraints in the formulation. Central optimal power flow (OPF), that has been traditionally used for offline designing and planning studies, has been recently studied as an online tool in distribution networks.

A centralised approach is proposed in [Kotsalos et al., 2019] based on the non-linear three-phase OPF formulation. The optimisation-based approach includes a time-horizon and controls multiple DERs to keep grid voltages and power flows within bounds. Again, due to the non-linear and non-convex nature of the full unbalanced three-phase PF formulation, it can be very challenging to solve within appropriate time frame, particularly for near-real-time applications required for controlling DERs.

Dobbe et al. [2020] proposed a machine learning approach to mimic OPF results and then decrease the dependence on communication. In this way, DERs can be controlled locally based on a learned model that approximates the optimal power injection. Machine learning approaches, however, usually requires large amount of data for training as well as representative and comprehensive scenarios of the grid operating condition in order to be reliable.

Arnold et al. [2016] derived a linearised three-phase PF model for unbalanced distribution networks, which is useful for convex OPF problems and online applications. This linear PF formulation is an extension of the well-known LinDistFlow equations first presented in [Baran and Wu, 1989a]. The model was used to cast an optimisation problem to dispatch reactive power of DER inverters to balance and regulate grid voltages. The optimisation objective was to minimise difference in voltage magnitude among phases at each node while decreasing reactive power usage of DERs.

Sankur et al. [2016] extended the linear network model shown in [Arnold et al., 2016] by simply adding the option to dispatch real power of DERs, rather than only reactive power. This formulation was tested in an OPF problem to minimise the real power required from the substation to supply the network demand. This study also proposed an iterative process to decrease the error of the linear OPF problem. Numerical simulation was carried out to compare the OPF with and without this iterative process for voltage balancing. Although the OPF with the iterative process has shown better performance, they have both shown appropriate results to balance voltage magnitude on the network.

The LinDistFlow equations are also used in [Joo et al., 2017] to regulate grid voltage magnitude by coordinating distributed flexible demand. The proposed approach is divided in a central OPF, responsible for requesting real power curtailment, and local controllers that receive the request and curtail based on the availability. The central OPF is formulated to minimise the real power required from the substation, while keeping voltages on the network within constraints. The local controllers then identify loads that can be curtailed to try to match the central request. Local controllers use the MPC method, in which a future time-horizon is included to prevent disruptive operation of load devices.

The broad literature review and critical reading carried out during the PhD program helped with several important decisions. Since optimal control enhances efficacy and it can easily incorporate network and device models, as well as their operational constraints, in this thesis we focus on optimisation-based control approaches. Optimisation-based control approaches are cast much like MPC problems. This is the subject of detailed investigation of Chapter 3 and Chapter 4.

Another local control investigated in this thesis is the proportional volt-var-watt (VVW) control – widely used in practical distribution networks nowadays. This simple yet fast and effective control for voltage regulation actuates real and/or reactive power with a proportional value to the voltage deviation value. Traditionally, gain (slope) coefficients and other parameters of VVW control have been obtained from off-the-shelf numbers that are not designed for the specific network in which controllers operate. Such coefficients have also been designed based on a single stability condition without considering other issues such as grid power losses, peak demands, or even the capacity of controllable DERs [Cavraro and Carli, 2018; IEEE, 2018]. This is the subject of investigation of Chapter 5 and Chapter 6.

In this thesis, original formulations that intrinsically captures the impedance characteristic of the grid are proposed for proportional VVW control (Chapter 5). We also propose convex optimisation problems to design parameters of local VVW controllers based on the actual grid operating point. Thus, controllers consider not only the grid model to capture the physics of the grid in which they operate, but also the present and future operating state of the network (Chapter 6).

One of the most pressing issues in distribution networks with massive penetration of DERs are: Excessive voltage deviations; unacceptably high grid power losses; and extreme peak demands (congestion) [IEA, 2022; Murray et al., 2021]. Therefore, we often minimise one or more of those issues in the objective functions of our optimisation problems.

We pursue simple and convex optimisation problems so our control approaches can be used online and respond quickly to demand and voltage variations on the grid. In this sense, the well-established linear network model LinDistFlow is largely used to model radial distribution networks within our control approaches. LinDistFlow equations typically provide errors smaller than 1% relative to its non-linear counterpart and, as opposed to the full PF equations, allow for convex optimisation problems Farivar et al. [2013].

2.2 Convex Optimisation

Convex optimisation problems are chiefly formulated as a linear program (LP), quadratic program (QP) and quadratically constrained quadratic program (QCQP) [Boyd and Vandenberghe, 2004]. A brief description of these classic optimisation formulations, which are more relevant for this PhD thesis, is presented in this section. More details on optimisation theory are found in [Borrelli et al., 2017; Boyd and Vandenberghe, 2004; Bertsekas, 1999].

For illustrative purposes, let us consider an optimisation-based control of DER power formulated as a standard LP problem. Define u as the controllable real power of a battery storage, for example, where an optimal value is pursued. We adopt the positive load convention for power flows, where positive values of u mean DER consuming power from the grid (e.g. charging battery) and negative values of u mean DER providing power to the grid (e.g. discharging battery).

Variable u is a real number $u \in \mathbb{R}^T$ and it can be a scalar ($T = 1$) or a vector ($T = 2, 3, ...$), and T represents the Total number of discrete future time steps, for instance. The limits of controllable real power of the battery storage are denoted by the lower bound $\underline{u}$ and the upper bound $\overline{u}$ constraint.

A given cost/weight/penalty for consuming power for each time step is denoted by $r \in \mathbb{R}^T$. Define a linear objective function as $r'u$, so the minimum cost for controlling u can be found[1]. An LP problem [Borrelli et al., 2017] is then formulated as:

$$
\begin{aligned}
\min_{u} \quad & r'u && \text{(2.1a)} \\
\text{s.t.} \quad & Au \le b, && \text{(2.1b)} \\
& A_e u = b_e, && \text{(2.1c)} \\
& \underline{u} \le u \le \overline{u}. && \text{(2.1d)}
\end{aligned}
$$

The optimisation problem (2.1) is composed of the objective function (a) and constraints (b)-(d). The last constraint (d) models the operational power limits of the battery. The linear inequality constraint (b) and the linear equality constraint (c) can model other operational limits and the physics of the system. Define the number of inequality constraints as s and thus matrix $A \in \mathbb{R}^{s \times T}$ and vector $b \in \mathbb{R}^s$. Similarly, define the number of equality constraints as c and thus $A_e \in \mathbb{R}^{c \times T}$ and $b_e \in \mathbb{R}^c$.

Here, controllable real power u is the unknown of the optimisation problem, also termed as the decision variable. By solving (2.1), optimal u is obtained, meaning the objective function is minimised and all constraints are satisfied. In this thesis, typical decision variables are u (controllable real power) of and v (controllable reactive power) of DERs. Other variables of interest that we seek to optimise in this thesis are parameters/coefficients of proportional VVW control.

In optimisation (2.1) both the objective function and constraints are linear (or affine) and therefore the problem is an LP. When the objective is a convex quadratic function and all constraints are linear (or affine) the optimisation problem is a QP [Borrelli et al., 2017; Boyd and Vandenberghe, 2004]. The QP optimisation is largely adopted in this thesis for modelling problems related

[1]Please note that T as in $(\cdot)^T$ denotes the size of the vector or matrix as the total number of discrete timeslots, whereas $'$ as in $(\cdot)'$ denotes the transpose of a vector or matrix.

to control (Chapters 3 and 4) and parameter design (Chapter 5). A QP can take the form:

$$\min_{u} \quad \frac{1}{2}u'Hu + r'u \tag{2.2a}$$
$$\text{s.t.} \quad Au \leq b, \tag{2.2b}$$
$$A_e u = b_e, \tag{2.2c}$$
$$\underline{u} \leq u \leq \overline{u}, \tag{2.2d}$$

where matrix $H \in \mathbb{R}^{T \times T}$ has to satisfy $H = H' \succ 0$ [Borrelli et al., 2017]. A QP provides the option to model the cost/weight/penalty as a quadratic expression via matrix H. Now, with the addition of convex inequality quadratic constraints, the optimisation problem is called a QCQP [Boyd and Vandenberghe, 2004]. An example of a QCQP problem used in Chapter 6 of this thesis is as follows:

$$\min_{u} \quad \frac{1}{2}u'H_0u + r_0'u \tag{2.3a}$$
$$\text{s.t.} \quad Au \leq b, \tag{2.3b}$$
$$A_e u = b_e, \tag{2.3c}$$
$$\underline{u} \leq u \leq \overline{u}, \tag{2.3d}$$
$$\frac{1}{2}u'H_iu + r_i'u \leq b_i, \quad i = 1, 2, ..., j, \tag{2.3e}$$

where j is the total number of convex quadratic inequality constraints. Convex problems as the LP, QP and QCQP presented in this section can be solved efficiently and reliably [Boyd and Vandenberghe, 2004; Borrelli et al., 2017].

LP is not a *strictly* convex problem, meaning there can be more than one optimal solution. Strictly convex problems have a unique minimiser and thus often reduces irregularities and fluctuations of the optimal u when solving the same optimisation multiple times. In this thesis, optimisation problems are mainly formulated as QP and QCQP. Even when problems can be treated as an LP, a small regularization quadratic term is often added to the objective function so that problems become a QP and thus strictly convex.

2.3 Framework for Numerical Simulations

This section presents the software used to implement the proposed optimisation problems and control approaches. We also briefly describe the distribution test feeders, the dataset, the PF calculation method and other implemented codes to run numerical simulations to test the proposed approaches during the PhD program.

Numerical simulations represent a convenient and accurate means of representing the physics of power systems. In fact, numerical simulations is one of the main practices in the power engineering literature for testing and investigating approaches [Robbins and Dominguez-Garcia, 2016; Franco et al., 2018; Mediwaththe et al., 2020]. PF simulations, more specifically, constitute one of the essential tools for steady-state offline studies, as well as for near-real-time decisions in distribution networks [Ahmadi et al., 2016]. In this thesis, the proposed approaches are tested and assessed by means of PF simulations.

Several commercial software are available for PF simulations. However, they are not always convenient to integrate with other software, datasets or optimisation and control approaches. Commercial software often protect their codes and the specific internal structure, limiting applications and detailed analyses.

In this sense, a simulation framework has been built during the first year of the PhD program to carry out experiments and to provide full access to internal variables and ease of integration with other parts. The framework consists of a set of codes in MATLAB, including: a full three-phase PF calculation; a clean, ready-to-use dataset with residential load and PV generation data for an entire year; localised and centralised optimisation-based approaches implemented as LP, QP and QCQP; local power control approaches of DER inverters, such as the VVW control; plot functions; etc. Since all codes are in MATLAB, or readily readable by MATLAB, they can be easily integrated to simulate many different scenarios in distribution networks. Original optimisation and control approaches to control real and reactive power of DERs can then be integrated and tested using this framework, assessing the effects on both the grid and customers.

The Gurobi Optimizer and MATLAB itself are used for solving optimisation problems in this thesis. Main optimisation solvers called within MATLAB are: *linprog* to solve LP problems [The MathWorks, Inc., 2023c]; *quadprog* to solve QP problems [The MathWorks, Inc., 2023d]; *fmincon* to solve QCQP and general optimisation problems [The MathWorks, Inc., 2023b,a]. MATLAB optimisation solvers are easy to integrate with the simulation framework, but have shown limited time efficiency when solving larger optimisation problems. Gurobi Optimizer has provided quicker solutions for large-scale problems and is mainly used in this thesis for solving QCQP problems in Chapter 6, where a system-wide optimisation problem is proposed.

The LinDistFlow model, largely used in this thesis, is a linear approximation of the full non-linear PF equations. To clarify, the optimisation and control proposed in this thesis are mostly based on the linear model, but they are tested under the full exact non-linear PF model. We adopt the non-linear PF calculation with the current injection method (CIM) [Garcia et al., 2000; Carvalho and Pesente, 2014]. We also often run numerical simulations with heavy load/PV generation conditions, where approximations are less accurate and thus LinDistFlow is really put to test. Even under extreme conditions, optimisation and control approaches have provided grid stability and have shown great efficacy, suggesting approximations are valid for the entire range of normal grid operation.

The implemented full three-phase non-linear PF calculation based on the CIM [Garcia et al., 2000; Carvalho and Pesente, 2014] is appropriate for both balanced and unbalanced, radial and mesh networks. Line segments are modelled as the well-known Pi model, and they can account for self and mutual series impedances as well as self and mutual shunt admittances. Loads can be delta (Δ) or star (Y) connected and can be modelled as the usual ZIP load model, i.e. constant impedance (Z), constant current (I), constant power (P and Q) values or a mix of the three. This implemented PF algorithm has been benchmarked with other commercial software and with available PF results from test feeders widely accepted in the community.

Several distribution test feeders are used for numerical simulation in this thesis, namely: IEEE 13-node test feeder (13NF) and IEEE 123-node test feeder (123NF) described in [Kersting, 2001]; the 8-node test feeder (8NF) described in [Zeraati et al., 2018; Mediwaththe and Blackhall, 2021]; and the 42-node test feeder (42NF) described in [Zhou et al., 2021]. Such test feeders present a good variety of medium-voltage (MV) and low-voltage (LV) distribution networks and are widely adopted in the power engineering research community [Dobbe et al., 2020; Islam et al., 2019; Joo et al., 2017; Niazazari and Livani, 2017; Arnold et al., 2016; Zeraati et al., 2018; Mediwaththe and Blackhall, 2021; Zhou et al., 2021].

The residential load and rooftop PV generation dataset are part of the Next Generation (NextGen) program that takes place in the Australian Capital Territory (ACT) [Shaw et al., 2019]. As a resulted of the cleaning process of 514 de-identified customers shown in [Shaw et al., 2019], a clean dataset composed of 100 different residential costumers have been organised for the entire year of 2018. The clean dataset with 100 de-identified customers was kindly provided by the authors of [Shaw et al., 2019].

With a suitable simulation framework in place, original approaches were proposed and developed during the course of the PhD program. The next chapter presents the first optimisation and control approaches of this thesis.

Chapter 3

Over-Voltage Disconnection of DERs: Assessing Grid and Customer Benefits

Over-voltage, often produced by excess PV generation during daylight, can cause inverters to frequently disconnect from the grid, affecting the operation of solar PV and batteries and, in turn, customer savings. In this chapter, we investigate how different local optimisation-based control to charge/discharge batteries can improve disconnections and customer savings.

We compare four QP approaches to schedule the day-ahead charge and discharge of residential batteries. The objective of the first optimisation is to increase the economic savings that PV customers with battery storage accrue. The second and the third approaches additionally modulate the power to and from the grid, reducing the occurrence of inverter-based disconnection and potentially also increasing economic savings for customers. The fourth approach directly manages customer-based power flows to and from the grid to smooth distribution load curve peaks and valleys, without explicitly considering energy savings that accrue to customers.

The second and the third approaches, named balanced quadratic program (B-QP) and alternate-balanced quadratic program (AB-QP), respectively, have the same objective function to balance between reducing grid power flow and increasing customer savings. In the AB-QP, however, a modification to promote the charging of the battery during the *peak* solar production is proposed to further reduce over-voltage disconnections.

With these four optimisation-based control, we assess the grid benefits in terms of inverter disconnections, where fewer over-voltage disconnections is the result of smaller voltage deviation from the nominal. In addition, we assess customer benefits in terms of financial savings accrued in a period of time. Although different customers sometimes accrue different amounts of savings, it is worth mentioning that fairness is not the focus of this thesis.

Relevant work on this subject has recently been published and can be found in [Poudel et al., 2023].

The key questions of this chapter are: how different local objectives, with local battery optimisation approaches, influence customer savings and inverter disconnections? Can a grid-focused objective, by improving grid voltages and thus disconnections, provide more savings for customers than the customer-savings-focused approach?

This chapter fully describes the paper presented in [de Carvalho et al., 2020]. The author of this thesis has opted for keeping most of the original structure of the paper in order to preserve coherence and clarity. This chapter is organised as follows: In Section 3.1, we introduce the specific context and problem being addressed here. In Section 3.2 we describe the residential system composed of load, rooftop solar PV generation and battery storage. The four optimisation for battery charge/discharge are presented in Section 3.3. The distribution network and simulation results are included in Section 3.4. Section 3.5 concludes this chapter with important remarks that also motivate the next chapter.

List of Main Symbols – Chapter 3

d	Residential real load demand
g	Real power of solar PV
$\hat{g}$	Processed real power of solar PV
p	Real power from the grid to residential system
$\hat{p}$	Processed real power from the grid to residential system
s	Charge level of battery storage
s_0	Initial charge level of battery storage
s_f	Final charge level of battery storage
$\overline{s}$	Energy capacity of battery storage
t	Discrete time index
T	Total number of time steps in the horizon
$\mathcal{T}$	Set of discrete time defined as $\{1, 2, ..., t, ..., T\}$
u	Real power of battery storage (controllable power)
$\overline{u}$	Maximum charging rate (absorbing power) of battery
$\underline{u}$	Maximum discharging rate (providing power) of battery
V	Voltage magnitude at point of connection of the residential system
Γ_g	Energy savings provided by solar PV
Γ_u	Energy savings provided by battery storage
Δ	Time length of a time interval
η	Electricity price
Ψ	Energy costs
ω	Weights of terms in objective function

3.1 Introduction

To manage voltages within an appropriate range, a number of different approaches have been adopted by distributors, such as limit maximum power export to the grid at 70% of the installed PV capacity [Marra et al., 2014] and restrict new installations of solar PV [Sayeef et al., 2012]. When voltage rise is significant, PV inverters are commanded to disconnect from the grid to prevent unacceptable high voltage levels on the feeder [Sayeef et al., 2012; Collins and Ward, 2015]. The subsequent loss of renewable generation, resulting from PV disconnection or curtailment, limits opportunities to store and dispatch the energy at a later time and impacts economic savings that solar PV would otherwise provide [Collins and Ward, 2015].

Among several methods for mitigating voltage rise and increasing the grid-connection of solar PV, is home- and business-scale battery storage solutions [Porteous et al., 2018]. As the technology continues to improve and prices fall, a greater number of PV customers are grid-connecting battery to provide both energy independence and, more frequently, increased economic benefits. Specifically, economic drivers such as time-of-use pricing have spurred customers to consider profit-based optimisation algorithms for designing the scheduling of battery storage charge and discharge cycles [Ranaweera and Midtgard, 2016].

Several authors have investigated approaches to balance distributor and customer benefits using home-battery co-located with solar PV. Ranaweera and Midtgard [2016] propose an objective function to maximise savings for customers while addressing voltage rise by limiting (with the battery) PV power exports to the grid. Several rule-based and voltage dependent control approaches for PV and battery inverters are proposed by von Appen et al. [2014]. The authors also consider PV self-consumption and the economic savings that accrue to the customer. Jayasekara et al. [2014] and Marra et al. [2014] propose different optimisation-based approaches to improve grid conditions and minimise operational costs for owners in terms of extending the battery life expectancy. Wang et al. [2015b] integrates batteries with solar PV by reserving specific amounts of the battery capacity to different tasks.

Although the aforementioned studies have provided important contributions to better integrate battery storage in the grid, they have not considered the disconnection of inverters caused by voltage rise. A typical threshold for disconnection is 1.10 p.u. Inverter disconnection impacts both battery storage control strategies and the economic savings that customers would otherwise accrue. The grid impact of wide-spread and frequent, inverter-based disconnection, is of growing concern to distribution network operators — see Collins and Ward [2015]; Sayeef et al. [2012]; Tonkoski et al. [2012]; Wang et al. [2012];

De Brabandere et al. [2004]; Ueda et al. [2008].

In this chapter we assess the customer and utility benefits of locally scheduling the charge and discharge of residential battery storage, considering the impact of DER inverter disconnection. We consider four QP optimisation problems to define the day-ahead battery charge and discharge schedule. The first QP, referred to as customer-focused quadratic program (CF-QP), increases operational savings for the battery owner while reducing battery cycling. The next two QPs, referred to as B-QP and AB-QP respectively, are two approach variations to balancing customer operational savings against PV self-consumption. By contrast, the objective function of the fourth QP, referred to as grid-focused quadratic program (GF-QP), is to flatten the residential load curve to improve supply voltages.

Our contribution is to provide a novel analysis of a range of QP approaches, benchmarking the impact on customer savings in cases where the over-voltage disconnection of inverters occurs. In addition, we introduce simple yet effective optimisation and control techniques in our formulations that contribute with less inverter disconnections. Numerical simulations are carried out on the 13NF that we populate with hundreds of residential systems that include solar PV and battery storage. The 13NF is a challenging feeder in terms of voltage regulation, proving to be appropriate to illustrate the impacts of over-voltage disconnection of inverters. Real-world, time-varying and de-identified data from the ACT, shown by Shaw et al. [2019], is used for residential loads and rooftop PV generation.

3.2 Residential System

Fig. 3.1 illustrates the residential system model considered in this chapter. For simplicity and clarity we adopt the load convention for power flows for all elements, including the solar PV. Positive power values represent that the element is absorbing power, whereas negative values imply element is producing power to the system. In that sense, PV power $g(t)$ is always negative or equal to zero.

Let $\mathcal{T} = \{1, 2, ..., t, ..., T\}$ be the steady-state discrete time set, where t is the discrete time index and T is the total number of time steps in the horizon. Symbols $d(t)$, $g(t)$, $u(t)$, $p(t)$ denote average real power flows (in kW) across time interval $((t-1)\Delta, t\Delta)$, where Δ is the time length. The battery charge/discharge scheduling horizon is then obtained by $T\Delta$. We introduce notation similar to that in [Ratnam et al., 2016].

The real-world load and PV generation dataset we use in this thesis is 5 minutes average power flows [Shaw et al., 2019]. Therefore, we often select

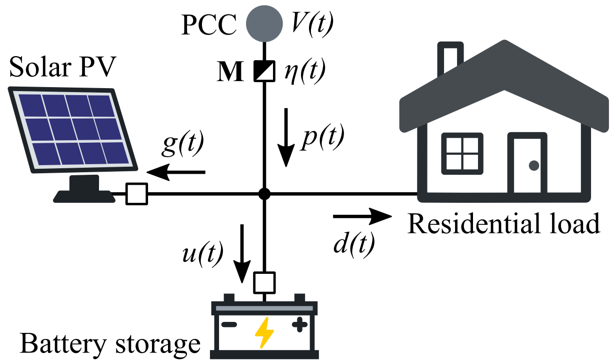

Figure 3.1: Residential system with average real power flows depicted for load demand $d(t)$, solar PV $g(t)$, the battery $u(t)$, and power to and from the grid $p(t)$. Battery is the only controllable element. Both the battery and solar PV can be disconnected. Arrows indicate the positive power flow direction. The PCC depicts the node where the customer is connected to the utility.

$\Delta = 5/60$ hour, the optimisation time window for a full day, $T\Delta = 24$ hours, and thus $T = 288$.

The residential system represented in Fig. 3.1 includes separate inverters for the solar PV and battery storage that facilitate the disconnection of DER when steady-state voltages measured at the PCC exceed an over-voltage threshold. The DER over-voltage trip protects both the devices and the surrounding grid infrastructure [Sayeef et al., 2012; Wang et al., 2012]. The DER inverter disconnection is either a physical separation from the system through a switch device or a virtual disconnection in which inverters set their power output to zero [EPRI, 2016]. In both cases, $g(t) = u(t) = 0$, when $V(t) > 1.10$, where $V(t)$ is the steady-state voltage magnitude (in per unit) as measured at the PCC.

Fig. 3.1 also depicts the bi-directional meter **M**, which applies a TOU price $\eta(t) \in \mathbb{R}_{\geq 0}$, $\forall t \in \mathcal{T}$, in \$/kWh across time interval $((t-1)\Delta, t\Delta)$. We also consider the financial policy of net metering, where the customer is billed for energy consumption at the same rate as they are compensated for exported energy to the grid. The power balance equation for Fig. 3.1 is

$$p(t) = d(t) + g(t) + u(t), \tag{3.1}$$

for all $t \in \mathcal{T}$, where $p(t)$ represents the grid real power provided to the residential system. Positive values of $p(t)$ indicate power flow to the residence and negative values correspond to power exported to the grid from the residence. Battery real power $u(t)$ is considered positive when charging and negative when discharging and is limited by

$$-\underline{u} \leq u(t) \leq \overline{u}, \qquad \forall t \in \mathcal{T}, \tag{3.2}$$

where $\underline{u}$ and $\overline{u}$ is the maximum discharging and charging rates in kW, respectively. Denote by $s(t)$ the battery charge level (in kWh) at time $t\Delta$, such that

$$s(t) = s_0 + \sum_{j=1}^{t} u(j)\Delta, \qquad \forall t \in \mathcal{T}, \tag{3.3}$$

where s_0 is the initial charge level of the battery in kWh. The charge level is limited by

$$0 \leq s(t) \leq \overline{s}, \qquad \forall t \in \mathcal{T}, \tag{3.4}$$

where $\overline{s}$ is the energy capacity of the battery (in kWh). At the end of the battery charge/discharge scheduling horizon, let the final charge level be

$$s(T) = s_f, \tag{3.5}$$

where s_f (in kWh) is the scheduled charge level at the end of time horizon. The compact battery model is consistent with [Ratnam et al., 2016], and more complex models such as [Reniers et al., 2018] are possible. We intentionally model the battery storage as the bucket model. Including efficiency and degradation in the battery storage model results in non-convex formulations, which negatively impacts solving efficiency and scalability of optimisation problems [Chen et al., 2023].

To further increase battery efficiency and lifespan, there are straightforward modelling techniques to include in the optimisation. The minimum and maximum charge level in (3.4) can easily be changed to 20% and 80%, for example, of the energy capacity to considerably reduce battery degradation [Martins et al., 2022]. Another option is to include regularisation penalty factors in the objective function of the optimisation problem to effectively reduce battery cycling. We include regularisation penalty factors in our proposed approaches, introduced in Section 3.3.

With net metering policy, the customer is billed for energy consumption over the entire time window $[0, T\Delta]$ by

$$\Psi = \sum_{t \in \mathcal{T}} \eta(t)p(t)\Delta = \sum_{t \in \mathcal{T}} \eta(t)\big(d(t) + g(t) + u(t)\big)\Delta.$$

As only g and u can be altered by disconnections, and only u is directly controlled, it is straightforward to see that by maximising savings with g and u, the bill cost as a whole is minimised. The savings accrued by a customer over the period $[0, T\Delta]$ with PV generation, or *PV savings*, is denoted by Γ_g, and the *battery savings* is denoted by Γ_u. Specifically,

$$\Gamma_g := -\sum_{t\in\mathcal{T}} \eta(t)g(t)\Delta, \qquad \Gamma_u := -\sum_{t\in\mathcal{T}} \eta(t)u(t)\Delta. \tag{3.6}$$

As PV power is always non-positive ($g(t) \in \mathbb{R}_{\leq 0}$, $\forall t \in \mathcal{T}$), PV savings is greater than or equal to zero. PV power is obtained from the real-world dataset, where inverters operates as per the maximum power point tracking (MPPT) algorithm. PV power $g(t)$ only differs from the dataset when $V(t) > 1.10$ and then inverters are disconnected from the grid. Therefore, the more over-voltage disconnections on the grid, the more PV is incapable of delivering power ($g(t) = 0$), and smaller the Γ_g. We aim at increasing PV savings by reducing voltage deviations and thus reducing disconnections from the network.

The battery storage is the only controllable element in the residential system of Fig. 3.1. As such, battery savings can be directly maximised by controlling u considering the electricity price $\eta(t)$. We aim at increasing battery savings by charging it when energy price is cheap (small $\eta(t)$) and discharging it when price is expensive (high $\eta(t)$). Controllable real power $u(t)$ can also be affected by battery inverter disconnections.

3.3 Problem Formulation

In this section we present four local optimisation-based approaches for scheduling the charge and discharge of residential battery storage. The first approach aims to maximise energy savings accrued through charging and discharging the battery. The second and third approach aims to balance the self-consumption of PV generation against increasing the energy savings accrued through charging and discharging the battery. By contrast, the fourth local approach flattens the residential load curve at the PCC, and in this way seeks to improve the voltage to reduce the occurrence of disconnections.

3.3.1 Customer-Focused CF-QP

The objective function of the CF-QP is designed to increase economic savings that accrue to residential battery owners whilst reducing battery cycling. Specifically,

$$\begin{aligned} \min_{u} \quad & \sum_{t\in\mathcal{T}} \omega(u(t))^2 + \eta(t)u(t)\Delta \\ \text{s.t.} \quad & (3.2) - (3.5), \end{aligned} \tag{3.7}$$

where ω is a weight designed to increase or reduce the importance of the battery cycling (first term in the objective function) and potentially reduce battery degradation. The second term in the objective function minimises the financial costs, i.e. maximises battery savings. The day-ahead time-of-use prices ($\eta(t)$ for all $t \in \mathcal{T}$) is provided by the electricity retailer. Note that when battery cycling is disregarded (3.7) can be cast as an LP. This optimisation problem is also used in Chapter 4 as a benchmark approach to other optimisation problem proposed in this thesis.

3.3.2 Balanced B-QP

The objective function of the B-QP is designed to balance increases in economic savings that accrue to residential battery owners against promoting the self-consumption of solar PV. Specifically, as proposed in [Ratnam et al., 2016],

$$\begin{aligned} \min_{u,p} \quad & \sum_{t\in\mathcal{T}} \omega(p(t))^2 + \eta(t)u(t)\Delta \\ \text{s.t.} \quad & (3.1) - (3.5), \end{aligned} \tag{3.8}$$

where the grid power is weighted by ω. Here the first term is designed to reduce peak power flows of $p(t)$, and promotes the self-consumption of PV generation. The first term is balanced against the second term designed to increase economic benefits associated with battery storage scheduling.

3.3.3 Alternate Balanced AB-QP

Over-voltage conditions in distribution networks typically occur when PV generation output peaks [Jayasekara et al., 2014]. As such, we design the AB-QP with the same objective function as the B-QP, but modify the power balance equation constraint to emphasises the charging of the battery when PV generation peaks. Let $\hat{g}(t)$ be the processed PV generation defined as

$$\hat{g}(t) := -\frac{(g(t))^2}{\|g\|_\infty}, \qquad \forall t \in \mathcal{T}, \tag{3.9}$$

where $\|g\|_\infty := max_{t\in\mathcal{T}}|g(t)|$. Then define processed grid power by

$$\hat{p}(t) = d(t) + \hat{g}(t) + u(t). \tag{3.10}$$

Finally, define the local AB-QP optimisation problem as

$$\begin{aligned} \min_{u,\hat{p}} \quad & \sum_{t\in\mathcal{T}} \omega(\hat{p}(t))^2 + \eta(t)u(t)\Delta \\ \text{s.t.} \quad & (3.2) - (3.5), (3.10). \end{aligned} \tag{3.11}$$

This modification to the B-QP further decreases PV exports during *peak* solar production, preventing over-voltage disconnection of DER inverters.

3.3.4 Grid-Focused GF-QP

The objective function of the GF-QP is designed to exclusively improve grid voltages by flattening the power curve measured at the PCC. Specifically,

$$\begin{aligned} \min_{u,p} \quad & \sum_{t\in\mathcal{T}} (p(t))^2 \\ \text{s.t.} \quad & (3.1) - (3.5). \end{aligned} \tag{3.12}$$

By reducing grid active power at the residence premises, the GF-QP approach potentially prevents voltage rise and thus economic losses caused by the frequent disconnection of inverters. Problem (3.12) is presented in the standard QP formulation in [Ratnam et al., 2015a].

3.4 Assessing the Benefits

In the numerical simulations that follow, the 13NF from [Kersting, 2001] represents the distribution network (see Fig. 3.2). The 13NF is the main distribution network model under consideration in this chapter [Kersting, 2001]. Due to its challenging configuration and electrical behaviour, the 13NF model is widely adopted in the power engineering research community [Dobbe et al., 2020; Islam et al., 2019; Joo et al., 2017; Niazazari and Livani, 2017].

This test feeder is comprised of both overhead and underground line segments, single-, two- and three-phase nodes and line segments, shunt capacitor banks and other components. The 13NF also presents negative mutual impedance in some line segments, meaning that voltage rise in one phase can contribute to significant voltage drop in another phase [Arnold et al., 2016]. All these characteristics of the 13NF, along with the fact that it is highly loaded and unbalanced, makes it a very challenging network in terms of voltage and power flow regulation. In other words, proposed optimisation and control approaches are really challenged by testing with the 13NF.

We replace the original spot loads with aggregated residential systems.

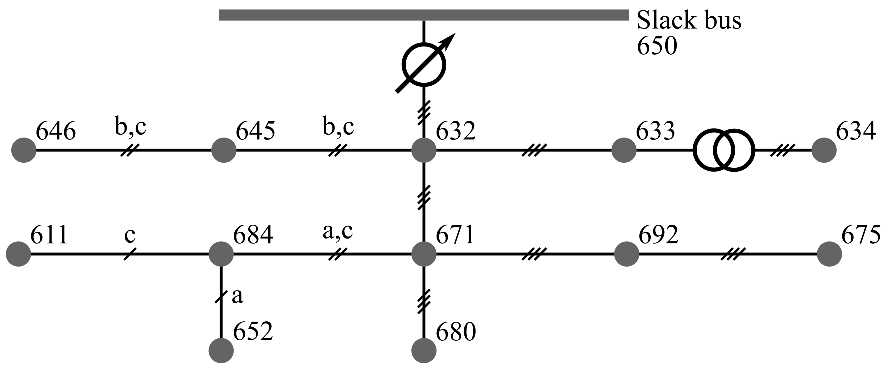

Figure 3.2: Diagram of IEEE 13-Node Test Feeder (13NF).

Real time-varying data from the Next Generation (NextGen) Energy Storage program at the ACT, Australia, is used for residential loads and solar PV generation [Shaw et al., 2019]. A clean NextGen dataset was obtained using the cleaning process presented in [Shaw et al., 2019], which excised both errors and customers with anomalous data. The cleaning process resulted in a 100-customer dataset for the entire year of 2018, which is used in this study. It is worth mentioning that each one of the 100 customers has their own solar PV system with a tailored power capacity.

Customers from this clean dataset were aggregated at each of the node on each phase (i.e., each point where there were a spot load in the 13NF) until the aggregated peak load reached approximately the original spot load value (in kW). A total of 1503 customers were connected to the 13NF, each one represented by the residential system shown in Fig. 3.1, although not all customers considered have a battery storage. To reach 1503 customers from the dataset, we repeated the selection of the 100 customers.

To calculate the unbalanced three-phase power flow for each t interval, residential loads, PV generation and battery power are represented by constant load (P) model. Solar PV and battery are considered to operate at unity power factor, whereas the load demand $d(t)$ power factor is considered to be equal to the respective original spot load of the 13NF. It is worth mentioning that the tap positions of the voltage regulator transformer is fixed at the original positions throughout the numerical simulations.

Each QP optimisation is executed at the beginning of each day (midnight) to obtain the day-ahead battery charge and discharge profile. With the exception of the CF-QP, each approach requires a day-ahead forecast of the load and the PV generation, which we emulated as per [Ratnam et al., 2016]. PV and battery inverters are configured to disconnect when voltage exceeds 1.10 p.u. as in [Sayeef et al., 2012; Tonkoski et al., 2012]. Batteries are allocated proportionally to the number of customers connected at each node. The max-

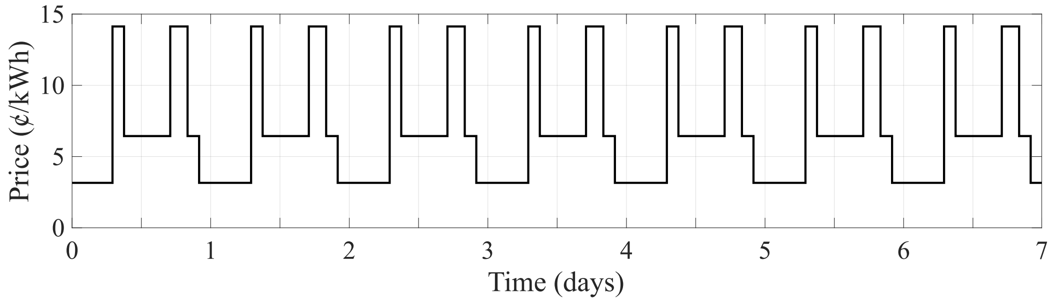

Figure 3.3: TOU tariff for an entire week.

imum continuous power of the battery is considered to be 5 kW for both charging and discharging ($\underline{u} = \overline{u} = 5$) and the energy capacity $\overline{s}$ is 10 kWh. To prevent an energy-shifting bias, both the initial and final charge level are selected as 2 kWh ($s_0 = s_f = 2$). However, note that s_0 is selected only at the beginning of the first day of the simulated week, whereas on the following days s_0 will be automatically updated to the battery charge level at midnight. Although the battery is scheduled to achieve s_f at the end of each day, it will not necessarily be s_f, since over-voltage disconnections will shutdown the battery for the duration of the over-voltage.

Load $d(t)$ and PV generation $g(t)$ data are 5 minutes average power flows, $\Delta = 5/60$ hour, the time window $T\Delta$ is 24 hours, and thus $T = 288$. The TOU tariff $\eta(t)$ is based on an Australian distributor that serves the de-identified customers from the NextGen dateset [Shaw et al., 2019; Evoenergy, 2019]. Specifically, $\eta(t) = 0.03154$ for $t = \{1, ..., 84, 265, ..., 288\}$ (*off-peak* price from midnight to 7 am and from 10 pm to midnight), $\eta(t) = 0.06438$ for $t = \{109, ..., 204, 241, ..., 264\}$ (*shoulder* price from 9 am to 5 pm and from 8 pm to 10 pm) and $\eta(t) = 0.14131$ for $t = \{85, ..., 108, 205, ..., 240\}$ (*peak* price from 7 am to 9 am and 5 pm to 8 pm). Fig. 3.3 illustrates these prices in cents/kWh over a week.

We prioritise increases in economic savings over other objectives when assigning the optimisation weights ω. That is, we carefully select $\omega = 10^{-5}$ for the CF-QP and $\omega = 10^{-4}$ for the B-QP and AB-QP. In this way, these weights work as bias factor to improve battery charge and discharge scheduling. Although these values seem too small, it is important to note that the savings term in the objective function is intrinsically multiplied by small values such as $2.6 \cdot 10^{-3}$, due to small η and Δ values. To further adjust the depth of battery cycling and potentially increase battery lifespan [Martins et al., 2022; Vonsien and Madlener, 2020], the ω value in CF-QP can be tuned up over time according to the preference of the customer.

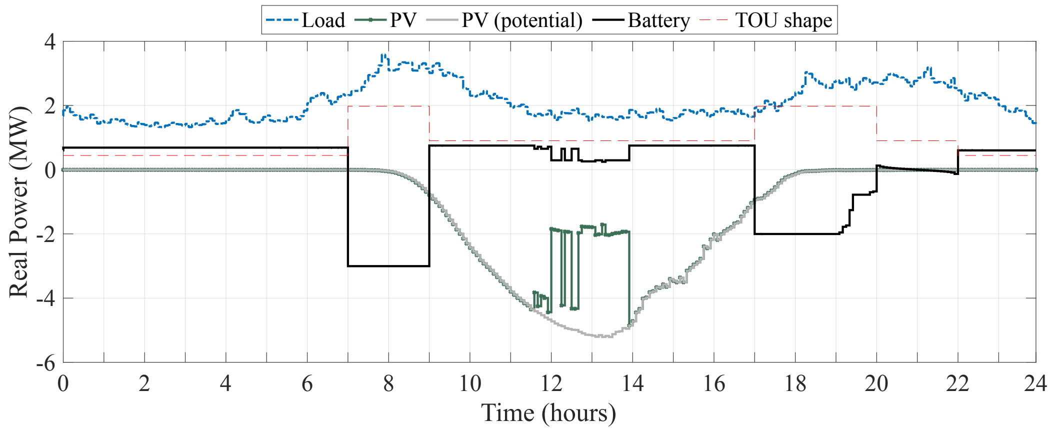

Figure 3.4: Network aggregate residential load, PV, and battery power. All battery storage are running the CF-QP. PV (potential) corresponds to the absence of inverter over-voltage disconnections.

3.4.1 Case Study

We consider data from 21-27 July 2018, a sequence of sunny days corresponding to PV generation peaks on the distribution network. A total of 601 residential customers (40% of customers) on the 13NF owns a residential battery storage. The feeder-level aggregated load, PV generation and battery power are shown in Fig. 3.4 for the last day (27 July 2018), with all batteries implementing the CF-QP approach.

In Fig. 3.4, observe the battery storage discharging (providing power) during the morning and evening peak pricing periods. The charging occurs overnight during the off-peak pricing period and also during the shoulder pricing period (between the morning and evening peak). As the CF-QP approach does not consider load and PV generation data, battery storage scheduling results in a flat power value for each pricing period. We also observe sharp variations on the aggregated PV and battery power due to inverter disconnections when voltages exceed 1.10 p.u. Note that disconnection of inverters occurs during peak PV generation combined with low demand, mainly shortly after 12 o'clock.

Fig. 3.5 presents simulation results for the entire week for each of the four local QP approaches. In Fig. 3.5(a) we note that many residential inverters are switched off for considerable intervals, specially on the fifth day. Simulation results for B-QP and AB-QP are presented in Fig. 3.5(b) and (c), respectively. We observe that both approaches reduce the disconnection of inverters. Also, with the AB-QP approach we observe no major disconnection of inverters on the last day, suggesting further improvement in supply voltages. In Fig. 3.5(d) we observe the GF-QP does not reduce over-voltage disconnection further,

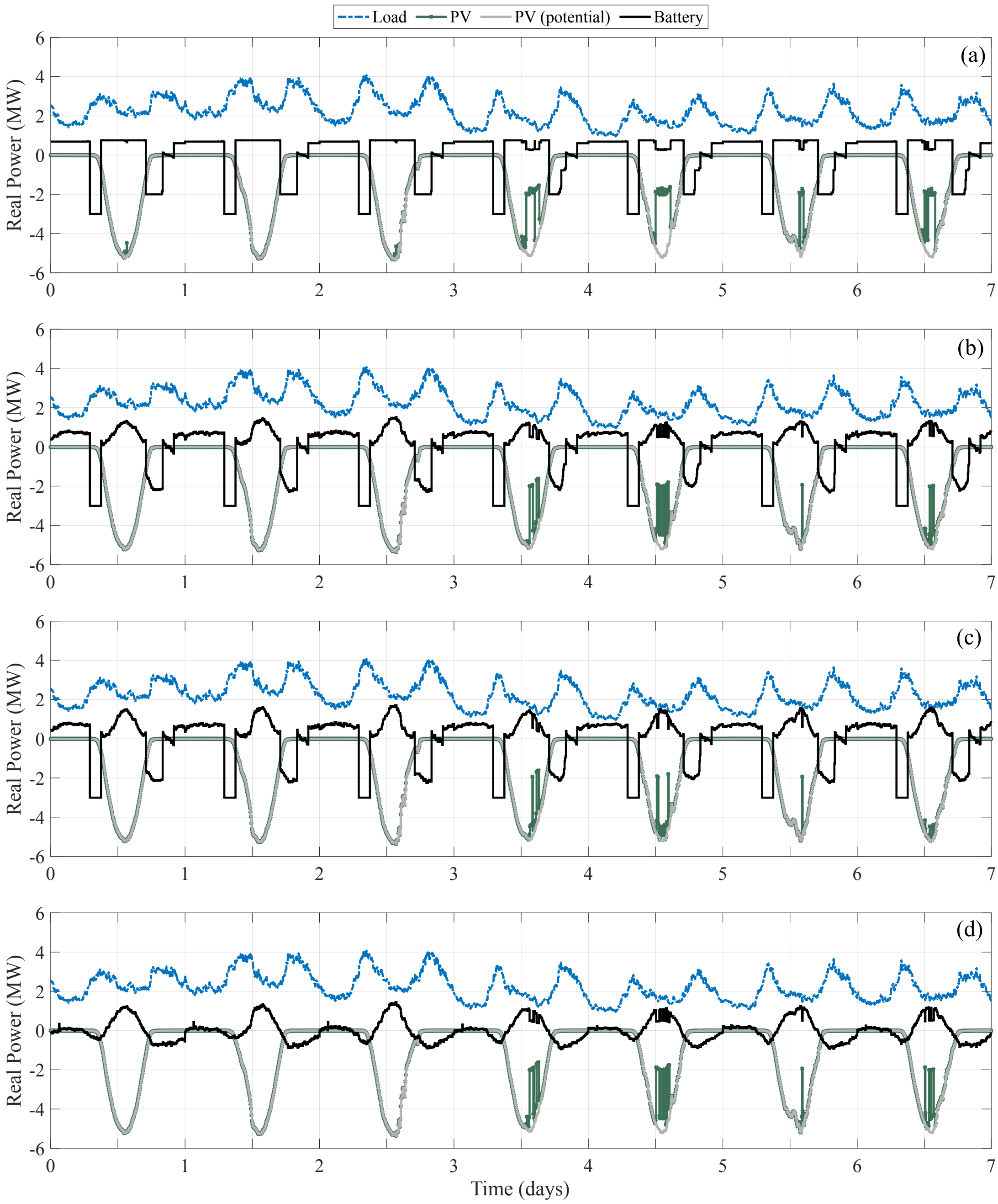

Figure 3.5: Network aggregate residential load, PV, and battery power corresponding to (a) CF-QP; (b) B-QP; (c) AB-QP; and (d) GF-QP.

when compared to the AB-QP approach.

Table 3.1 presents the average savings per customer accrued in the simulated week. PV savings represent the average savings accrued per solar PV customer (1503 customers), computed by Γ_g in (3.6) over the entire week. Bat-

Table 3.1: Average savings accrued per customer[1].

	CF-QP	**B-QP**	**AB-QP**	**GF-QP**
PV savings	\$7.86	\$8.45	\$8.67	\$8.36
Battery savings	\$12.60	\$12.73	\$12.90	\$2.34

tery savings represent the average savings accrued per battery customer (601 customers), computed by Γ_u in (3.6) over the entire week. It is worth mentioning that the potential PV generation across the week is the same for all four cases, so increases in PV savings corresponds to a reduction in PV inverter disconnections caused by over-voltage.

In Table 3.1, we observe that AB-QP, by improving grid supply voltages, increases the customer solar PV savings. In comparing the CF-QP to the GF-QP approach, we observe GF-QP improves PV savings, however, the battery savings are drastically reduced. Recall that the objective of the CF-QP battery scheduling approach is to increase savings customers with battery storage accrue. However, we observe inverter disconnection results in reduced battery savings (when compared to B-QP and AB-QP). Furthermore, the battery savings are greater for the AB-QP approach, suggesting an appropriate balance between improving grid voltage and earnings for battery owners.

Fig 3.6 presents the savings accrued in the week for each customer. In Fig 3.6(a) we observe that some battery owners enjoyed higher earnings than others, although all batteries were scheduled to accrue the exact same savings under the same TOU tariff. The variation in customer savings is attributed to the customer location in the 13NF, that is, voltage rise occurs more frequently on some nodes and thus customers experience more frequent inverter disconnections. Customers more affected by over-voltage disconnection are mainly connected at nodes at the end of the feeder and on phases in which the tap position is higher. Nodes 675 and 611 contain shunt capacitors connected and are specially affected by voltage rise during high PV generation. It can be seen in Fig 3.6(b) and (c) that B-QP and AB-QP have a similar distribution of savings, although AB-QP enables customers to accrue more earnings. In Fig 3.6(d) we observe that the majority of battery owners accrued just a few dollars in the week. Furthermore, we observe cases where battery storage

[1]In Table 3.1, saving values are shown as the amount accrued during 21-27 July 2018 period only. Note that if a similar over-voltage disconnection pattern repeats over that year, the average difference between AB-QP and GF-QP, for instance, would have been of \$565, considering a single customer with both PV and battery storage.

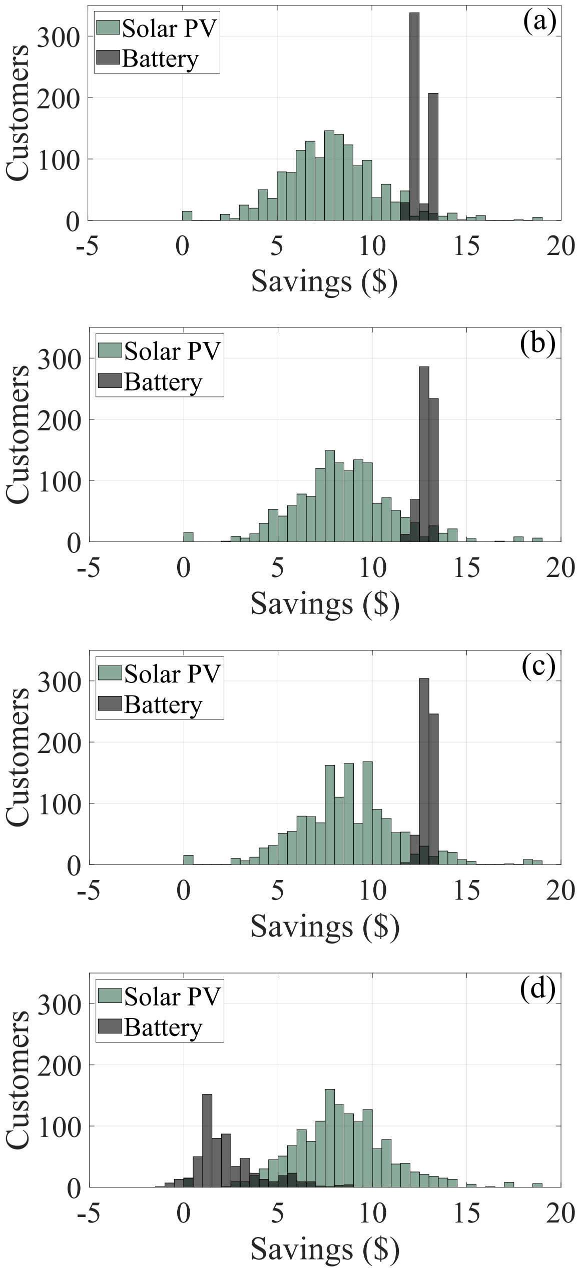

Figure 3.6: Distribution of customer savings accrued in the week from PV generation and from battery storage: (a) CF-QP; (b) B-QP; (c) AB-QP; and (d) GF-QP.

scheduling corresponds to an economic loss for some customers[2].

In Fig. 3.7 we present average savings accrued in the same week for different proportions of customers with battery storage. In Fig. 3.7(a) we observe

[2]In this thesis, we do not further investigate such differences in financial savings as fairness is not the focus of investigation. Relevant work and discussions on this subject has recently been published and can be found in [Poudel et al., 2023] and other references therein.

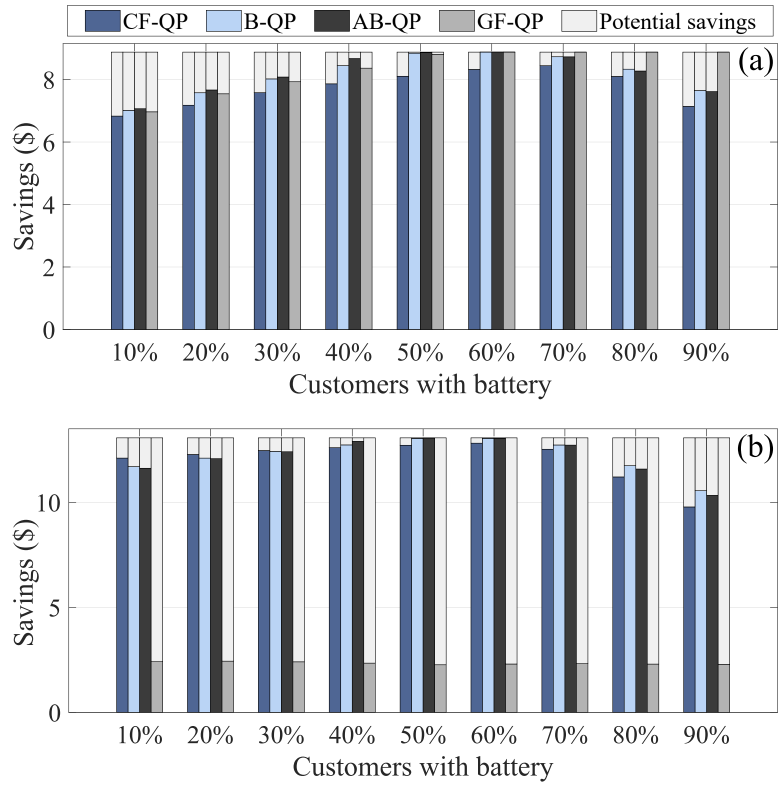

Figure 3.7: Average savings accrued in the week considering different percentage of customers with battery on the distribution network. (a) PV savings; and (b) battery savings.

that AB-QP battery scheduling provides moderately higher savings from PV generation until we reach 60% of customers with battery storage. When 50% and 60% of customers install battery storage, AB-QP prevents all cases of over-voltage disconnection for PV inverters. In the context of total earnings (from PV and battery storage) for all customers in the network, AB-QP provides higher savings until we reach 60% of customers with battery storage.

We observe in Fig. 3.7(b) that for low percentages of customers with battery storage, CF-QP provides higher savings for battery owners than the other approaches. Here, the population of battery storage is not significant enough to prevent widespread over-voltage disconnections. In Fig. 3.7(b) we also observe the average earnings from battery for the GF-QP approach is low for all percentages of battery populations, suggesting that the distributor would be required to incentivise such an approach.

GF-QP battery scheduling considers only grid power to and from the PCC of the residential system. As such, this optimisation does not necessarily assist grid voltages if customer is not contributing to the general demand profile of the distribution feeder. Battery scheduling approaches that directly consider customer savings according to TOU tariffs, at times improve the general demand profile of the feeder. Accordingly, at times, voltages across the feeder are potentially improved with price-based schemes, reducing inverter disconnection attributed to voltage-rise.

From the case study we observe that, except for GF-QP, customer savings decrease once the battery population reaches 70% – attributed to more frequent over-voltage inverter disconnections on the grid. With battery populations of 70% or more, the morning discharge of battery storage becomes significant, which creates voltage rise and resulting in the disconnection of inverters. Incapable of fully discharging energy in the early morning, batteries have limited room to charge from solar PV during daylight, resulting in further disconnections.

3.4.2 Analysis of Charging and Discharging Efficiency on Financial Benefits

When considering the TOU tariff in the optimisation problem, we observe batteries perform two cycles on each day. In the first cycle, a residential battery charges overnight with the off-peak price (0.03154 $/kWh) and discharges in the morning under the peak price (0.14131 $/kWh). In the second cycle, the battery charges during the day under the shoulder price (0.06438 $/kWh) and discharges during the evening peak price (0.14131 $/kWh). As such, the maximum savings for our battery of 5kW and 10kWh can be calculated as: $-0.03154 \cdot 10 + 0.14131 \cdot 10 - 0.06438 \cdot 10 + 0.14131 \cdot 10$, which amounts to \$1.867 per day.

Now consider a battery storage with 90% round-trip efficiency – 95% charging efficiency and 95% discharging efficiency [Tesla, 2024]. To charge 10kWh in the battery storage, it is required an amount of $10/0.95 = 10.526$ kWh. Then the energy the battery is able to deliver back to the grid is $10 \cdot 0.95 = 9.5$ kWh. The maximum savings in this case is computed as: $-0.03154 \cdot 10.526 + 0.14131 \cdot 9.5 - 0.06438 \cdot 10.526 + 0.14131 \cdot 9.5$, which amounts to \$1.675 per day. The amount of savings is approximately 90% of the savings considering full efficiency.

Battery technologies are getting more affordable and efficient over the years, allowing even further financial and grid benefits. This chapter focused on the financial impact of DER disconnection considering different optimisation approaches. Further details on the impact of charging and discharging efficiency on financial savings is presented in [Vonsien and Madlener, 2020].

Another important aspect to note is the influence of the difference between high and low electricity prices on customer profits. The difference between charging and discharging prices dictates the financial benefits provided by the battery. In case price goes negative during day-time solar production in our simulations scenarios, the customer would accumulate savings while charging the battery, rather than paying for it, and further increase overall revenue.

3.5 Conclusions

The AB-QP optimisation results in fewer over-voltage disconnection cases until 60% of battery penetration on the grid. After that level, batteries themselves start causing over-voltage disconnection of inverters due to significant combined discharging power. At battery integration levels beyond 60%, only the fourth approach, named GF-QP, continues to improve grid voltages and preventing inverter disconnections. However, the GF-QP approach results in much lower savings for customers, with some experiencing financial losses, since batteries are dispatched without considering the TOU tariff.

Different approaches presented better results for different penetration levels of residential battery. Whilst some approaches improve disconnections and savings when the number of batteries are low, others reduce disconnections only when a great number of batteries are connected to the grid. These results suggest that more effective use of controllable DERs to regulate grid voltages are needed.

In this chapter, the network model is not regarded within optimisation problems. That is, optimisation-based approaches are *network-agnostic* in the sense that they do not require any information from the specific grid the residential systems are connected to. Rather, approaches take into account only real power measurements of each element in the residential system and seek to improve grid voltages by proxy, i.e., by improving their own *real* power profile.

Both solar PV and battery inverters have the potential to inject or sink *reactive* power. Reactive power is not as effective for voltage regulation in distribution as in transmission networks. Nevertheless, knowing the R/X ratio and the actual voltage magnitude of the grid, the readily available resource can be carefully controlled to complement real power control. The impedance characteristic of the network mathematically describes how effective real and reactive power are to regulate grid voltages; and proper control of reactive power can further improve voltage regulation and even grid power losses.

This work motivates the development and proposal of more sophisticated *network-cognisant* approaches to control DERs. In the next chapter, we propose a local QP that includes reactive power control as well as the impedance characteristic of the network and grid voltage measurements.

Chapter 4

Local Network-Cognisant Approach: Optimisation-Based Control of Real and Reactive Power of DERs

Voltage regulation is one of the most urgent issues in distribution networks with high penetration levels of DERs. Small-scale behind-the-meter battery storage is a key element in effectively overcoming such a challenge, while offering financial benefits for customers.

In this chapter, we propose an optimisation-based approach for controlling power from battery storage for grid support and customer savings, considering only local (behind-the-meter) measurements. The proposed approach takes into account the physics of the grid and both real and reactive power (coupled) for voltage regulation and grid loss reduction. The proposed optimisation-based control, termed local quadratic program (L-QP), is formulated based on linear power flow equations (LinDistFlow).

The proposed L-QP in this chapter is benchmarked against an approach in which real power is used to maximise the customer benefit, as the CF-QP in Chapter 3, while reactive power is dedicated for voltage regulation. Numerical simulations with the 13NF and 123NF demonstrate the technical advantages of the proposed optimisation-based control.

This chapter fully describes the paper presented in [de Carvalho et al., 2023]. The author of this thesis has opted for keeping most of the original structure of the paper in order to preserve coherence and clarity. This chapter is organised as follows: In Section 4.1, we introduce the specific context and problem being addressed in this chapter. The LinDistFlow equations together with the residential system are introduced in Section 4.2. We derive grid voltage and resistive loss equations, and formulate the L-QP approach in Section 4.3. Numerical simulations follow in Section 4.4. Section 4.5 concludes this chapter with important remarks that also motivate the next chapter.

List of Main Symbols – Chapter 4

c	Customer index
C_m	Total number of customers at node m
$\mathcal{C}_m$	Set of customers at node m
d_m^c	Real power of residential load
e_m^c	Reactive power of residential load
E_m	Voltage deviation at node m relative to the reference
E_t	Voltage deviation threshold
$\hat{E}_m^c$	Extended voltage deviation of customer c at node m
$\overline{E}_m^c$	Voltage regulation capacity of customer c at node m
$\boldsymbol{E}$	Voltage deviation vector over nodes
$\mathcal{E}$	Set of all line segments on the network
g_m^c	Real power of solar PV
I_{mn}	Current magnitude in line segment (m, n)
L_m	Resistive power losses in the path $\mathcal{L}_m$
L_m^c	Resistive power losses related only to residential system c
$\mathcal{L}_m$	Set of line segments in the unique path from node 0 to node m
N	Total number of nodes downstream of the slack bus
$\mathcal{N}_o$	Set of all nodes on the network defined as $\{0, 1, ..., l, m, n, ..., N\}$
$\mathcal{N}$	Set of downstream nodes defined as $\{1, ..., l, m, n, ..., N\}$
p_m^c	Real power consumption of residential system
P_m	Aggregate real power consumption at node m
P_{mn}	Real power flow in line segment (m, n)
$\widetilde{P}_{mn}$	Real power flow in line segment (m, n) not delivered to customer c
$\boldsymbol{P}$	Real power consumption vector over nodes
q_m^c	Reactive power consumption of residential system
Q_m	Aggregate reactive power consumption at node m

Q_{mn}	Reactive power flow in line segment (m, n)
$\widetilde{Q}_{mn}$	Reactive power flow in line segment (m, n) not delivered to customer c
$\boldsymbol{Q}$	Reactive power consumption vector over nodes
r_{mn}	Resistance of line segment (m, n)
R_{mm}	Resistance (multiplied by 2) of the unique path from node 0 to m
$\boldsymbol{R}$	Resistance matrix
s_m^c	Charge level of battery storage of customer c at node m
s_0	Initial charge level of battery storage
s_f	Final charge level of battery storage
$\bar{s}$	Energy capacity of battery storage
t	Discrete time index
T	Total number of time steps in the horizon
$\mathcal{T}$	Set of discrete time defined as $\{1, 2, ..., t, ..., T\}$
u_m^c	Real power of battery storage (controllable power)
$\overline{u}$	Maximum charging rate (absorbing power) of battery
$\underline{u}$	Maximum discharging rate (providing power) of battery
v_m^c	Reactive power of battery storage (controllable power)
$\overline{v}$	Maximum absorption of reactive power
$\underline{v}$	Maximum supply of reactive power
V_m	Voltage magnitude at node m
V_t	Voltage magnitude threshold
V_r	Reference voltage magnitude
x_{mn}	Reactance of line segment (m, n)
X_{mm}	Reactance (multiplied by 2) of the unique path from node 0 to m
$\boldsymbol{X}$	Reactance matrix

α_m^c	Extension (or gain) coefficient
Γ_m^c	Energy savings provided by battery storage for customer c at node m
Δ	Time length of a time interval
ζ	Design parameter of optimisation problem
η	Electricity price
σ	Design parameter of optimisation problem
Ψ	Energy costs

4.1 Introduction

The dramatic increase of solar PV penetration in recent years has caused significant challenges for distribution network operators. High rooftop PV generation combined with low power demand can result in reverse power flow along line segments and an unacceptably high grid voltage. Significant voltage rise can limit customer-owned solar PV generation and, in turn, potentially reduces financial saving that a PV customer accrues [Palmintier et al., 2016]. Among different measures to mitigate voltage issues posed by distributed PV, including grid reinforcement or the installation of on-load tap changing transformers, are increasingly affordable battery storage solutions. Residential-scale battery storage that charges when solar generation is in excess, potentially reduces grid voltage deviations at the source of the problem [AEMO, 2020a].

Approaches to charge and discharge residential-scale battery storage are typically designed to solely provide financial benefits to the battery owner [Petrou et al., 2018]. However, purely economic-based methods do not consider the local impact on the grid voltage [Procopiou et al., 2020]. To improve voltages, it is also possible to inject/absorb inverter-based reactive power from residential battery systems [Smith et al., 2011]. However, using reactive power alone can lead to unsatisfactory voltage regulation with excessive power losses in the distribution network. Decoupling real power for customer economic-benefit and reactive power for voltage regulation, while sensible in transmission networks, has fundamental limitations in distribution grids. The higher resistance over reactance (R/X) ratio of lines in the distribution realm couples both real and reactive power flows to over-voltage or under-voltage conditions, limiting the long-term applicability of the aforementioned decoupled approaches [von Meier et al., 2020].

Several papers in the literature have proposed new approaches for controlling real and reactive power of residential battery systems for both grid and customer benefit. An optimisation-based approach is proposed in [Ranaweera et al., 2017] to use real power from the battery for customer financial benefit, while promoting charging during the peak PV generation period. When the grid voltage exceeds a threshold, both real and reactive power from the battery are dispatched to drive the grid voltage closer to the nominal voltage. In [Hashemi and Østergaard, 2018] the reactive power is constantly dispatched for voltage regulation, while real power is reserved for correcting voltage excursions beyond a nominal threshold. The authors in [Hashmi et al., 2020] propose a method to dispatch real power from the battery to maximise customer financial savings, while reactive power is reserved for power factor correction of the residential system. A variety of rule-based approaches for real and reactive power dispatch have been proposed and compared in [von Appen et al., 2014] to provide customer benefit and grid voltage regulation.

Due to the limited efficacy of reactive power for voltage regulation in distribution networks, other studies [Ratnam et al., 2016; Yao et al., 2016; Procopiou et al., 2019; Wang et al., 2016; Zeraati et al., 2018] have focused only on dispatching real power, i.e. charging/discharging battery storage. Several behind-the-meter optimisation-based approaches have been proposed in the previous chapter and in [Ratnam et al., 2016] to reduce real power imports/exports from/to the grid while considering customer savings. The authors in [Yao et al., 2016; Procopiou et al., 2019] propose to use the real power of the battery to improve grid voltages alongside customer benefit. However, in [Yao et al., 2016] the proposed optimisation-based approach includes an additional cost when real power exports exceeds a threshold, whereas in [Procopiou et al., 2019] a time-based approach is proposed to prevent overvoltage by charging the battery proportional to the amount of PV generation. In [Wang et al., 2016; Zeraati et al., 2018] real power is dispatched for grid voltage regulation, disregarding the benefits provided for the battery owner.

Although reactive power for voltage regulation in the distribution grid is not as effective as in the transmission network, it can still contribute to improve grid voltages and reduce grid power losses. Ultimately, it is the grid impedance characteristic that determines how effective real and reactive power is to regulate grid voltage and the impact on grid power losses. It follows that the authors in [Cavraro and Carli, 2018; Molzahn et al., 2017; Joo et al., 2017; Antoniadou-Plytaria et al., 2017; Sankur et al., 2016, 2018; Arnold et al., 2016] have described centralised and distributed approaches to dispatch real and reactive power from DERs, which incorporate network models that capture the relationship of grid impedance to grid voltages and power losses. However, a key challenge that exists is to capture such a relationship with a formulation that considers only local (behind-the-meter) measurements, which are fast-acting to system variability, robust to communication failures, and privacy preserving [Antoniadou-Plytaria et al., 2017]. This motivates us to consider more directly the impedance characteristic of the electrical network in the formulation of a local optimisation problem.

In this chapter, we propose a local optimisation-based approach for controlling residential battery storage. The optimisation problem incorporates both real and reactive power (coupled) for grid voltage regulation and grid power loss reduction. The formulation is based on the impedance characteristics of the network, which fundamentally dictates the relation of real and reactive power with grid voltages and losses. Specifically, the proposed optimisation-based approach, labelled L-QP, incorporates a linearised model of the distribution grid power flow equations (i.e., LinDistFlow) together with behind-the-meter (local) voltage and power flow measurements. The optimisation objective is to increase the customer financial benefits, while improving grid voltages and power losses.

The contributions of this chapter are: (i) the derivation of an equation with both real and reactive power coupled for voltage regulation considering only behind-the-meter variables; (ii) the derivation of mathematical terms to express grid resistive power losses using only behind-the-meter variables; and (iii) the formulation of a local optimisation-based approach for behind-the-meter battery storage operation that seeks to minimise grid voltage deviations, grid resistive losses and customer electricity billing costs. Importantly, the derivation of (i) and (ii) culminate in the proposed local optimisation problem (iii). Contributions (i) and (ii) can underpin other applications, including the design of new tariff structures for individual customers.

We benchmark our proposed L-QP algorithm against an alternative approach similar to CF-QP that also ingresses local measurements, however, separates real power for maximising customer savings and reactive power for voltage regulation. Numerical simulations are carried out with challenging distribution test feeders and with actual time-varying data for residential load and PV generation [Shaw et al., 2019].

4.2 Preliminaries

Consider a single-phase radial distribution network modelled as a connected graph as in Fig. 4.1. The set of nodes is denoted by $\mathcal{N}_o = \{0, 1, \ldots, N\}$, where 0 is the source node, also referred as slack or substation bus, and N is the total number of nodes downstream of node 0 (i.e. $|\mathcal{N}_o| = N + 1$). The set of edges is denoted by $\mathcal{E} \subseteq \mathcal{N}_o \times \mathcal{N}_o$, where edge $(m, n) \in \mathcal{E}$ represents a line segment from node m to node n. The distribution network can then be represented by the graph $\mathcal{G} = (\mathcal{N}_o, \mathcal{E})$. We more often refer to the set of nodes downstream of node 0, denoted by $\mathcal{N} = \mathcal{N}_o \backslash \{0\}$.

In Fig. 4.2 we present our distribution network and residential system notation. Denote a set of customers by $\mathcal{C}_m = \{1, \ldots, c, \ldots, C_m\}$ connected to each node $m \in \mathcal{N}$. The voltage magnitude at node m is denoted by V_m and the impedance of the edge $(m, n) \in \mathcal{E}$ is represented by $r_{mn} + jx_{mn}$, where r_{mn} is the resistance and x_{mn} is the reactance of the line segment. Variable P_{mn} is the real power and Q_{mn} is the reactive power flow in the edge (m, n). Whereas P_m and Q_m is the *aggregate* real and reactive power consumption, respectively, at node m, consistent with the positive load convention. For a customer c connected to node m, p_m^c denotes the real power and q_m^c denotes the reactive power consumption, with positive load convention. The relationship of

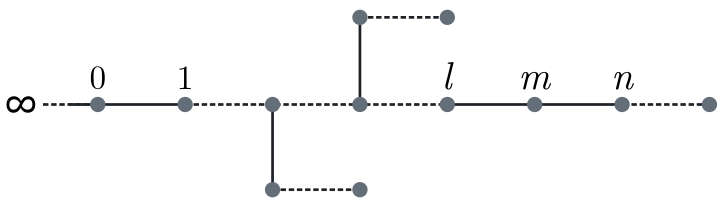

Figure 4.1: Distribution network modelled as a connected graph. Node 0 is the source node, also referred as slack or substation bus, and l, m, n are indices used to represent nodes and line segments.

aggregate power consumption to customer power consumption is given by

$$P_m = \sum_{c \in \mathcal{C}_m} p_m^c, \quad Q_m = \sum_{c \in \mathcal{C}_m} q_m^c, \tag{4.1}$$

for all $m \in \mathcal{N}$. Throughout, V_m^2 is referred to as voltage magnitude squared. Further, we refer to the deviation of the voltage magnitude squared relative to node 0, denoted by $E_m = V_0^2 - V_m^2$, by simply *voltage deviation*. Note that a positive voltage deviation ($E_m > 0$) represents a voltage drop between the nodes, whilst a negative voltage deviation ($E_m < 0$) represents voltage rise between the nodes.

As in [Farivar et al., 2012; Baran and Wu, 1989a], the DistFlow power flow equations to model the distribution network are as follows:

$$P_{lm} = r_{lm} I_{lm}^2 + P_m + \sum_{n:(m,n) \in \mathcal{E}} P_{mn}, \tag{4.2}$$

$$Q_{lm} = x_{lm} I_{lm}^2 + Q_m + \sum_{n:(m,n) \in \mathcal{E}} Q_{mn}, \tag{4.3}$$

$$V_l^2 = V_m^2 + 2 r_{lm} P_{lm} + 2 x_{lm} Q_{lm} - (r_{lm}^2 + x_{lm}^2) I_{lm}^2, \tag{4.4}$$

for all $(l, m) \in \mathcal{E}$ in the distribution circuit, where I_{lm} is the current magnitude of line segment (l, m). The DistFlow equations to model radial distribution networks are complex and originally non-linear. Optimisation problems with such a model are cast as a non-convex problem, which presents poor scalability and solving efficiency and cannot guarantee the global minimiser Borrelli et al. [2017].

The higher order, non-linear terms associated with current in (4.2)-(4.4) are typically orders of magnitude smaller than other terms and can be neglected to result in a linear power flow model [Turitsyn et al., 2010a]. The linear equations typically provide errors smaller than 1 per cent relative to its non-linear counterpart Farivar et al. [2013]; Turitsyn et al. [2010b]. The linear

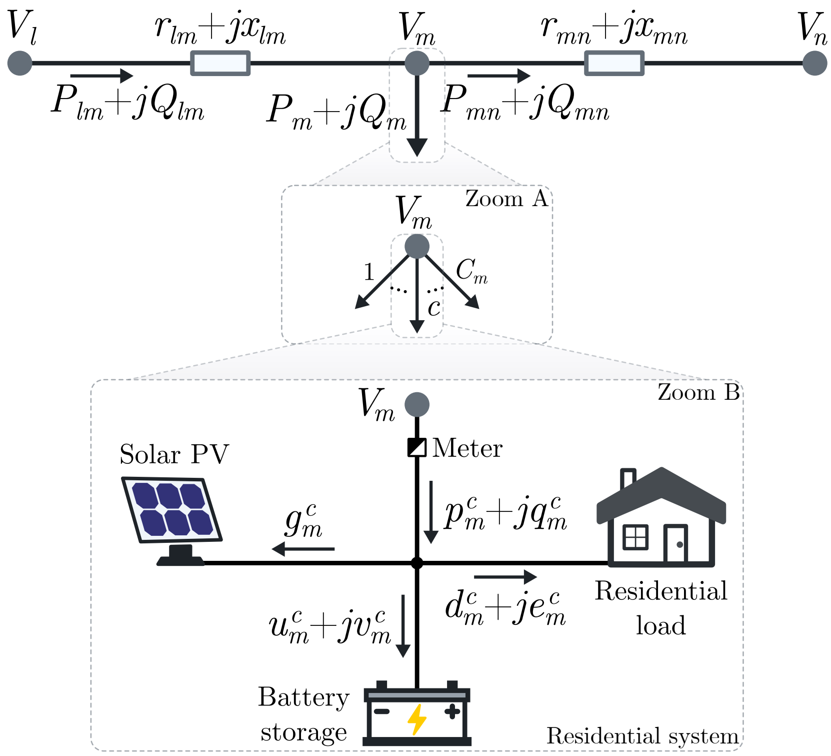

Figure 4.2: Distribution network serving residential systems. Arrows indicate the positive direction of power flow. Zoom A depicts the disaggregation of load P_m, Q_m, consisting of the load drawn by each customer in the set $\{1, \ldots, c, \ldots, C_m\}$, e.g., customer c draws load p_m^c, q_m^c. Zoom B depicts a residential system for customer c connected to node m. All customers prescribe to a time-of-use (TOU) pricing tariff with the net-metering policy.

model, called as LinDistFlow, with our notation in Fig. 4.2 are as follows:

$$P_{lm} = P_m + \sum_{n:(m,n)\in\mathcal{E}} P_{mn}, \quad \forall m \in \mathcal{N}, \tag{4.5}$$

$$Q_{lm} = Q_m + \sum_{n:(m,n)\in\mathcal{E}} Q_{mn}, \quad \forall m \in \mathcal{N}, \tag{4.6}$$

$$V_l^2 = V_m^2 + 2r_{lm}P_{lm} + 2x_{lm}Q_{lm}, \quad \forall (l,m) \in \mathcal{E}. \tag{4.7}$$

Such LinDistFlow equations are well established in the literature and are used to model the network within our control approach. Specifically, we are motivated to consider the LinDistFlow equations as they support the development of convex optimisation problems. The LinDistFlow equations assume negligible power losses in line segments, yet are able to model power networks with satisfactory accuracy and still approximate grid power losses [Lin and Bitar, 2018; Sankur et al., 2016, 2018; Arnold et al., 2016; Baran and Wu, 1989b].

We derive equations to represent power losses with the LinDistFlow in Section 4.3.

As in [Baran and Wu, 1989a; Lin and Bitar, 2018], define a path $\mathcal{L}_m \subseteq \mathcal{E}$ as the set of edges (line segments) on the unique path from node 0 to node m. Define matrices $\boldsymbol{R}, \ \boldsymbol{X} \in \mathbb{R}^{\mathrm{N}\times\mathrm{N}}$, such that elements in the matrices can be computed as:

$$R_{hk} = \sum_{(m,n)\in\mathcal{L}_h\cap\mathcal{L}_k} 2r_{mn}, \qquad X_{hk} = \sum_{(m,n)\in\mathcal{L}_h\cap\mathcal{L}_k} 2x_{mn}, \tag{4.8}$$

where $h, \ k \in \mathcal{N}$ represent the row and column index, respectively, of the matrices. Conceptually, the elements in the matrices $\boldsymbol{R}, \ \boldsymbol{X}$ represent the total resistance and reactance, respectively, of the path that is common for both nodes h and k. When $h = k$, R_{hh} is the summation of the resistance (multiplied by 2) of each line segment along the unique path from node 0 to node h. Likewise, X_{hh} is the summation of the reactance (multiplied by 2) of each line segment along the unique path from node 0 to node h.

The LinDistFlow equations are then written in compact form [Lin and Bitar, 2018] as follows

$$\boldsymbol{E} = \boldsymbol{RP} + \boldsymbol{XQ}, \tag{4.9}$$

where $\boldsymbol{E} = [E_1, \cdots, E_N]'$, $\boldsymbol{P} = [P_1, \cdots, P_N]'$, $\boldsymbol{Q} = [Q_1, \cdots, Q_N]'$. Note that all elements in the column vector $\boldsymbol{E}$ are voltage squared deviations relative to node 0 (e.g. $E_N = V_0^2 - V_N^2$). It is worth mentioning that (4.9) is formulated with nodal aggregate power, instead of line power flows as in (4.7).

4.2.1 Residential System

Fig. 4.2 depicts a residential system connected to node m for a customer $c \in \mathcal{C}_m$. The residential system includes a load, solar PV, and battery storage. The battery storage represents the controllable resource, whereas load and PV generation are considered uncontrollable resources. Although PV inverters are usually able to dispatch reactive power, in this study, for simplicity, the controllable reactive power (v_m^c) is provided by the battery inverter only.

Let $\mathcal{T} = \{1, 2, ..., t, ..., T\}$ be the steady-state discrete time set, where t is the discrete time index and T is the total number of time steps in the horizon. Denote by Δ the length of one time interval (i.e., $((t-1)\Delta, t\Delta)$), and compute the time horizon by $T\Delta$, where $[0, T\Delta]$ is the time window.

In Fig. 4.2, $p_m^c(t)$, $d_m^c(t)$, $g_m^c(t)$ and $u_m^c(t)$ represent average real power flows (in kW) across time interval $((t-1)\Delta, t\Delta)$. Similarly, $q_m^c(t)$, $e_m^c(t)$ and $v_m^c(t)$ denote average reactive power flows (in kvar) across time interval $((t-1)\Delta, t\Delta)$. The real and reactive power consumed by the entire residential system is represented by $p_m^c(t)$ and $q_m^c(t)$, respectively. The power flows from the grid to the residence are positive, whereas power flows from the residence exported to the grid are negative.

We represent real and reactive residential load by $d_m^c(t),\ e_m^c(t) \in \mathbb{R}_{\geq 0}$, $\forall t \in \mathcal{T}$, respectively, and $g_m^c(t) \in \mathbb{R}_{\leq 0}$, $\forall t \in \mathcal{T}$, represents the solar PV real power. The real and reactive battery power is denoted by $u_m^c(t)$ and $v_m^c(t)$, respectively, where positive power flows represent the battery absorbing power and negative power flows represent the battery generating power. The real and reactive power balance equations for the residential system, corresponding to Fig. 4.2, are:

$$p_m^c(t) = d_m^c(t) + g_m^c(t) + u_m^c(t), \tag{4.10}$$

$$q_m^c(t) = e_m^c(t) + v_m^c(t), \tag{4.11}$$

for all $t \in \mathcal{T}$. Next we consider a battery with charging and discharging constraints (in kW) given by

$$-\underline{u} \leq u_m^c(t) \leq \overline{u}, \quad \forall t \in \mathcal{T}, \tag{4.12}$$

where $\underline{u}$ is the maximum discharging constraint and $\overline{u}$ is the maximum charging constraint. The battery charge level $s_m^c(t)$ (in kWh) at time $t\Delta$ is given by:

$$s_m^c(t) = s_0 + \sum_{i=1}^{t} u_m^c(i)\Delta, \quad \forall t \in \mathcal{T}, \tag{4.13}$$

where s_0 is the initial charge level. The battery charge level is limited by the energy capacity $\overline{s}$ (in kWh) as:

$$0 \leq s_m^c(t) \leq \overline{s}, \quad \forall t \in \mathcal{T}, \tag{4.14}$$

We also restrict the charge level of the battery at the end of the time horizon by

$$s_m^c(T) = s_f, \tag{4.15}$$

where s_f is the final charge level (in kWh). The dispatchable reactive power v_m^c is constrained independently from the dispatchable real power u_m^c. In practice, this can be achieved by over-sizing the battery inverter or requesting reactive power from the PV system [Yao et al., 2016]. That is, v_m^c can represent the controllable reactive power from one or more inverter in a residential system. The dispatchable reactive resource is limited by

$$-\underline{v} \leq v_m^c(t) \leq \overline{v}, \quad \forall t \in \mathcal{T}, \tag{4.16}$$

where $\underline{v}$ is the maximum supply and $\overline{v}$ is the maximum absorption of reactive power (in kvar). This model where real and reactive power is limited separately can be interpreted as a linear square constraint as opposed to the traditional apparent power circle constraint. We consider that the square (regular 4-sided polygon) is inscribed in the circle, resulting in a feasible region and small errors. More detailed linear approximation of the apparent power circle constraint can be achieved with the n-sided polygon [Abadi et al., 2021]. We include the regular 8-sided polygon approximation in the work of Chapter 6.

Next, the customer of the residential system subscribes to the financial policy of net metering, where the customer is billed for energy consumption at the same rate as it is compensated for exported energy to the grid. With a TOU tariff η (in \$/kWh), supported by the net-metering policy, the cost of energy consumption (in \$) across one time interval $((t-1)\Delta, t\Delta)$ is defined by

$$\Psi_m^c(t) := \eta(t) p_m^c(t) \Delta. \tag{4.17}$$

With the net-metering policy, the corresponding financial savings provided by the battery across $[0, T\Delta]$ are shown in [Ratnam et al., 2015b] to be simply

$$\Gamma_m^c = -\sum_{t \in \mathcal{T}} \eta(t) u_m^c(t) \Delta. \tag{4.18}$$

That is, we consider the net-metering policy as in [Hashmi et al., 2020; Ratnam et al., 2015b], however, other policies and tariff structures are possible.

4.3 Problem Formulation

In this section we propose a local optimisation-based approach for scheduling day-ahead real and reactive power from a residential battery system. Our proposed L-QP approach is designed to enhance voltage regulation and reduce grid resistive losses, while increasing financial savings that accrue to a customer. This L-QP approach incorporates physics-based models of the grid, and relies on measurements collected at the customers premise (i.e., within the residential system as per Fig. 4.2).

In what follows we derive voltage deviation and power loss equations, which support the formulation of the L-QP optimisation problem. We seek mathematical expressions to identify the share of voltage deviation and grid power loss that can be allocated to a customer. We then include and minimise those expressions in local optimisation problems (individual for each residential system). To reduce notational overhead, we omit the time index (t) in the following equations.

4.3.1 Voltage Deviation Equations

Following on from (4.9), the voltage deviation at node m relative to node 0 can be written as:

$$E_m = \sum_{n \in \mathcal{N}} (R_{mn} P_n + X_{mn} Q_n), \tag{4.19}$$

where R_{mn} and X_{mn} are defined in (4.8). Next expand (4.19),

$$E_m = (R_{mm} p_m^c + X_{mm} q_m^c) + \sum_{\substack{i \in \mathcal{C}_m \\ i \neq c}} (R_{mm} p_m^i + X_{mm} q_m^i) + \sum_{\substack{n \in \mathcal{N} \\ n \neq m}} (R_{mn} P_n + X_{mn} Q_n).$$

and rewrite it as follows

$$E_m = E_m^c + E_m^C + E_m^N, \tag{4.20}$$

where

$$\begin{aligned} E_m^c &= (R_{mm} p_m^c + X_{mm} q_m^c), \\ E_m^C &= \sum_{\substack{i \in \mathcal{C}_m \\ i \neq c}} R_{mm} p_m^i + X_{mm} q_m^i, \\ E_m^N &= \sum_{\substack{n \in \mathcal{N} \\ n \neq m}} R_{mn} P_n + X_{mn} Q_n. \end{aligned}$$

Here E_m^c represents the voltage deviation attributed to customer c, E_m^C represents the voltage deviation attributed to other customers connected to the same node m, and E_m^N represents the voltage deviation attributed to other nodes along the circuit. (Note that (4.20) can be used as a voltage deviation allocation method and support a market-based operation of distribution networks.)

Next we denote by $\hat{E}_m^c$ the *extended voltage deviation*, which is defined by

$$\hat{E}_m^c := E_m^c + \alpha_m^c (E_m^C + E_m^N), \tag{4.21}$$

where $\alpha_m^c \geq 0$ is a parameter termed the *extension (or gain) coefficient*. If $\alpha_m^c = 1$, equation (4.21) is identical to (4.20). If $\alpha_m^c = 0$ the extended voltage deviation, $\hat{E}_m^c$, is representative of voltage deviation stemming from residential system c itself. It is worth mentioning that in distribution grids with many nodes and customers, voltage deviation caused by a single customer is much smaller than the combined voltage deviation associated with all other customers and nodes. Consequently, we approximate from (4.20) that

$$E_m \approx E_m^C + E_m^N. \tag{4.22}$$

We then approximate the extended voltage deviation, $\hat{E}_m^c$, by

$$\hat{E}_m^c \approx E_m^c + \alpha_m^c (E_m). \tag{4.23}$$

We then expand (4.23) as follows

$$\hat{E}_m^c \approx (R_{mm} p_m^c + X_{mm} q_m^c) + \alpha_m^c (V_0^2 - V_m^2). \tag{4.24}$$

Assuming the voltage at the substation, V_0, is known, and the impedance of the path, R_{mm} and X_{mm}, is also known, the extended voltage deviation $\hat{E}_m^c$ in (4.24) can be computed from measurements within the residential system c (i.e., from the measurement of p_m^c, q_m^c, and V_m) as per Fig. 4.2. Voltage V_0 in (4.24) can also represent the nominal voltage magnitude of the network.

The voltage deviation $(V_0^2 - V_m^2)$ in (4.24) encapsulates the impact of other customers, from everywhere in the network, on node m. In practice, such deviation can be much larger than the voltage regulation capacity of a residential battery system. In such cases, a large extension coefficient α_m^c (e.g. $\alpha_m^c = 1$) might result in voltage deviations beyond the battery capacity for voltage regulation, whereas a small extension coefficient (e.g. $\alpha_m^c = 0$) might result in insufficient voltage regulation from the battery system. As such, we design the gain coefficient α_m^c to scale voltage deviation to an appropriate size in the context of the regulation capacity of the residential battery system.

In what follows, we present our approach to designing the gain coefficient α_m^c. First, we define the *voltage regulation capacity* ($\overline{E}_m^c$) of a customer by

$$\overline{E}_m^c := (R_{mm}\overline{u} + X_{mm}\overline{v}). \tag{4.25}$$

Here $\overline{E}_m^c$ represents the extent that the battery is able to reduce the voltage (i.e. reduce voltage rise). In (4.25), we include the maximum real and reactive power limits of the battery, $\overline{u}$ and $\overline{v}$, respectively, and the network impedances R_{mm} and X_{mm}. Importantly, it is straightforward to represent the capacity of the battery to raise the voltage (e.g. in cases of steady-state voltage drop), by replacing $\overline{u}$ and $\overline{v}$ with $\underline{u}$ and $\underline{v}$, respectively, in (4.25). Next we define a *voltage deviation threshold* denoted by E_t,

$$E_t := V_r^2 - V_t^2, \tag{4.26}$$

where V_r is the nominal voltage magnitude of the distribution circuit and V_t is the voltage magnitude threshold. Specifically, the voltage magnitude threshold, V_t, represents either the maximum or the minimum voltage magnitude limit for the network, e.g., 1.10 or 0.90 p.u. Compute parameter α_m^c as

$$\alpha_m^c = \left| \frac{\overline{E}_m^c}{E_t} \right|. \tag{4.27}$$

Computing the extension coefficient as in (4.27) enables the battery to regulate the local grid voltage in accordance with its capacity $\overline{E}_m^c$.

Variable E_t is used in (4.27) to obtain the voltage regulation capacity as a fraction of the acceptable voltage deviation. Note that the absolute value of E_t in (4.26) represents the distance of the voltage threshold from the nominal value. As such, both $|1^2 - 1.10^2| = 0.21$ and $|1^2 - 0.90^2| = 0.19$ produce similar values.

4.3.2 Grid Resistive Power Loss Equations

Here we derive power loss expressions of a distribution circuit that can be computed by a customer using behind-the-meter measurements. It's worth mentioning that even though power losses are neglected in the LinDistFlow equations, it is still possible to approximate power losses with the linear equations as in [Baran and Wu, 1989b; Turitsyn et al., 2010a].

Let's consider the path $\mathcal{L}_m \subseteq \mathcal{E}$ connecting the substation bus to node m, where customer c is connected. The resistive power loss in the path $\mathcal{L}_m \subseteq \mathcal{E}$ can be calculated as

$$L_m = \sum_{(h,k) \in \mathcal{L}_m} r_{hk} I_{hk}^2, \tag{4.28}$$

where r_{hk} is the resistance of line segment (h,k) and I_{hk} is the current magnitude flowing in the line segment (h,k). The current magnitude can be written in terms of power and voltage, using the complex power equation, as in [Baran and Wu, 1989b],

$$L_m = \sum_{(h,k) \in \mathcal{L}_m} r_{hk} \frac{(P_{hk}^2 + Q_{hk}^2)}{V_h^2}. \tag{4.29}$$

During normal operation of distribution networks, the voltage magnitude of all nodes have to be maintained close to the nominal value. We approximate the resistive losses by assuming the voltage V_h^2 is approximately equal to the nominal ($V_h^2 \approx V_r^2$) [Baran and Wu, 1989b; Turitsyn et al., 2010a], yielding:

$$L_m \approx \frac{1}{V_r^2} \sum_{(h,k)\in\mathcal{L}_m} r_{hk}(P_{hk}^2 + Q_{hk}^2). \tag{4.30}$$

The power flow in line segment $(h,k) \in \mathcal{L}_m$ that is not delivered to customer c is given by

$$\widetilde{P}_{hk} = \sum_{\substack{i\in\mathcal{C}_m \\ i\neq c}} p_m^i + \sum_{\substack{n\in\mathcal{N}:\mathcal{L}_n\supseteq(h,k) \\ n\neq m}} P_n, \tag{4.31}$$

and similar for the reactive power ($\widetilde{Q}_{hk}$) that is not delivered to customer c. We now rewrite (4.30) as follows

$$L_m \approx \frac{1}{V_r^2} \sum_{(h,k)\in\mathcal{L}_m} r_{hk}\big((p_m^c + \widetilde{P}_{hk})^2 + (q_m^c + \widetilde{Q}_{hk})^2\big). \tag{4.32}$$

Next, expand and simplify (4.32), and rewrite the resistive power loss in the path $\mathcal{L}_m$ by

$$L_m \approx L_m^c + L_m^b + L_m^x, \tag{4.33}$$

where

$$L_m^c = \frac{R_{mm}}{2V_r^2}((p_m^c)^2 + (q_m^c)^2), \tag{4.34}$$

$$L_m^b = \frac{2}{V_r^2} \sum_{(h,k)\in\mathcal{L}_m} r_{hk}(p_m^c\widetilde{P}_{hk} + q_m^c\widetilde{Q}_{hk}),$$

$$L_m^x = \frac{1}{V_r^2} \sum_{(h,k)\in\mathcal{L}_m} r_{hk}(\widetilde{P}_{hk}^2 + \widetilde{Q}_{hk}^2).$$

Importantly, L_m^c is the resistive power loss related only to residential system c, whereas L_m^b and L_m^x incorporate the external customers and nodes. Assuming that R_{mm} and V_r are known parameters, L_m^c in (4.34) can be computed by customer c using behind-the-meter measurements (see Fig. 4.2). (Note that (4.33) can also be used as a power loss allocation method in distribution networks and support a market-based operation of the network.)

4.3.3 L-QP: Local Optimisation-Based Approach

To dispatch real and reactive power from the battery system we propose an optimisation-based control termed L-QP. Our L-QP objectives are threefold: (i) reduce energy costs for the customer; (ii) reduce grid voltage deviations; and (iii) reduce power losses on the electric grid. The optimisation problem is formulated to reduce these three terms across the entire time window $[0, T\Delta]$. Specifically, we formulate the L-QP optimisation problem by

$$\begin{aligned} \min_{\substack{u_m^c, p_m^c \\ v_m^c, q_m^c, \hat{E}_m^c}} \quad & \sum_{t \in \mathcal{T}} \eta(t) p_m^c(t)\Delta + \sigma(t)(\hat{E}_m^c(t))^2\Delta + \zeta(t) L_m^c(t)\Delta \\ \text{s.t.} \quad & (4.10) - (4.16), (4.24), \end{aligned} \tag{4.35}$$

where the first term in the objective function is $\Psi_m^c(t)$ as in (4.17), $\hat{E}_m^c(t)$ is as in (4.24), $L_m^c(t)$ is as in (4.34), and $\sigma(t)$, $\zeta(t)$ are design parameters. In more detail, $L_m^c\Delta$ represents the energy loss (in kWh) along the path $\mathcal{L}_m$ and Ψ_m^c is the cost of energy consumption for customer c at node m. Design parameters $\sigma(t)$, $\zeta(t)$ are selected to balance reductions in energy consumption cost against improvements in voltage regulation and reductions in grid power losses. Reductions in the Euclidean distance of the voltage deviation in either direction (e.g., voltage rise or drop) are regulated by the design of $\sigma(t)$, and reductions in grid power losses are regulated by the design of $\zeta(t)$.

Careful selection of design parameters $\sigma(t)$, $\zeta(t)$ will support both reductions to voltage deviations and power losses without significantly reducing the financial savings accrued by the customer. Extensions to include a method for selecting $\sigma(t)$ and $\zeta(t)$ are possible. Since the loss term in (4.35) is an energy value representing the losses in the grid associated only with customer c, parameter $\zeta(t)$ can be computed based on the energy price. Similarly, in a scenario in which customers are compensated for their contribution on voltage, parameter $\sigma(t)$ could represent the price for voltage regulation.

The constraints in (4.35) include battery constraints, the power balance equation, and the proposed extended voltage deviation equation based on the LinDistFlow model. In the process of solving (4.35), we obtain the real (u_m^c) and reactive (v_m^c) battery power to be dispatched across time window $[0, T\Delta]$. The optimisation problem (4.35) is solved by a residential customer, with information of the network impedances and with their (local) behind-the-meter measurements (see Fig. 4.2). The optimisation problem in (4.35) can be cast as a QP for which there are many commercially available solvers.

In cases where the network topology in a distribution grid changes, updates to R_{mm} and X_{mm} parameters are potentially required for customers connected to nodes along the path $\mathcal{L}_m$. In such cases, customers along the path

$\mathcal{L}_m$ will still operate inverters according to the L-QP formulation, to drive measured supply voltages towards the nominal ahead of updates to R_{mm} and X_{mm} parameters.

4.3.4 Benchmark Approach with Droop-Based Volt-Var Control

We introduce an important benchmark approach to assess the effectiveness of our proposed L-QP algorithm. Here, the real power of the battery storage is dedicated to maximise financial savings for the customer, whereas the reactive power is dedicated to voltage regulation. Similar to the network-agnostics control approaches in Chapter 3, this benchmark control does not include the impedance information of the network.

We consider an optimisation problem equivalent to the CF-QP in Chapter 3 for charging/discharging the battery across $[0, T\Delta]$ [Hashmi et al., 2020; Ratnam et al., 2015b]. Specifically, the optimisation problem is

$$\begin{aligned} \min_{u_m^c, p_m^c} \quad & \sum_{t \in \mathcal{T}} \eta(t) p_m^c(t) \Delta \\ \text{s.t.} \quad & (4.10), (4.12) - (4.15). \end{aligned} \tag{4.36}$$

The optimisation (4.36) minimises the energy consumption costs for the customer, subject to battery constraints and the power balance equation. In the process of solving (4.36) we obtain the battery real power dispatch (u_m^c) across the time window $[0, T\Delta]$.

Next, to dispatch reactive power of the battery system, we consider the volt-var droop curve in accordance with the IEEE Standard 1547 [IEEE, 2018]. Droop-based volt-var control has been considered in [Cavraro and Carli, 2018; Smith et al., 2011; Hashemi and Østergaard, 2018] and is also a mandatory control requirement for new connections of battery storage in several real-world distribution networks [AusNet Services, 2021; Victorian DNSP, 2019].

Fig. 4.3 illustrates the droop-based volt-var function that we incorporate in the benchmark approach for dispatching reactive power. In this chapter, we adopt the default volt-var droop function for distribution networks with a high penetration of distributed resources as per [IEEE, 2018]. The maximum reactive power is 44% of the apparent power rating of the inverter as per the standard in [IEEE, 2018].

Volt-var droop functions with a steeper slope and a smaller dead-band potentially provide enhanced voltage regulation; but it might also impact grid power losses and, more importantly, system stability. Locally regulating the grid voltage, without coordinating the response of customers along a feeder,

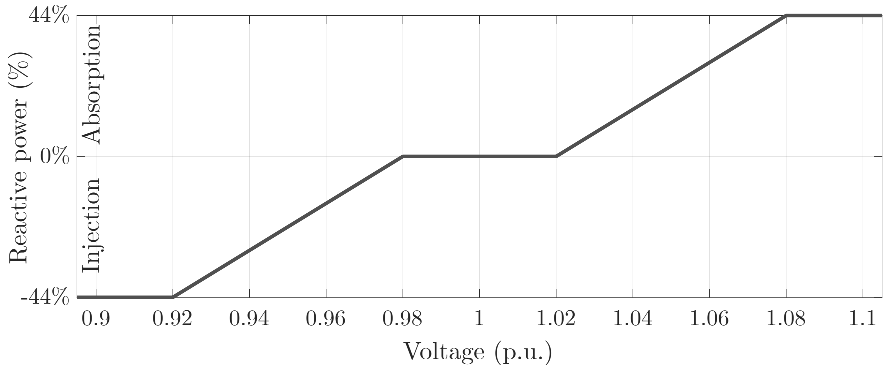

Figure 4.3: Droop-based volt-var function, with reactive power as a percentage of the nameplate apparent power rating for an inverter [IEEE, 2018].

as in both volt-var and the proposed L-QP in this chapter, potentially creates adverse interactions between controllers as reported in [IEEE, 2018; Jahangiri and Aliprantis, 2013; Schoene et al., 2017; Chakraborty et al., 2015; Abadi et al., 2019; Swartz et al., 2021; Cavraro and Carli, 2018; Singhal et al., 2019; Baker et al., 2018]. Adverse interactions between controllers is underpinned by a number of factors, including the network impedance and the location of inverters in the network, the operating state of the system, and the number and size of inverters along a feeder [IEEE, 2018; Jahangiri and Aliprantis, 2013; Schoene et al., 2017; Chakraborty et al., 2015; Abadi et al., 2019; Swartz et al., 2021; Cavraro and Carli, 2018].

Approaches proposed in the literature to avoid controller interactions include: (i) increasing or decreasing inverter response times to avoid interactions [Jahangiri and Aliprantis, 2013; Abadi et al., 2019; Schoene et al., 2017; Maharjan et al., 2021]; (ii) the careful placement of inverters along a feeder so as to critically dampen or avoid adverse inverter interactions [Swartz et al., 2021]; and more importantly (iii) the careful design of control parameters for local controllers located along a feeder so as to preserve system stability (convergence to steady-state voltages) [IEEE, 2018; Cavraro and Carli, 2018; Chakraborty et al., 2015; Singhal et al., 2019; Baker et al., 2018]. The design of control parameters for system stability is presented in more detail in the next two chapters (Chapter 5 and 6).

4.4 Numerical Simulations

In Fig. 4.4 a single line diagram of the 13NF, a three-phase unbalanced distribution network, is depicted. In our numerical simulations the 13NF is selected for the voltage regulation challenges it presents — stemming from being highly loaded, unbalanced, and its inclusion of mutual line impedances

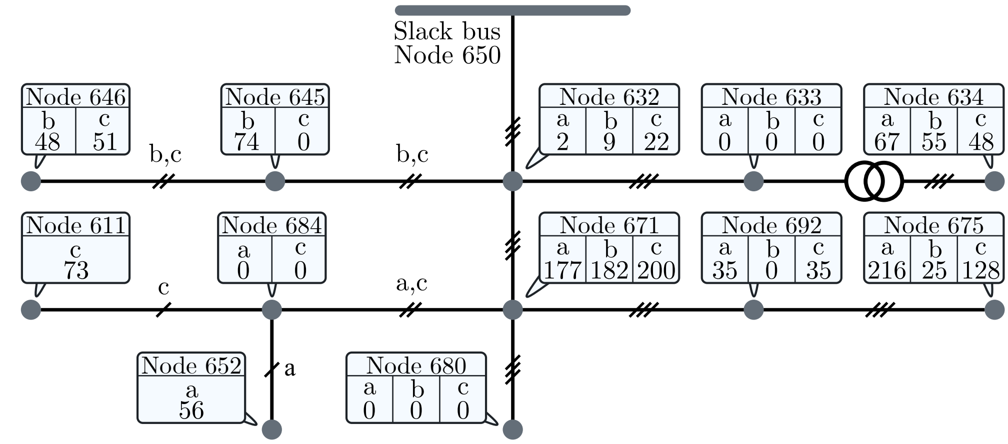

Figure 4.4: The IEEE 13-Node Test Feeder, where boxes represent the number of residential customers connected to the phases of each node.

[Arnold et al., 2016; Kersting, 2001]. In other words, proposed optimisation and control approaches are really challenged by testing with the 13NF. This is specially the case with the optimisation-based approaches using the LinDistFlow, in which the linear model considers no losses in line segments [Sankur et al., 2018]. Another test feeder with more nodes and line segments is also used in this chapter.

We assign slack bus 650 as node 0, with a fixed and nominal voltage magnitude $V_0 = V_r = 1$ p.u. The nominal line-to-ground voltage is 2.4 kV, and the voltage threshold, V_t, is 1.10 p.u. The 13NF includes a transformer between nodes 633 and 634, allowing for an analysis across both the primary and secondary side of the transformer.

We modify the 13NF by removing the voltage regulator transformer and the capacitors, and in this way we exacerbate underlying over-voltage and under-voltage conditions that the residential battery systems are designed to regulate. In the modified 13NF we connect 1,503 residential systems, where each residential system is connected to a phase at each of the nodes, as illustrated in Fig. 4.4.

Similar to Chapter 3, each residential system includes real time-varying load and PV generation data obtained from one of the 100 de-identified customers [Shaw et al., 2019], with average power values reported in 5-min intervals. Specifically, we replace the fixed load in the 13NF with time-varying load and PV generation data, where the substitution of aggregate customer load data at each node is approximately equal to the original fixed load values (with respect to the peak load conditions). Each customer is connected to a single-phase and we use the constant power load characteristic. Reactive loads are obtained by using the original 13NF power factor for each phase at each node.

In our numerical simulations, we also consider the more extensive 123NF. For the 123NF, we apply the same methodology described to populate the 13NF with real time-varying data, which corresponds to the inclusion of 1,145 residential systems in total in the 123NF.

It's worth mentioning that customers connected to different phases of the same node measure the voltage magnitude for the respective phase. The residential battery is thus dispatched according to the voltage measurements for the respective phase. Accordingly, R_{mm} and X_{mm} is composed of the self-resistance and self-reactance, respectively, of the line segments of the respective phase. For the 13NF, the R/X ratio of paths range from 0.32 to 0.58, and for the 123NF the R/X ratio of paths range from 0.42 to 0.86. As per the IEEE test feeder documentation [Kersting, 2001], the power factor for all residential loads connected to the 13NF range from 0.75 to 0.93, with a mean load power factor of 0.86. The loads on the 123NF have a power factor ranging from 0.80 to 0.91, with a mean load power factor of 0.87.

In what follows, we assume each customer has a solar PV system, and 30% of customers have a battery storage system. In our numerical simulations, we focus on the distinctive impact of the battery operation on the network and assume the PV inverters do not operate according to a volt-var control strategy. Customers with a battery storage system schedule their battery power flows for the day-ahead, i.e., $T\Delta = 288 \cdot 5/60 = 24$ h. We consider a 5 kW, 10 kWh residential battery ($\underline{u} = \overline{u} = 5$ kW and $\overline{s} = 10$ kWh) and a 6 kVA inverter. The dispatchable reactive power limit is 3.3 kvar ($\underline{v} = \overline{v} = 3.3$ kvar). We set the battery charge level at the end of the day equal to the charge level at the beginning of the day, i.e., $s_0 = s_f = 2$ kWh.

The distributor serving the 100 de-identified customers reported in the dataset (described more fully in [Shaw et al., 2019]) has published a TOU tariff η [Evoenergy, 2020] which we use in our simulations. Specifically, $\eta(t) = 0.032$ from midnight to 7 am and from 10 pm to midnight, $\eta(t) = 0.065$ from 9 am to 5 pm and from 8 pm to 10 pm and $\eta(t) = 0.144$ from 7 am to 9 am and 5 pm to 8 pm. We assume each day begins at midnight, and the day-ahead load, PV generation and voltage forecasts (with uncertainty) are computed using the procedure described in [Ratnam et al., 2016].

Note that we use a three-phase, non-linear, full power flow model based on the current injection method [Garcia et al., 2000] to simulate the respective IEEE test feeders, enabling a comprehensive analysis and benchmark for the L-QP approach. That is, the proposed L-QP in this chapter incorporates the linear approximate power flow equations, but it is assessed under the full non-linear model that more precisely represents distribution networks.

In our numerical simulations, the simulation time step is 5 minutes (i.e.,

$\Delta = 5/60$ h and $T = 288$). Using an Intel Core i7-8700 CPU @ 3.20GHz, it takes approximately 2 seconds to solve the L-QP with the MATLAB optimisation solver *quadprog*.

For the 13NF, coefficient α_m^c computed as in (4.27) ranges from 0.003 to 0.011, and for the 123NF, α_m^c ranges from 0.0007 to 0.014. Next, we carefully select our design parameters σ and ζ to prioritise financial savings for the customer. We tune the design parameters such that they result in smaller values for the voltage deviation and power loss terms in the optimisation problem in (4.35). We select $\zeta(t)$ to reflect the energy price in \$/kWh, i.e., $\zeta(t) = \eta(t), \forall t \in \mathcal{T}$, since parameter $\zeta(t)$ is associated with energy losses on the grid allocated to the customer. To prioritise earnings for customers, let $\sigma(t) = 0.01, \forall t \in \mathcal{T}$. In what follows, we consider the L-QP the benchmark approach as described in 4.3, in the context of network voltages, network losses, and customer daily operational savings.

4.4.1 Assessing Utility and Customers Benefits

Fig. 4.5 presents real and reactive power of load, PV and battery storage for a residential system connected to node 675 in the 13NF. In Fig. 4.5(a,b) we present their real power considering the benchmark and the proposed L-QP approach, respectively. In Fig. 4.5(c,d) we present the reactive power considering the benchmark and the L-QP approach, respectively.

In Fig. 4.5(a) observe that our benchmark approach results in real power of the battery that is solely determined by the TOU tariff, as the CF-QP of the previous chapter. In Fig. 4.5(b) observe that the L-QP control results in battery real power that is also influenced by the TOU tariff, as we prioritised savings for customer in (4.35). We further observe that the battery charges when PV generation *peaks*, resulting in reduce real power exports from the customer which potentially reduces grid resistive losses. In Fig. 4.5(c), according to the volt-var of the benchmark approach, the battery reactive power is essentially proportional to the local voltage. In Fig. 4.5(d), with the L-QP control, reactive power is dispatched to support voltage regulation but it is not solely a function of the local voltage, since real and reactive power are coupled for voltage regulation as in (4.24).

In Fig. 4.6 we present voltages envelopes for the IEEE 13NF considering all phases of all nodes across the feeder — excluding node 650 (the slack bus). Each envelope represents the range between the maximum and the minimum voltage magnitude across the network at each time step. In Fig. 4.6 the baseline envelope represents the case where no customer along the feeder has a battery (i.e., $u = v = 0$ for all customers). In Fig. 4.6 observe that the baseline envelope encompasses two significant voltage drops at 08:00 and again

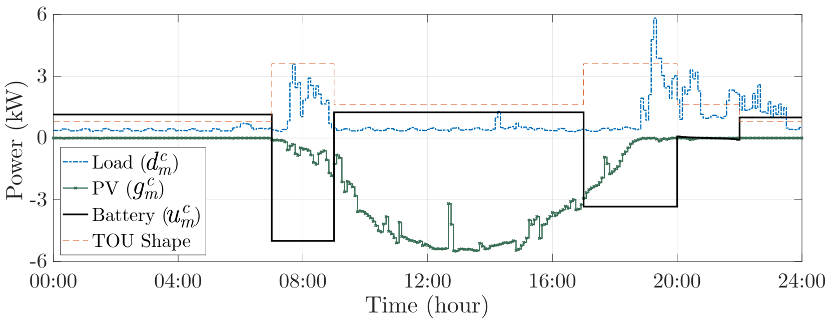

(a)

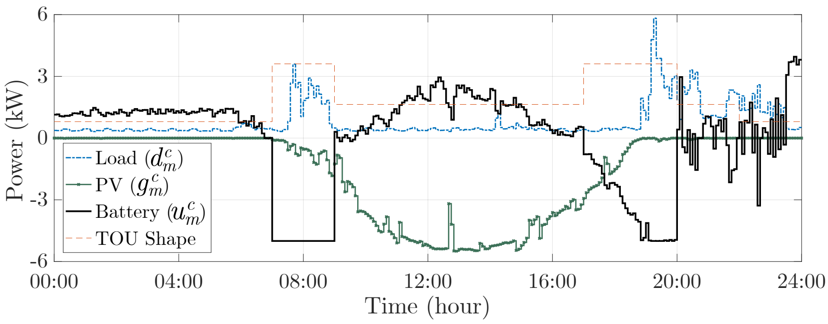

(b)

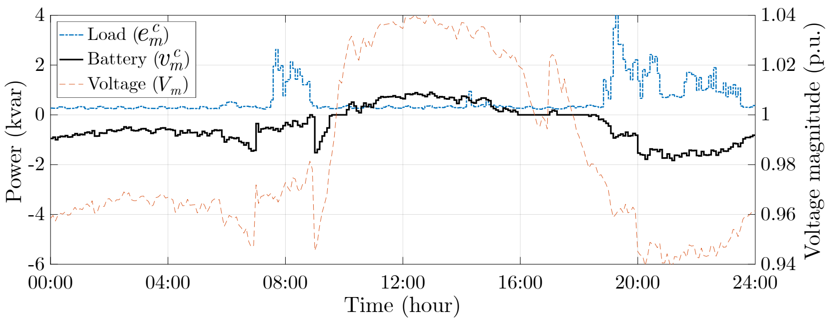

(c)

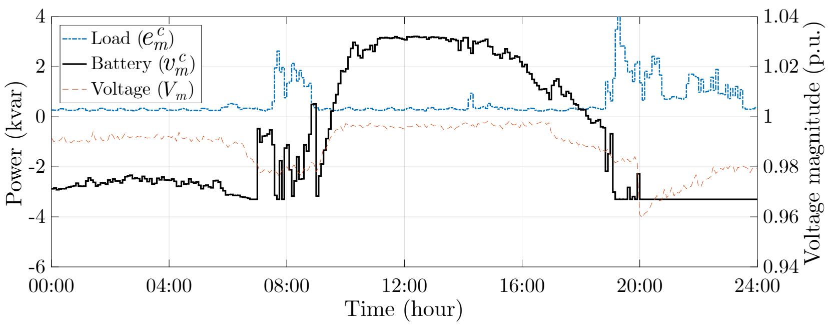

(d)

Figure 4.5: Residential system connected at node 675 phase C along the 13NF. Real power of elements for (a) benchmark approach (b) proposed L-QP. Reactive power for (c) benchmark approach (d) proposed L-QP approach.

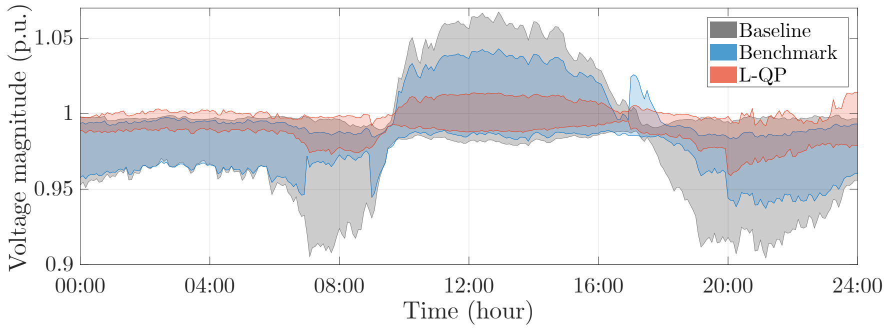

Figure 4.6: Voltage magnitude envelopes for the entire IEEE 13NF. The baseline voltage envelope represents the case where no customer installs a battery.

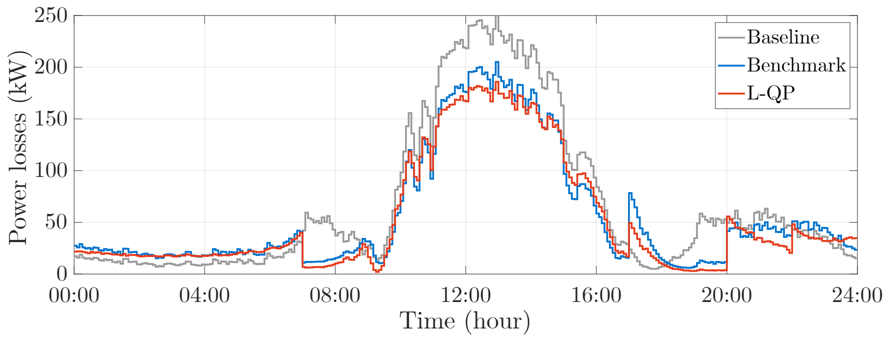

Figure 4.7: Grid resistive power losses across a day for the entire 13NF. Baseline represents the case where no customer installs a battery.

at 20:00, which coincides with peak demand across the feeder. Furthermore, we observe voltage rise occurs at 12:00, which is also coincident with peak PV production across the feeder. The proposed L-QP approach significantly reduces voltage deviations from the nominal in comparison with both the baseline and the benchmark approach.

Fig. 4.7 illustrates the grid resistive power losses across the day, where the baseline approach represents the situation where no customer has installed a battery. We observe that in all three approaches, Baseline, Benchmark and L-QP, the most significant losses occur during the middle of the day when PV generation peaks. During peak PV generation, large quantities of real power (P_{mn}) flow back along line segments resulting in significant power losses across the network, in accordance with (4.29). We also observe that the proposed L-QP offers a greater reduction in peak power losses, a result of charging of batteries during peak PV generation.

Table 4.1 presents a summary of numerical simulations that were carefully curated to be representative of summer and winter days, considering sunny and cloudy conditions — where the load and PV generation profiles vary considerably. The selected days are representative of extreme cases, where large voltage deviations and power losses are prevalent throughout the network. Note that the first selected day (Summer Sunny Day) summarises the results previously presented in Figs. 4.5-4.7.

Table 4.1 presents the maximum and minimum voltage magnitude and the total energy loss across the 13NF, in addition to the average savings per customer provided by batteries on that day. The average savings are calculated as the average of Γ_m^c in (4.18) for all customers with battery storage. The impact of inverter disconnections on savings is the focus of Chapter 3, and it is not included here.

In Table 4.1 both the benchmark and the L-QP approaches provide savings for customers and reduce the grid losses from the reported baseline. The benchmark approach provided a maximum savings of \$1.912 on all selected days, whereas the proposed L-QP approach reduced grid power losses and provided significant voltage improvement at a marginal cost to the customer (e.g., savings reduced from \$1.912 to \$1.829 on the Winter Cloudy Day).

In Table 4.1, the distribution network presents voltage violations when batteries employ the benchmark approach (0.88 p.u.) and voltages are kept within suitable range ($>$0.91 p.u.) when batteries employ the proposed L-QP approach. The L-QP approach also considerably reduced grid power losses. The valuable and significant reduction in voltage deviation and grid power losses when customers employ the L-QP approach does not reflect in greater financial benefits for the customer as those two terms were not monetised in the objective function. Future work can investigate how those terms could financially compensate customers for their invaluable ancillary services to the grid. In that case, the total financial savings for a customer providing such ancillary services plus the energy arbitrage (L-QP approach) could easily be greater than a customer that only provides energy arbitrage (benchmark approach).

In Table 4.2, we present a summary of the numerical simulations completed with the 123NF. Specifically, we carefully consider the two most extreme days, and we observe that in this larger-scale distribution network the L-QP approach reduces voltage deviations and resistive losses when compared to the baseline and the benchmark. The numerical simulation for the L-QP approach are completed within 2 seconds, for each customer, consistent with the reported simulation time for the 13NF.

In Fig. 4.8 we present voltage envelopes for the Summer Sunny Day for the 13NF, considering the L-QP approach with three different sets of weights as reported in Table 4.3. Note that Set 1 is consistent with our previous numerical simulations, whereas Set 2 considers a larger weight for grid losses (ζ) and Set 3 considers a larger weight for both grid voltage (σ) and grid losses (ζ). That is, we carefully select our three sets of weights for our simulations,

Table 4.1: Financial savings, energy losses and voltage envelopes for the IEEE 13NF.

Day	**Baseline**	**Benchmark**	**L-QP (Set 1)**
Summer Sunny Day	N/A 1609 kWh 1.07-0.90 p.u.	$ 1.912 1348 kWh 1.04-0.94 p.u.	$ 1.890 1261 kWh 1.01-0.96 p.u.
Summer Cloudy Day	N/A 968 kWh 1.06-0.91 p.u.	$ 1.912 847 kWh 1.04-0.94 p.u.	$ 1.904 768 kWh 1.01-0.96 p.u.
Winter Sunny Day	N/A 1565 kWh 1.02-0.81 p.u.	$ 1.912 1045 kWh 1.01-0.88 p.u.	$ 1.843 810 kWh 1.02-0.91 p.u.
Winter Cloudy Day	N/A 1569 kWh 1.00-0.83 p.u.	$ 1.912 1184 kWh 1.00-0.90 p.u.	$ 1.829 979 kWh 1.01-0.91 p.u.

Table 4.2: Financial savings, energy losses and voltage envelopes for the IEEE 123NF.

Day	**Baseline**	**Benchmark**	**L-QP (Set 1)**
Summer Sunny Day	N/A 713 kWh 1.04-0.94 p.u.	$ 1.912 689 kWh 1.03-0.95 p.u.	$ 1.889 669 kWh 1.02-0.97 p.u.
Winter Sunny Day	N/A 943 kWh 1.01-0.89 p.u.	$ 1.912 779 kWh 1.00-0.93 p.u.	$ 1.822 571 kWh 1.00-0.95 p.u.

with extension to systematic tuning possible. In Fig. 4.8 and Table 4.3 we observe that, according to the change in priority, Set 2 considerably reduced grid energy loss compared to Set 1, while decreasing savings and voltage regulation performance. Set 3 resulted in improved grid voltage and losses compared to Set 1, while providing lower savings.

Including the approximate loss equation (4.34), developed in this chapter for a local control approach as the L-QP, has shown significant reduction in grid power losses across the network, as presented in Table 4.3. By removing the loss term from the L-QP optimisation in (4.35), i.e. $\zeta(t) = 0$, the energy losses across the network increase to 1411 kWh.

Prioritizing voltage and loss terms in (4.35), as with Set 3, shifts the bat-

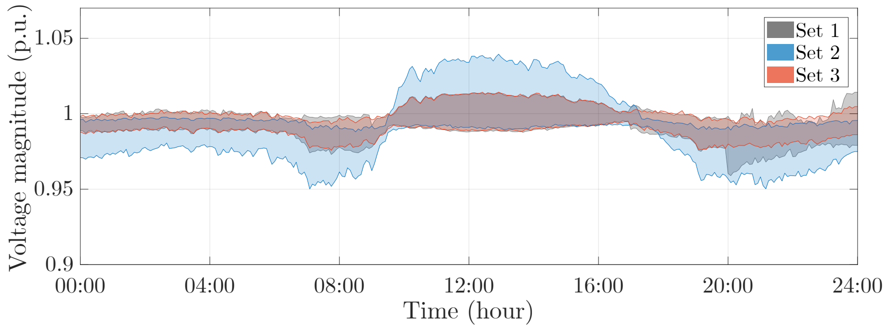

Figure 4.8: Voltage magnitude envelopes for the IEEE 13NF with three sets of L-QP weights.

Table 4.3: Introducing three sets: L-QP design parameters

	Set 1	**Set 2**	**Set 3**
Design parameters: σ, ζ	0.01, η	0.01, 10^3	1, 10^3
Average savings	\$ 1.890	\$ 0.492	\$ 0.511
Total energy losses	1261 kWh	1082 kWh	1090 kWh

tery real power flows from a trajectory guided by the TOU tariff to a trajectory that directly reduces both grid voltage deviation from the nominal and feeder losses. We observed that the coupled action of real and reactive power intensifies voltage regulation performance with the L-QP approach, however, the average savings per customer fell to around \$0.50 per day. In this context, financially compensating customers for their grid voltage regulation services and for reducing feeder losses could potentially create greater benefits for both the customer and utility.

4.4.2 Interaction Between Inverters

This section presents numerical simulations to illustrate the effect of extension coefficient α_m^c on the grid voltage stability due to interactions between inverters. Analogous to the gain in a proportional controller or the droop slope in the volt-var control, coefficient α_m^c has direct influence on stability, convergence rate and steady-state voltage deviation of the system. More precise details are presented in Chapter 5 and Chapter 6.

Here, for illustrative purposes, consider a single-phase two-node network with two batteries alternately updating their output for grid voltage regulation with the L-QP control. In this simulation, customers have enough resources to fully minimise the voltage regulation term $(\hat{E}_m^c)^2$ in (4.35). In

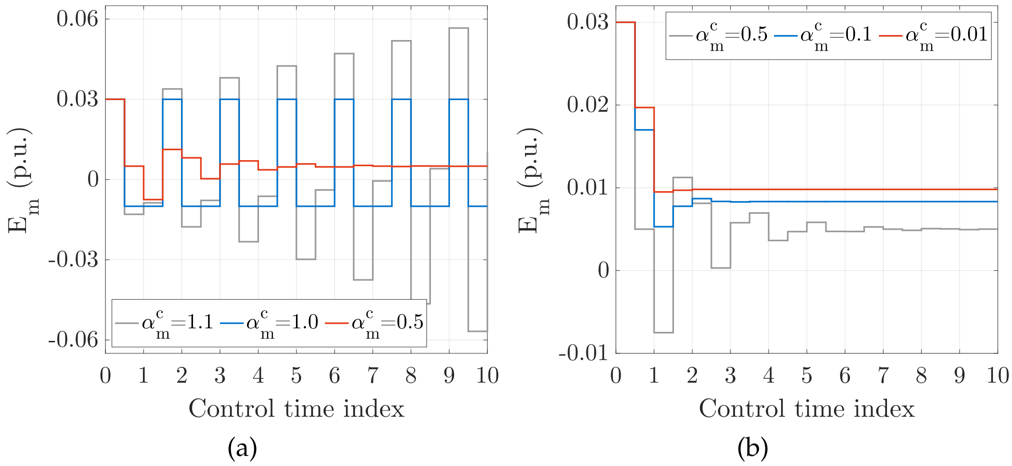

Figure 4.9: Grid voltage deviation for different values of the extension coefficient α_m^c. Effect of the coefficient α_m^c on (a) voltage stability and (b) on convergence rate and steady-state voltage deviation.

what follows, we numerically assess the impact of gain coefficient α_m^c on grid voltage stability, convergence rate and steady-state voltage deviation.

Fig. 4.9 depicts the grid voltage deviation behavior for different values of coefficient α_m^c. In Fig. 4.9(a) we observe that $\alpha_m^c > 1$ resulted in ever-increasing voltage deviation (unstable system); $\alpha_m^c = 1$ resulted in a sustained interaction between inverters (marginally stable system); and $\alpha_m^c < 1$ resulted in a convergent grid voltage (stable system). In Fig. 4.9(b) we observe that smaller coefficient values reduce interactions between inverters, whereas larger values reduce steady-state voltage deviation.

Analogous to other local (fully decentralised) approaches [Singhal et al., 2019; Baker et al., 2018], coefficient α_m^c can be adjusted to balance convergence rate and steady-state voltage deviation. Equation (4.27) computes coefficient α_m^c according to the voltage regulation capacity of the battery storage. However, in case of significant interactions between local controllers, there can be a tuning-down factor in (4.27) that reduces α_m^c proportionally to the battery regulation capacity. A similar strategy is proposed in [Singhal et al., 2019] to adaptively adjust the coefficients of the local volt-var control.

Analytical investigation of coefficient α_m^c can provide further insights on its relation with convergence and steady-state voltage deviation. Such a strategy is presented in [Baker et al., 2018], where a convex optimisation problem is formulated to obtain the coefficients of a fully decentralised approach to minimise voltage deviation while ensuring system stability. A similar strategy is undertaken in this thesis and presented in Chapter 5 and Chapter 6.

4.4.3 L-QP vs VVW

We finalise this section by drawing a brief parallel between the optimisation-based L-QP approach and a proportional VVW control. The insights provided here can be used to analytically design gain parameters of L-QP (and also VVW control) to preserve system stability.

In the L-QP optimisation in (4.35), for a customer with enough resources, the voltage deviation term is minimised when

$$(\hat{E}_m^c)^2 = 0. \tag{4.37}$$

Then from the extended voltage deviation in (4.24), it holds that

$$\hat{E}_m^c = R_{mm} p_m^c + X_{mm} q_m^c + \alpha_m^c (V_0^2 - V_m^2) = 0 \tag{4.38}$$

$$R_{mm} p_m^c + X_{mm} q_m^c = -\alpha_m^c (V_0^2 - V_m^2) \tag{4.39}$$

$$R_{mm} p_m^c + X_{mm} q_m^c = -\alpha_m^c E_m \tag{4.40}$$

On the right-hand side (RHS) of (4.40), we observe coefficient α_m^c multiplying the voltage deviation E_m. That is, similar to a proportional control, the proportional gain coefficient is multiplying the error (difference of measured value from reference). On the left-hand side (LHS) of (4.40), real and reactive power, multiplied by their respective sensitivities, are adjusted to match the RHS.

In control systems, a standard proportional control aims at actuating a resource to counteract a deviation of a variable from the reference value [Åström and Murray, 2020]. Similarly in (4.40), two resources are available to counteract the grid voltage deviation from the nominal.

In Chapter 5 and Chapter 6 we focus on proportional VVW control approaches. The design of VVW parameters for system stability can then be translated to the L-QP control of this chapter. Additionally, by following the reverse derivation of this section, original VVW control can be cast as a convex optimisation problem to consider other objectives and constraints.

4.5 Conclusion

Control approaches separating real power for economic purposes and reactive power for voltage regulation have their fundamental limitations in distribution networks. In this chapter, we proposed a local optimisation-based control, L-QP, that enables both real and reactive power coupled for grid voltage regulation and loss reduction, while considering the financial savings for the battery owner.

With a small reduction in the financial savings that accrue to customers, our proposed approach has shown higher technical performance in simulation in terms of grid voltage regulation and reduced power losses across the feeder. By carefully selecting the design parameters for enhanced voltage regulation and further feeder loss reduction, we observed residential batteries operated according to the proposed L-QP approach offered significant opportunities for improved grid operations.

Other possible investigations in the context of this chapter are: assessment of battery degradation; the systematic tuning of σ and ζ; and detailed investigation on the impact of gain coefficients on interaction between local controllers and system stability. In the next chapter, the stability condition is analytically determined for gain coefficients of proportional control. We leverage on the stability condition and the local linear formulation derived in this chapter to propose an original VVW proportional control. An optimisation problem that is solved locally and analytically is also proposed to design other parameters of the proportional control.

Chapter 5

Local Volt-Var-Watt Control: Network-Cognisant Formulation for Proportional Control

This chapter proposes a local volt-var-watt (VVW) control to effectively regulate voltages while reducing the impact on grid power losses. We incorporate the impedance characteristic of the network in the control algorithm to actuate real and reactive power of DERs. A local and convex optimisation problem is proposed to obtain the optimal relation of real to reactive power control for voltage regulation. The gain coefficients of the local proportional controllers are designed such that convergence (asymptotic stability) is guaranteed. Numerical simulations with a realistic 8-node distribution feeder and real-world demand data show the effectiveness of the proposed controller compared to available alternatives in the literature.

This chapter fully describes the paper presented in [de Carvalho et al., 2022]. The author of this thesis has opted for keeping most of the original structure of the paper in order to preserve coherence and clarity. This chapter is organized as follows. Section 5.1 gives the motivation, literature review and research gaps specific to this chapter. Section 5.2 presents the linear network model using the tailored notation of this chapter. Section 5.3 introduces the proposed VVW control, the optimisation and design of its coefficients, and a performance index to measure efficacy of the voltage regulation. Section 5.4 presents the conventional VVW formulation for benchmarking. Section 5.5 presents numerical simulations to assess convergence and steady-state performance, and Section 5.6 concludes this chapter with important remarks that also motivates the next one.

List of Main Symbols – Chapter 5

$\boldsymbol{A}$	Diagonal matrix with proportional gain of all nodes
d_m	Non-controllable real load of participating user at node m
$\boldsymbol{d}$	Vector of non-controllable real load of participating users
e_m	Non-controllable reactive load of participating user at node m
$\boldsymbol{e}$	Vector of non-controllable reactive load of participating users
E_m	Voltage deviation at node m relative to the reference
E_m^w	Controllable part of the voltage deviation at node m
$\boldsymbol{E}$	Voltage deviation vector
$\widetilde{\boldsymbol{E}}$	Underlying voltage deviation vector
$\mathcal{E}$	Set of all line segments on the network
g	Gain coefficient of benchmark proportional control
$\overline{g}$	Critical gain coefficient of benchmark proportional control
$\boldsymbol{H}$	Matrix that captures sensitivities
I_{mn}	Current magnitude in line segment (m, n)
k	Control iteration index
L	Total resistive power losses on the network
L^{bl}	Total resistive power losses on the network with no control
L^{reg}	Total resistive power losses on the network with control
$\mathcal{L}_m$	Set of line segments in the unique path from node 0 to node m
N	Total number of nodes downstream of the slack bus
$\mathcal{N}_o$	Set of all nodes on the network defined as $\{0, 1, ..., l, m, n, ..., N\}$
$\mathcal{N}$	Set of downstream nodes defined as $\{1, ..., l, m, n, ..., N\}$
p_m	Real power consumption of participating user at node m
$\widetilde{p}_m$	Real power consumption of non-participating user at node m
$\boldsymbol{p}$	Vector of real power consumption of participating users
$\widetilde{\boldsymbol{p}}$	Vector of real power consumption of non-participating users
P_{mn}	Real power flow in line segment (m, n)

q_m	Reactive power consumption of participating user at node m
$\widetilde{q}_m$	Reactive power consumption of non-participating user at node m
$\boldsymbol{q}$	Vector of reactive power consumption of participating users
$\widetilde{\boldsymbol{q}}$	Vector of reactive power consumption of non-participating users
Q_{mn}	Reactive power flow in line segment (m, n)
r_{mn}	Resistance of line segment (m, n)
R_{mm}	Resistance (multiplied by 2) of the unique path from node 0 to m
$\boldsymbol{R}$	Resistance matrix
$\boldsymbol{R}_d$	Diagonal resistance matrix with only diagonal elements of $\boldsymbol{R}$
u_m	Controllable real power of participating user at node m
$\boldsymbol{u}$	Vector of controllable real power of participating users
v_m	Controllable reactive power of participating user at node m
$\boldsymbol{v}$	Vector of controllable reactive power of participating users
V_m	Voltage magnitude at node m
V_m^{bl}	Voltage magnitude at node m for the baseline (no control) case
V_m^{reg}	Voltage magnitude at node m when regulated by control
V_0	Reference voltage magnitude (voltage magnitude at node 0)
x_{mn}	Reactance of line segment (m, n)
X_{mm}	Reactance (multiplied by 2) of the unique path from node 0 to m
$\boldsymbol{X}$	Reactance matrix
$\boldsymbol{X}_d$	Diagonal reactance matrix with only diagonal elements of $\boldsymbol{X}$
$\boldsymbol{Y}$	Diagonal matrix with coupling factor of all nodes
α_m	Proportional gain coefficient
$\overline{\alpha}$	Critical proportional gain coefficient
γ_m	Coupling factor between real and reactive power
$\rho(\cdot)$	Spectral radius of matrix (maximum absolute eigenvalue of matrix)
σ	Index of loss reduction per voltage regulated

5.1 Introduction

Distribution networks are experiencing increasingly high penetration of solar PV and other DERs. While these zero-emission technologies bring several benefits they also bring challenges to operate distribution networks and maintain an appropriate voltage magnitude for energy users. In this new distributed paradigm, the proper operation of DERs scattered across the network is paramount to keep voltages within an adequate range [AEMO, 2020b; ENEA et al., 2020; Scott, 2016].

As described in more detail in Section 1.1, there are three main categories of control approaches in distribution networks to perform voltage regulation: centralised, distributed and local/autonomous approaches [Mahmud and Zahedi, 2016]. Centralised and distributed approaches can both achieve global objectives in the distribution network, while keeping voltages within the bounds [Cavraro and Carli, 2018; Arnold et al., 2016]. The high communication and computational costs, along with convergence challenges, can make these approaches complex and insufficiently fast to respond to quick voltage variations [Singhal et al., 2019]. Local approaches are limited to local measurements and might not achieve globally optimum solutions. With minimal or no communication, local approaches are privacy strengthening, robust to communication failures, autonomous and can respond quickly to sudden voltage variations [Antoniadou-Plytaria et al., 2017].

Locally controlling many DERs across the grid and achieving steady-state voltages is challenging and the focus of many research works [Cavraro and Carli, 2018; Singhal et al., 2019; Baker et al., 2018; Spanias et al., 2019; Hashemi and Østergaard, 2018; de Carvalho et al., 2023]. In [Cavraro and Carli, 2018], two variations of the local volt-var approach are proposed for voltage regulation, where coefficients are analytically designed to guarantee convergence to steady-state voltages. In [Singhal et al., 2019], an adaptive volt-var control with real-time update of coefficients is proposed to reduce voltage deviations and maintain convergence. However, the relatively high R/X ratio of distribution networks limits the efficacy of pure volt-var approaches for voltage regulation, and can result in unacceptably high grid power losses [von Meier et al., 2020]. Real power has also been included in proportional controllers to increase the voltage regulation performance, resulting in volt-var-watt control strategies, such as [Baker et al., 2018; Spanias et al., 2019]. In [Hashemi and Østergaard, 2018], the reactive power is used in a droop-based volt-var approach, while the controllable real power is used to prevent excessive PV generation export. In contrast, real and reactive power are jointly controlled in the L-QP in Chapter 4 for voltage regulation and power loss reduction, with coefficients designed based on the size and location of controllable DER.

In this chapter, we propose a volt-var-watt control approach for voltage regulation and grid loss reduction where coefficients are designed to guarantee overall system stability (convergence). The proposed approach, termed voltage-based volt-var-watt (VB-VVW), is a local proportional controller such that each DER inverter in the network acts autonomously and requires only local measurements. The control approach is formulated based on the LinDistFlow model to incorporate the impedance characteristics of the network. Control parameters are optimised based on a local optimisation problem to reduce the amount of controllable real power and injection of reactive power into the grid. We benchmark VB-VVW with a pure volt-var approach as well as a conventional VVW formulation. Numerical simulations are carried out on a realistic 8-node low voltage distribution feeder [Zeraati et al., 2018; Mediwaththe and Blackhall, 2021] populated with real-world customer data [Shaw et al., 2019].

5.2 Preliminaries

Fig. 5.1 illustrates a radial distribution network modelled as a connected graph (repeated here for convenience). The network contains $N+1$ nodes where node 0 is the source node, also known as substation or slack bus. Similar to the notation introduced in Chapter 4, the set $\mathcal{N} := \{1, ..., l, m, n, ..., N\}$ collects all nodes downstream from the source node and $\mathcal{E}$ is the set that collects all line segments.

In Fig. 5.2 we present the distribution network notation of this chapter. The impedance of the line segment $(l, m) \in \mathcal{E}$ is represented by $r_{lm} + jx_{lm}$, where r_{lm} is the resistance and x_{lm} is the reactance of the line segment. The real and reactive power flows in the line segment $(l, m) \in \mathcal{E}$ are denoted by P_{lm} and Q_{lm}, respectively. At each node $m \in \mathcal{N}$, we divide between users (customers) that do not participate in the control approach (non-participating users) and users with controllable DERs that participate in the control approach (participating users). The real and reactive load of non-participating users are denoted by $\widetilde{p}_m$ and $\widetilde{q}_m$, respectively, and the real and reactive load of participating users are denoted by p_m and q_m, respectively.

Within the participating user, the non-controllable real and reactive load is denoted by d_m and e_m, respectively, whereas the controllable real and reactive power is denoted by u_m and v_m, respectively. Finally, V_m denotes the voltage magnitude at node $m \in \mathcal{N}$.

We again use the LinDistFlow equations derived in [Baran and Wu, 1989a] to model the distribution network. The linear model supports the development of convex optimisation problems and selection of coefficients for overall

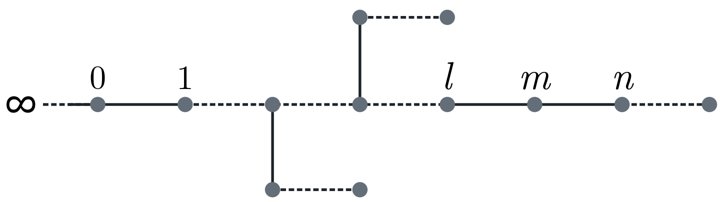

Figure 5.1: A connected graph is used to model the distribution network.

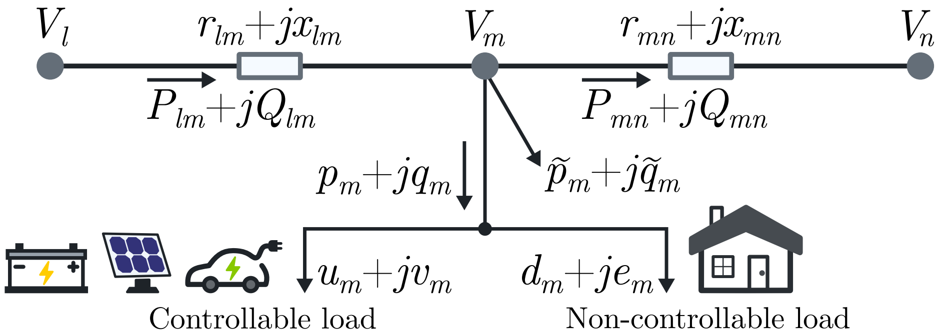

Figure 5.2: Distribution network notation, where arrows indicate direction of positive power flow. Load of non-participating users are denoted by $\widetilde{p}_m$ and $\widetilde{q}_m$, whereas power of participating users are denoted by p_m and q_m. Examples of controllable DERs are battery energy storage, solar PV and electric vehicle.

system convergence. In this chapter, the accuracy of the linear model is compared to the exact non-linear model and presented in the numerical simulations. The LinDistFlow equations [Baran and Wu, 1989a] with the notation presented in Fig. 5.2 are written as:

$$P_{lm} = p_m + \widetilde{p}_m + \sum_{n:(m,n)\in\mathcal{E}} P_{mn}, \quad \forall m \in \mathcal{N}, \tag{5.1}$$

$$Q_{lm} = q_m + \widetilde{q}_m + \sum_{n:(m,n)\in\mathcal{E}} Q_{mn}, \quad \forall m \in \mathcal{N}, \tag{5.2}$$

$$V_l^2 = V_m^2 + 2r_{lm}P_{lm} + 2x_{lm}Q_{lm}, \quad \forall (l,m) \in \mathcal{E}. \tag{5.3}$$

Define a path with the unique set of line segments from node 0 to node m as $\mathcal{L}_m \subseteq \mathcal{E}$ [Lin and Bitar, 2018]. Then the resistance and reactance matrix $\boldsymbol{R}, \boldsymbol{X} \in \mathbb{R}^{\mathrm{N}\times\mathrm{N}}$ have their entries computed as:

$$R_{hk} = \sum_{(m,n)\in\mathcal{L}_h\cap\mathcal{L}_k} 2r_{mn}, \quad X_{hk} = \sum_{(m,n)\in\mathcal{L}_h\cap\mathcal{L}_k} 2x_{mn}, \tag{5.4}$$

where h and k are the indices for the row and column of the matrices. We additionally define the voltage deviation squared at each node $m \in \mathcal{N}$ as

$E_m := V_0^2 - V_m^2$, where V_0 is the nominal voltage and the voltage at node 0. We can then formulate the compact LinDistFlow equation in matrix format as in [Lin and Bitar, 2018] as:

$$\boldsymbol{E} = \boldsymbol{R}(\boldsymbol{p} + \widetilde{\boldsymbol{p}}) + \boldsymbol{X}(\boldsymbol{q} + \widetilde{\boldsymbol{q}}), \tag{5.5}$$

where $\boldsymbol{E}, \boldsymbol{p}, \widetilde{\boldsymbol{p}}, \boldsymbol{q}, \widetilde{\boldsymbol{q}} \in \mathbb{R}^{\mathrm{N}}$ are vectors in which each row represents the variable of the respective node $m \in \mathcal{N}$. Expand (5.5) as

$$\boldsymbol{E} = \boldsymbol{R}(\boldsymbol{u} + \boldsymbol{d} + \widetilde{\boldsymbol{p}}) + \boldsymbol{X}(\boldsymbol{v} + \boldsymbol{e} + \widetilde{\boldsymbol{q}}), \tag{5.6}$$

where $\boldsymbol{u}, \boldsymbol{d}, \boldsymbol{v}, \boldsymbol{e} \in \mathbb{R}^{\mathrm{N}}$ are vectors in which each row represents the variable of the respective node $m \in \mathcal{N}$. We now expand (5.6) for a single node $m \in \mathcal{N}$ as

$$E_m = E_m^w + \sum_{\substack{n \in \mathcal{N} \\ n \neq m}} (R_{mn} u_n + X_{mn} v_n) + \sum_{n \in \mathcal{N}} (R_{mn}(d_n + \widetilde{p}_n) + X_{mn}(e_n + \widetilde{q}_n)), \tag{5.7}$$

where

$$E_m^w = R_{mm} u_m + X_{mm} v_m. \tag{5.8}$$

E_m^w represents the controllable part of voltage at node m by the local DER. The two summation terms in (5.7) are, respectively, the controllable voltage at node m attributed to external DERs and the voltage deviation at node m attributed to the non-controllable power consumption across the grid.

Remark: As presented in (5.7)-(5.8), the local controllable real and reactive power (u_m and v_m) changes the local grid voltage according to the resistance and reactance of the path (R_{mm} and X_{mm}). As such, R_{mm} and X_{mm} dictates which power has greater effectiveness for voltage regulation; therefore, the R_{mm}/X_{mm} ratio can be interpreted as the effectiveness of real power relative to the effectiveness of the reactive power for voltage regulation. For example, a R_{mm}/X_{mm} of 2 indicates that real power provides twice the voltage regulation the reactive power provides with the same amount of power.

5.3 Problem Formulation

We formulate a proportional control termed VB-VVW based on the locally controlled voltage equation, E_m^w, such that the network impedance is intrinsically incorporated in the approach. We initially formulate the proportional control law for a participating user as:

$$E_m^w(k) = -\alpha_m E_m(k-1), \tag{5.9}$$

where k is the control iteration index and $\alpha_m \geq 0$ is the gain coefficient to be designed for the proportional controller. Substituting from (5.8) for E_m^w, we get

$$R_{mm} u_m(k) + X_{mm} v_m(k) = -\alpha_m E_m(k-1). \tag{5.10}$$

Note that $E_m = V_0^2 - V_m^2$ is the local voltage deviation and can be computed by measuring the local voltage V_m. The controllable reactive power v_m have negligible impact on the energy reserve of DERs and it can also be used to locally supply the reactive load e_m of the participating user. As such, we adapt (5.10) to consider the total reactive power of the participating user for voltage regulation as

$$R_{mm} u_m(k) + X_{mm} q_m(k) = -\alpha_m E_m(k-1), \tag{5.11}$$

where $q_m(k) = v_m(k) + e_m$. Note that both real and reactive power can be actuated in the proportional control in (5.11) for voltage regulation. We seek for an optimal balance of real and reactive power. Consider the additional equation that gives the relation between real and reactive power to be used in the control law in (5.11):

$$u_m(k) = \gamma_m q_m(k), \tag{5.12}$$

where $\gamma_m \in \mathbb{R}$ is the coupling factor that is designed by an optimisation problem in this chapter. For $\gamma_m = 0$, for example, the control is a volt-var only with no real power actuation for voltage regulation. For $\gamma_m = \infty$ the control is a volt-watt only with no reactive power for voltage regulation. Combining (5.11) and (5.12), the controllable real and reactive power for each control iteration k are be computed as

$$u_m(k) = -\frac{\gamma_m \alpha_m}{R_{mm}\gamma_m + X_{mm}}(V_0^2 - V_m^2(k-1)), \tag{5.13}$$

$$v_m(k) = -\frac{\alpha_m}{R_{mm}\gamma_m + X_{mm}}(V_0^2 - V_m^2(k-1)) - e_m, \tag{5.14}$$

for $m \in \mathcal{N}$. The proposed VB-VVW approach is given by (5.13)-(5.14). Considering the control and grid parameters are known, the controllable real and reactive power at each control step k can be locally and autonomously computed in real time behind-the-meter based on the local voltage magnitude V_m and the local reactive power consumption e_m. Note that V_0 is the voltage at node 0, but it can also be a reference value that proportional controllers follow, such as the constant nominal voltage magnitude of the network.

In (5.14), note that when the voltage is close to the nominal ($V_m \approx V_0$), the controllable reactive power fully produces the reactive power consumption of the residential system, i.e., $v_m \approx -e_m$. Locally producing their own reactive power consumption can potentially result in less power flowing in line segments and in turn reduce resistive power losses across the feeder [Turitsyn et al., 2010b]. Now as the voltage deviates from the nominal, v_m gradually deviates from fully supplying the reactive load to perform grid voltage regulation. The controllable real power in (5.13) is only actuated for grid voltage regulation. In the following subsections, we design parameters γ_m and α_m for the VB-VVW approach.

5.3.1 Design of Coupling Factor

We now design parameter γ_m to determine the controllable real to reactive power ratio for voltage regulation. Each node $m \in \mathcal{N}$ locally optimise parameter γ_m to increase efficacy of the voltage regulation. That is, a specific γ_m is designed for each node to perform voltage regulation with less controllable resources and lower power losses in the distribution network. Specifically, the optimisation problem is formulated as:

$$\begin{aligned} \min_{u_m, q_m, \gamma_m} \quad & \big(u_m(k)\big)^2 + \big(q_m(k)\big)^2 \\ \text{s.t.} \quad & (5.11), (5.12), \end{aligned} \tag{5.15}$$

for all $m \in \mathcal{N}$ and control step k. The optimisation problem minimises the usage of real power resources u_m and import/export of the reactive power q_m from/to the grid, obeying the VB-VVW proportional control law. Less import/export of reactive power can potentially reduce the amount of reactive power flowing in line segments and, therefore, reduce grid resistive power losses and alleviate congestion on the distribution network. The constraints (5.11) and (5.12) are the proportional control equations.

Note that optimisation problem (5.15) can be solved locally and has a closed form solution. Combining (5.11) and (5.12) with the objective function in (5.15) gives

$$(\gamma_m^2 + 1)\frac{\big(- \alpha_m E_m(k-1)\big)^2}{(R_{mm}\gamma_m + X_{mm})^2}. \tag{5.16}$$

The minimum can be found by taking the derivative of (5.16) with respect to γ_m and setting it equal to zero. The minimum in (5.15) is obtained when

$$\gamma_m = R_{mm}/X_{mm}, \tag{5.17}$$

for $m \in \mathcal{N}$ and all control iteration k. The optimal value of the coupling coefficient is the R/X ratio of the impedance of the path between the source node and the local node m.

5.3.2 Design of Gain Coefficient for Convergence

To design coefficient α_m, we first formulate the control law for the entire network considering that each node has a participating user with controllable power. We define a diagonal matrix $\boldsymbol{A} \in \mathbb{R}^{\mathrm{N}\times\mathrm{N}}$ in which each diagonal entry is the gain of the respective node as $\boldsymbol{A} := \mathrm{diag}(-\alpha_1, ..., -\alpha_N)$. Similarly, we define a diagonal matrix $\boldsymbol{Y} \in \mathbb{R}^{\mathrm{N}\times\mathrm{N}}$ in which each diagonal entry is the coupling factor of the respective node as $\boldsymbol{Y} := \mathrm{diag}(\gamma_1, ..., \gamma_N)$. We also define diagonal matrices $\boldsymbol{R}_d, \boldsymbol{X}_d \in \mathbb{R}^{\mathrm{N}\times\mathrm{N}}$ in which each diagonal entry is the resistance and reactance of the path, respectively, of the respective node as $\boldsymbol{R}_d := \mathrm{diag}(R_{11}, ..., R_{NN})$ and $\boldsymbol{X}_d := \mathrm{diag}(X_{11}, ..., X_{NN})$. Finally, we can write the local control law in (5.11)-(5.12) for the entire system as:

$$\boldsymbol{R}_d\boldsymbol{u}(k) + \boldsymbol{X}_d\boldsymbol{q}(k) = \boldsymbol{A}\boldsymbol{E}(k-1), \tag{5.18}$$

$$\boldsymbol{u}(k) = \boldsymbol{Y}\boldsymbol{q}(k), \tag{5.19}$$

where $\boldsymbol{q}(k) = \boldsymbol{v}(k) + \boldsymbol{e}$. Combining the linear network model in (5.6) with the control law in (5.18)-(5.19), results in

$$\boldsymbol{E}(k) = \boldsymbol{H}\boldsymbol{A}\boldsymbol{E}(k-1) + \widetilde{\boldsymbol{E}},$$

where $\boldsymbol{H} := (\boldsymbol{R}\boldsymbol{Y} + \boldsymbol{X})(\boldsymbol{R}_d\boldsymbol{Y} + \boldsymbol{X}_d)^{-1}$ and $\widetilde{\boldsymbol{E}} := \boldsymbol{R}(\boldsymbol{d} + \widetilde{\boldsymbol{p}}) + \boldsymbol{X}\widetilde{\boldsymbol{q}}$. Matrix $\boldsymbol{H} \in \mathbb{R}^{\mathrm{N}\times\mathrm{N}}$ represents the impact of the voltage regulation of each node on each other node, whereas vector $\widetilde{\boldsymbol{E}} \in \mathbb{R}^{\mathrm{N}}$ represents the underlying voltage deviation attributed to non-controllable loads, except for the reactive load $\boldsymbol{e}$.

Remark: Matrix $(\boldsymbol{R}_d\boldsymbol{Y} + \boldsymbol{X}_d)$ is invertible and it is the inverse of each entry of the diagonal. Matrix $\boldsymbol{H}$ captures topology and the impedance characteristic of the network and it represents how nodes are coupled across the network in terms of voltage regulation. It can be seen that the diagonal of $\boldsymbol{H}$ is composed of ones, meaning that a voltage regulation at node m fully reflects on node m itself. The special case of a radial feeder with no laterals results in a matrix $\boldsymbol{H}$ where the entire lower triangular is equal to one, meaning that every upstream node has full voltage regulation impact on its downstream nodes.

Finally, we can write the system model with the proportional control in the state space format as follows:

$$\boldsymbol{E}(k+1) = \boldsymbol{H}\boldsymbol{A}\boldsymbol{E}(k) + \widetilde{\boldsymbol{E}}. \tag{5.20}$$

Similar to [Baker et al., 2018], during the fast actuation of the electronic power inverters to regulate the voltage, we consider in (5.20) that the non-controllable load does not change significantly.

The system in (5.20) achieves asymptotic stability and convergence to steady-state voltages when [Singhal et al., 2019; Cavraro and Carli, 2018; Baker et al., 2018],

$$\rho(\boldsymbol{H}\boldsymbol{A}) < 1, \tag{5.21}$$

where $\rho(\cdot)$ is the spectral radius defined as $\rho(\boldsymbol{M}) := \max\{|\lambda_1|, ..., |\lambda_N|\}$, with matrix $\boldsymbol{M} \in \mathbb{R}^{\mathrm{N}\times\mathrm{N}}$ and $\lambda_1, ..., \lambda_N$ as the eigenvalues of $\boldsymbol{M}$. For simplicity, we consider that coefficient $\alpha_m = \alpha$, $\forall m \in \mathcal{N}$. As such, we have that $\boldsymbol{A} = -\alpha\boldsymbol{I}$, where $\boldsymbol{I}$ is the $\mathrm{N} \times \mathrm{N}$ identity matrix. From (5.21) we can then directly compute coefficient α as:

$$\alpha < \overline{\alpha} = \frac{1}{\rho(\boldsymbol{H})}, \tag{5.22}$$

where $\overline{\alpha}$ is the critical gain coefficient in which the system presents marginal stability. For any value of $\alpha < \overline{\alpha}$, the linear system in (5.20) is proved to converge [Singhal et al., 2019; Cavraro and Carli, 2018; Baker et al., 2018].

5.3.3 Performance Index

Considering that the total resistive power loss in the network can be computed as [Turitsyn et al., 2010b]

$$L = \sum_{(m,n)\in\mathcal{E}} r_{mn} \frac{P_{mn}^2 + Q_{mn}^2}{V_m^2}, \tag{5.23}$$

we introduce a performance index σ to measure efficacy of the voltage regulation. Index σ, also termed loss reduction per voltage regulated (LRVR) index, indicates how much power loss is reduced on the entire network for each unit of regulated voltage in the network. Specifically,

$$\sigma = \frac{L^{bl} - L^{reg}}{\sum_{n \in \mathcal{N}} \left(|V_0 - V_n^{bl}| - |V_0 - V_n^{reg}| \right)}, \tag{5.24}$$

where L^{bl} and L^{reg} is the total resistive power loss in the network as in (5.23) for the baseline case (no control) and the case with voltage regulation, respectively. Similarly, V_n^{bl} and V_n^{reg} is the voltage magnitude at node $n \in \mathcal{N}$ for the baseline case (no control) and the case with voltage regulation, respectively.

Considering the overall regulated voltage with the proportional controllers is closer to the nominal than the baseline voltage, the denominator in (5.24) is always positive. Therefore, positive values of σ represents loss reduction for each unit of voltage regulation in the network, whereas negative values represents loss increase for each unit of voltage regulation in the network. LRVR values close to zero represent that the grid voltage was regulated with small impact on the grid power loss, compared to the no control case.

5.4 Benchmark Approach

A benchmark approach with the conventional formulation is presented for a volt-var-watt proportional controller. Here, the controllable real and reactive power are computed as [Baker et al., 2018]

$$u_m(k) = -g_m^u(V_0 - V_m(k-1)), \tag{5.25}$$

$$v_m(k) = -g_m^v(V_0 - V_m(k-1)), \tag{5.26}$$

where g_m^u and g_m^v are the controller gain for the real and reactive power, respectively. The controller is designed based on the linear equations (5.1)-(5.2) and the linear voltage equation presented in [von Meier et al., 2020] as

$$V_m = V_n + r_{mn}P_{mn} + x_{mn}Q_{mn}, \quad \forall (m,n) \in \mathcal{E}. \tag{5.27}$$

In order to compute the critical gain directly and design the controller gains, we make $g_m^u = g_m^v = g$ for all $m \in \mathcal{N}$. The critical gain $\overline{g}$ for marginal stability can then be easily obtained by following similar steps presented for the design of coefficient α in (5.22).

5.5 Numerical Simulations

Numerical simulations are carried out in a realistic 8-node ($N+1=8$) low-voltage feeder [Zeraati et al., 2018; Mediwaththe and Blackhall, 2021]. Node 0 is assigned as the slack bus with single-phase nominal voltage of 230 V (1 p.u.). The distribution feeder is populated with real-world, time-varying data of de-identified residential systems with solar PV generation from the NextGen dataset [Shaw et al., 2019]. The reactive power demand was obtained by assuming a constant power factor of 0.90, and all loads are modelled as constant power loads. Two residential systems are connected at each of the downstream nodes, resulting in a total of 14 users on the feeder. One residential system at each node (50% of users) has controllable DER with abundant controllable real and reactive power to investigate the full potential of each approach [Arnold et al., 2016].

Numerical simulations are carried out with the full non-linear power flow model [Garcia et al., 2000] and also with the linear model (5.1)-(5.3) used to design the coefficients of the proportional controllers. The critical gain coefficient is $\overline{\alpha} = 0.21$ p.u. for the proposed approach and $\overline{g} = 0.23$ kVA/V for the conventional volt-var-watt approach in (5.25)-(5.26). We also consider the pure volt-var approach ($u_m = 0$ in (5.25)-(5.26)), which results in $\overline{g} = 1.15$ kvar/V. We first present numerical simulations on the convergence performance of the proposed approach (VB-VVW) for voltage regulation.

5.5.1 Convergence Performance of the VB-VVW

Fig. 5.3 presents the voltage magnitude at node 7 and the proximity of the linear model (dashed lines) to the exact non-linear model (solid lines) for larger and smaller values of coefficient α. Fig. 5.3(a) illustrates the case that controllers are regulating a significant voltage drop, whereas Fig. 5.3(b) illustrates the case of a significant voltage rise. Observe that smaller coefficients converge to the steady-state voltage with fewer iterations, whereas larger coefficients result in more iterations before convergence, as expected. In contrast, large gain coefficients result in steady-state voltages closer to the nominal, whereas smaller coefficients result in larger voltage deviations and potentially in insufficient voltage regulation.

It is worth mentioning that for each iteration k the local controller can quickly measure, compute and actuate real and reactive power, taking approximately 100 milliseconds to complete each control step k [Baker et al., 2018; Maharjan et al., 2021]. In Fig. 5.3, we also observe a close match between the linear and the non-linear power flow models. To exacerbate the dynamic response in Fig. 5.3, the initial values of the controllable variables

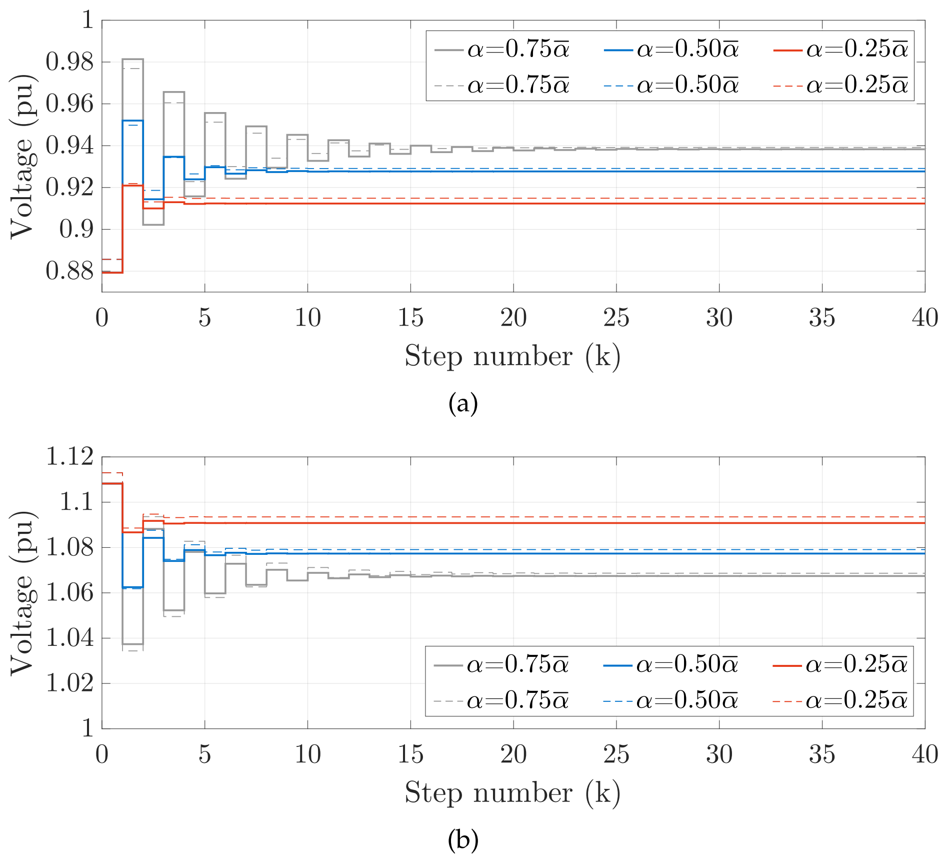

Figure 5.3: Voltage magnitude behavior at node 7 for different values of coefficient α for the VB-VVW approach: Voltage regulation of (a) voltage drop and (b) voltage rise case in the network. Dashed lines represent the linear model, whereas solid lines represent the exact non-linear model.

are considered as zero, i.e., $u_m(0) = v_m(0) = 0,\ \forall m \in \mathcal{N}$.

Fig. 5.4 illustrates the same case presented Fig. 5.3(b) with coefficient $\alpha = 0.75\overline{\alpha}$ for initial values equal to zero (grey lines) and where initial values are the steady-state values of the previous time step (blue lines). The case where initial values are as in the previous time step, the convergence is quicker and the voltage oscillations are much less significant.

5.5.2 Steady-State Results and Comparisons

We now compare four different approaches for the steady-state results. The baseline approach represents the case with no voltage regulation (no control); volt-var is the case with only reactive power and volt-var-watt is the case with real and reactive power with the conventional formulation; and VB-VVW is the proposed approach. In what follows, the exact non-linear power flow

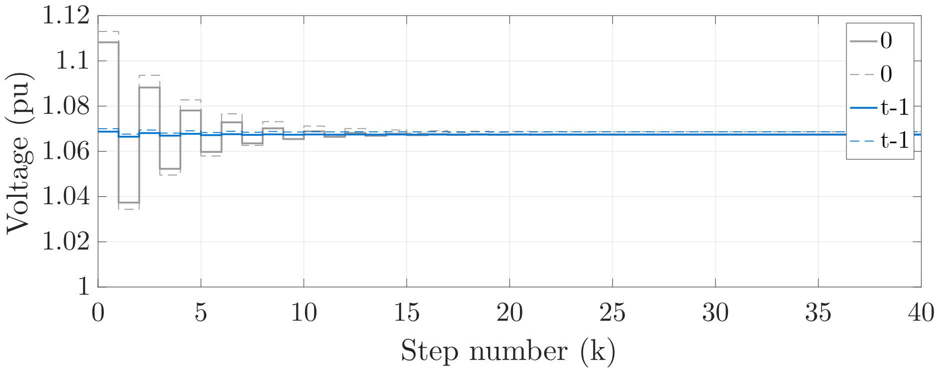

Figure 5.4: Voltage magnitude behavior at node 7 with coefficient $\alpha = 0.75\overline{\alpha}$ for the VB-VVW approach with initial values for u_m and v_m as zero (gray lines) and as the steady-state value of the previous time step (blue lines). Dashed lines represent the linear model, whereas solid lines represent the exact non-linear model.

model is used to run numerical simulations.

Fig. 5.5 illustrates the steady-state simulation results for an entire day with severe voltage deviations and power losses on the feeder. Fig. 5.5(a) illustrates the range of all voltages V_m, $m \in \mathcal{N}$, and Fig. 5.5(b) illustrates total grid power losses. Fig. 5.5(c) illustrates the controllable real (solid lines) and reactive (dashed lines) power for a participating user at node 7. The gain coefficients of all approaches are tuned to 50% of their own critical value.

In Fig. 5.5(a) we observe that all approaches provided similar voltage regulation on the grid, since they all have the same relative gain coefficient, driving grid voltages to within 0.90 and 1.10 values. However, observe in Fig. 5.5(b) that the volt-var approach resulted in a significant increase in grid power losses compared to the baseline. In contrast, both approaches that includes real power for voltage regulation resulted in smaller power losses compared to the baseline. VB-VVW resulted in smaller grid power losses particularly during peak PV generation. In Fig. 5.5(c) the pure volt-var approach resulted in large amount of reactive power control to provide voltage regulation. The VB-VVW approach presented less real and reactive power control at node 7 compared to the other approaches.

Table 5.1 presents the LRVR index for different days and gain coefficients for the exact non-linear model for steady-state results. The volt-var approach presented negative LRVR for all cases, except for Day 2 with gain as 0.25 of the critical. Such negative values are in accordance with Fig. 5.5, where the voltage regulation on the grid came at the cost of greater power losses. In contrast, both approaches with real and reactive power for voltage regulation resulted in positive LRVR, meaning a loss reduction in the network while performing voltage regulation. VB-VVW presented higher LRVR values for

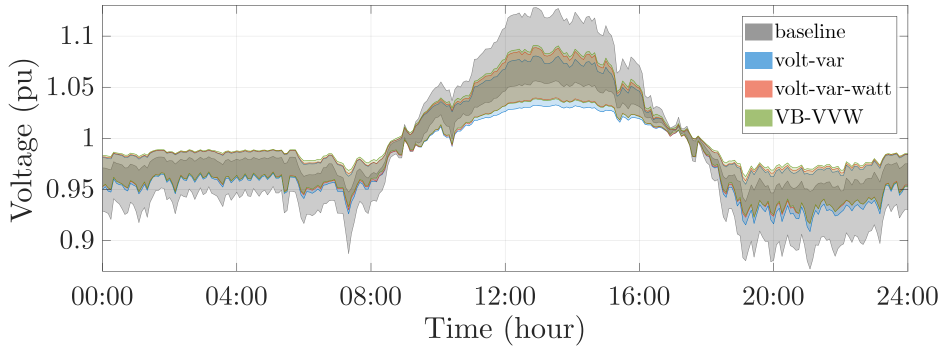

(a)

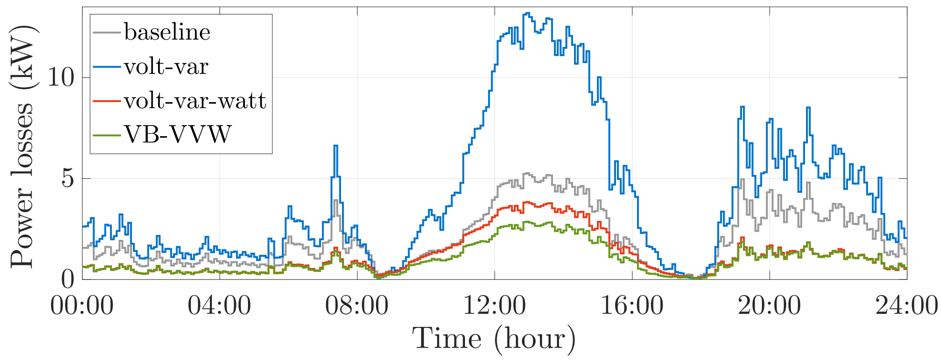

(b)

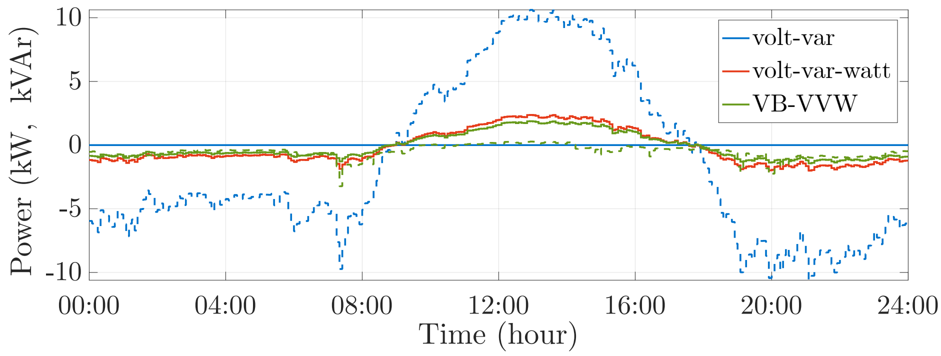

(c)

Figure 5.5: Steady-state results for gain coefficient of 0.50 of the critical: (a) Voltage magnitude of the entire network; (b) total resistive power losses in the network; and (c) controllable real (u_m, solid lines) and reactive (v_m, dashed lines) power of participating user at node 7. Reported values are from the exact non-linear model.

all cases, suggesting higher efficacy for voltage regulation on the distribution network. We can also observe that, in general, smaller gain values result in higher efficacy, that is, more loss reduction per unit of voltage regulated in the distribution network. As in Table 5.1, the LRVR index for higher gains of the volt-var approach was not possible to compute due to non-convergence to

Table 5.1: LRVR index for different gains and days.

Day	Gain	volt-var	volt-var-watt	VB-VVW
Day 1	0.75	N/A	5.99	7.58
	0.50	-16.24	6.58	8.10
	0.25	-6.57	7.40	9.07
Day 2	0.75	N/A	8.13	8.37
	0.50	-13.22	8.77	9.00
	0.25	0.50	9.72	10.12

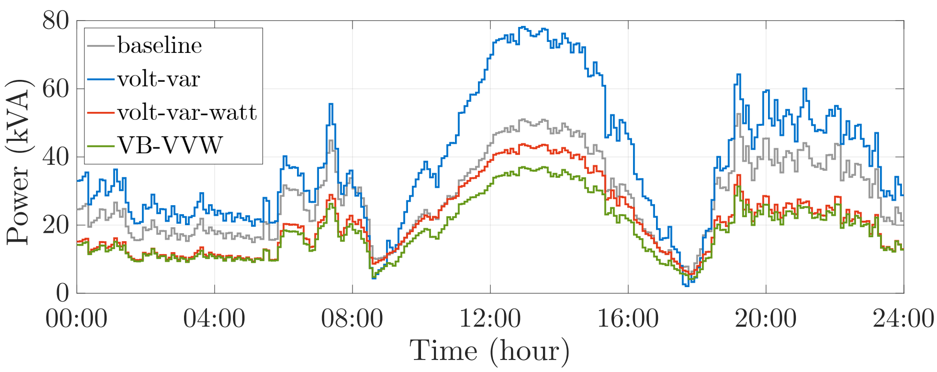

Figure 5.6: Steady-state apparent power provided by substation bus with gain coefficient as 0.50 of the critical value. Reported values are from the exact non-linear power flow model.

steady-state voltages with the exact non-linear model. The non-convergence of the pure volt-var case is correlated with periods of high grid power losses.

Fig. 5.6 presents the substation apparent power for all four cases for the same day as in Fig. 5.5. Observe that, similar to the grid resistive power loss in Fig. 5.5(b), the volt-var results in increased apparent power through the head of the feeder compared to the baseline case. In contrast, the VB-VVW approach presented reduced apparent power at the head of the feeder, potentially contributing to reduce congestion in the distribution network.

5.6 Conclusion

In this chapter, we propose a network-cognisant formulation for the proportional VVW control for effective real-time voltage regulation. The VB-VVW approach takes into account the LinDistFlow model to incorporate the impedance information of the network in the control algorithm. The coefficients of the VB-VVW are designed to provide convergence and are locally optimised to reduce grid power losses in the distribution network.

Numerical simulations with the exact non-linear network model have shown convergence to steady-state voltages and greater loss reduction per unit of regulated voltage when employing the VB-VVW control. With locally tuned coefficients and local and autonomous actuation for voltage regulation, the proposed approach can be easily scaled up to larger distribution networks. Interesting options for further investigation in the context of this chapter are: extend the formulation to mesh distribution networks; and design globally optimal coefficients for proportional VVW control.

In this chapter, the gain coefficients are designed analytically based on the stability criterion. Note that no specific optimal value is given, but rather a range of values that preserve system stability ($\alpha < \overline{\alpha}$). The real to reactive power control ratio is optimised based on a local optimisation problem, which only considers variables within the participating user perimeter.

In the next chapter, we present a central (global) optimisation problem to design coefficients of the proportional VVW local control. The global optimisation problem gives specific optimal gain coefficients for every DER and considers not only the impedance characteristic of the network, but also the operating state of the entire distribution network. The system-wide optimisation problem computes new coefficients at the minute timescale and send them to the local VVW controllers, which in turn provide voltage regulation at the millisecond timescale. This central-local control approach is proposed and discussed in more detail in the next chapter.

Chapter 6

Central-Local Control Approach: System-Wide Optimisation for Gain Coefficients of Local Proportional Controllers

In this chapter, we propose a combined global-local control approach to perform voltage regulation and minimise power losses in distribution networks with high integration of DERs. Local controllers embed the fast acting proportional volt-var-watt (VVW) control law and have their gain (slope) coefficients updated regularly by a global optimisation problem at a slower timescale.

Optimal gain coefficients preserve overall system stability and encapsulate inverter and energy limits of controllable DERs. The proposed approach is formulated based on the linear network model (LinDistFlow) and suitable approximations to produce a convex multi-period optimisation problem. Numerical simulations with real-world customer data and two different distribution feeders revealed that our approach provides substantial voltage regulation, while reducing losses by 11 per cent and peak substation power by 26 per cent compared to other state-of-the-art algorithms.

This chapter fully describes the paper in preparation [de Carvalho et al., 2024]. This chapter is organised as follows. Section 6.1 presents the motivation, literature review and the main problems to be investigated in this chapter. Section 6.2 presents the notation and linear model for distribution networks of this chapter. Section 6.3 presents the control law equations and stability criterion. Section 6.4 introduces the original non-convex optimisation problem and approximations to formulate the convex, multi-period optimisation. Section 6.5 describes the receding-horizon method to run the time-horizon approach. In Section 6.6, two benchmark approaches to design gain coefficients are described. Numerical simulations are presented in Section 6.7 and conclusions of this chapter drawn in Section 6.8.

List of Main Symbols – Chapter 6

$\boldsymbol{A}$	Diagonal matrix with proportional gains for real power
$\boldsymbol{B}$	Diagonal matrix with proportional gains for reactive power
$\boldsymbol{D}$	Node-arc incidence matrix
E_m	Voltage deviation at node m relative to the reference
$\boldsymbol{E}$	Voltage deviation vector
$\widetilde{\boldsymbol{E}}$	Underlying voltage deviation vector
$\mathcal{E}$	Set of all line segments on the network
g	Gain coefficient of proportional control of Direct approach
$\boldsymbol{G}$	Gain matrix
$\boldsymbol{H}$	Resistance and reactance matrix
I_{mn}	Current magnitude in line segment (m, n)
$\boldsymbol{I}$	Identity matrix
k	Control iteration index
$\boldsymbol{L}$	Lower triangular matrix composed of time lengths
$\mathcal{L}_m$	Set of line segments in the unique path from node 0 to node m
N	Total number of nodes downstream of the slack bus
$\mathcal{N}_o$	Set of all nodes on the network defined as $\{0, 1, ..., l, m, n, ..., N\}$
$\mathcal{N}$	Set of downstream nodes defined as $\{1, ..., l, m, n, ..., N\}$
$\widetilde{p}_m$	Non-controllable real load at node m
$\widetilde{\boldsymbol{p}}$	Vector of non-controllable real load of nodes
P_{mn}	Real power flow in line segment (m, n)
$\boldsymbol{P}$	Vector of real power in line segments of the network

$\widetilde{q}_m$	Non-controllable reactive load at node m
$\widetilde{\boldsymbol{q}}$	Vector of non-controllable reactive load of nodes
Q_{mn}	Reactive power flow in line segment (m, n)
$\boldsymbol{Q}$	Vector of reactive power in line segments of the network
r_{mn}	Resistance of line segment (m, n)
$\boldsymbol{R}$	Resistance matrix
$\overline{s}_m$	Maximum charge level of battery storage at node m
$\underline{s}_m$	Minimum charge level of battery storage at node m
s_m	Initial charge level of battery storage at node m
$\hat{s}_m$	Scheduled final charge level of battery storage at node m
t	Discrete time index
T	Total number of time steps in the horizon
$\mathcal{T}$	Set of discrete time defined as $\{1, 2, ..., t, ..., T\}$
u_m	Controllable real power at node m
$\boldsymbol{u}_m$	Vector of controllable real power at node m over time steps
$\boldsymbol{u}$	Vector of controllable real power of nodes
v_m	Controllable reactive power at node m
$\boldsymbol{v}$	Vector of controllable reactive power of nodes
V_m	Voltage magnitude at node m
V_0	Reference voltage magnitude (voltage magnitude at node 0)
$\overline{w}_m$	Rated apparent power of controllable inverter
x_{mn}	Reactance of line segment (m, n)
$\boldsymbol{X}$	Reactance matrix

α_m	Proportional gain coefficient for controllable real power
β_m	Proportional gain coefficient for controllable reactive power
Δ	Time length of a time interval
ϵ	Stability margin
$\rho(\cdot)$	Spectral radius of matrix (maximum absolute eigenvalue of matrix)
$\|\cdot\|_F$	Frobenius norm of matrix

6.1 Introduction

As prices steadily drop for low-carbon technologies, distribution networks are undergoing a massive uptake of DERs such as solar PV, battery storage and EVs [NREL, 2019a; IEA, 2022]. If not properly coordinated, DERs introduce unprecedented variability and technical challenges in distribution grids, including undesirable voltage deviations, power losses and peak demands [IEA, 2022]. Excess PV generation can cause adverse voltage rise, whereas EV charging can intensify voltage drop during peak demand and push grid voltages beyond operating limits [ENEA et al., 2020]. When properly controlled, the same DERs provide many opportunities to overcome such operational challenges [Zeraati et al., 2018].

Control approaches of DERs can simply be categorised as system-wide communication-based approaches (e.g. centralised approaches) or autonomous/local approaches. A central optimisation problem has been formulated in [Arnold et al., 2016] to control DERs in the distribution grid to provide voltage regulation and balancing. Similarly, a central OPF-based approach is proposed in [Nazir and Almassalkhi, 2021] to minimise voltage deviation with DERs and legacy devices. Other centralised approaches are presented in [Torbaghan et al., 2020; Robbins and Dominguez-Garcia, 2016; Joo et al., 2017]. While central approaches provide system-wide optimal performance, solving global optimisation problems can be insufficiently fast to respond to quick load and generation variations [Antoniadou-Plytaria et al., 2017].

Local (fully decentralised) approaches act fast and autonomously to voltage variations, while offering simple and scalable implementation [Alonso et al., 2022]. Various local control approaches have been presented in this thesis and in [Procopiou et al., 2019; Cavraro and Carli, 2018; Singhal et al., 2019; Farivar et al., 2013; Zhou et al., 2021; Zhu and Liu, 2016] to control real and reactive power to reduce grid voltage deviations. Local approaches lack system-wide visibility and thus often achieve lower overall performance when compared to central approaches [Antoniadou-Plytaria et al., 2017].

A combination of both categories, where parameters of fast local controllers are regularly updated by global optimisation problems with a slower timescale, often achieve better outcomes [NREL, 2019b; Annaswamy et al., 2023]. Combined central-local approaches are proposed in [Alonso et al., 2022; Abadi et al., 2021; Maharjan et al., 2021; Baker et al., 2018]. In [Abadi et al., 2021; Maharjan et al., 2021] local controllers respond with reactive power to voltage deviations and receive updated parameters from global optimisation problems. In [Baker et al., 2018], proportional gains of local VVW controllers are updated regularly by a global optimisation that minimises grid voltage deviations.

Controlling power from many DERs across the network for voltage regulation can intensify grid power losses and impact system stability. Nonetheless, aforementioned works do not explicitly account for power losses in the design of proportional controllers. Losses are considered in [Abadi et al., 2021] yet only for a base parameter where no control is required and the design of gain coefficients neglects a stability criterion. Disregarding stability constraints can lead to sustained grid voltage oscillations and interactions between inverters [Baker et al., 2018]. Aforementioned approaches also do not consider a multi-period optimisation with future time horizons to design proportional gains, which is critical when considering DERs with limited energy reserve such as battery storage and EVs.

In this chapter, we propose a combined global-local approach to provide grid voltage regulation, while minimising grid power losses, keeping overall system stability, and incorporating DERs limits in a multi-period (time-horizon) framework. Local controllers follow the VVW proportional control law, responding fast and autonomously with real and reactive power changes to local voltage measurements. Optimal proportional gains are provided regularly at a slower time-scale by a global OPF-based optimisation problem. The optimisation is formulated with the LinDistFlow and valid approximations to result in a convex problem. The two-layer control approach proposed in this chapter is referred to as optimal-power-flow-based proportional control (OPF-PC).

The main contributions of this chapter are: The computation of globally optimal coefficients for local VVW proportional controllers that (i) minimise grid power losses while performing voltage regulation; (ii) provide overall system stability (convergence to steady-state voltages) and encapsulate inverter and energy constraints of DERs; (iii) are updated regularly based on a convex multi-period optimisation solved in a receding-horizon fashion. Compared to other approaches to design proportional gains of local controllers, OPF-PC have shown significant improvement of grid operation.

6.2 Preliminaries

A radial distribution network is modelled as a connected graph with $1 + N$ nodes as in Fig. 6.1 (repeated here for convenience). Node 0 represents the slack (substation) bus and N is the number of downstream nodes. Similar to the previous chapter, let $\mathcal{N} := \{1, ..., l, m, n, ..., N\}$ denote the set of all downstream nodes and $\mathcal{E}$ the set of all line segments of the distribution network.

Fig. 6.2 illustrates the notation of the distribution network in this chapter.

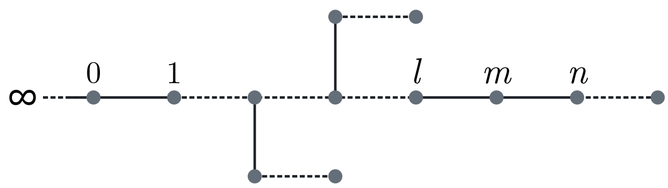

Figure 6.1: Distribution network represented by a connected graph.

Let r_{lm} denote the resistance and x_{lm} the reactance of line segment $(l, m) \in \mathcal{E}$. The real power flowing in the line segment $(l, m) \in \mathcal{E}$ is denoted by P_{lm} and the reactive power by Q_{lm}. Voltage magnitude is denoted by V_m and load is divided between controllable and non-controllable load, at each node $m \in \mathcal{N}$. The non-controllable real and reactive load is represented by $\widetilde{p}_m$ and $\widetilde{q}_m$, respectively. The controllable resource is represented by an inverter-based energy storage device, with real (u_m) and reactive (v_m) power available to promptly respond to local voltage deviations.

Power flow equations to model radial distribution networks are complex and originally non-linear. optimisation problems with such equations are cast as a non-convex problem, which presents poor scalability and solving efficiency and cannot guarantee the global minimiser [Borrelli et al., 2017]. We again consider the established LinDistFlow equations [Baran and Wu, 1989a] to model the network within our control approach. The linear model supports the development of convex optimisation problems and facilitates the design of feedback controller gains for overall system stability, and typically provides errors smaller than 1 per cent relative to its non-linear counterpart [Farivar et al., 2013]. The LinDistFlow equations with our notation in Fig. 6.2 are as follows:

$$P_{lm} = u_m + \widetilde{p}_m + \sum_{n:(m,n)\in\mathcal{E}} P_{mn}, \quad \forall m \in \mathcal{N}, \tag{6.1}$$

$$Q_{lm} = v_m + \widetilde{q}_m + \sum_{n:(m,n)\in\mathcal{E}} Q_{mn}, \quad \forall m \in \mathcal{N}, \tag{6.2}$$

$$V_m^2 = V_n^2 + 2r_{mn}P_{mn} + 2x_{mn}Q_{mn}, \quad \forall (m,n) \in \mathcal{E}. \tag{6.3}$$

As in the previous chapter, let $\mathcal{L}_m \subseteq \mathcal{E}$ be the set with line segments of the unique path from node 0 to node m, as in [Lin and Bitar, 2018; Farivar et al., 2013]. We then compose the resistance and reactance matrix $\boldsymbol{R}, \boldsymbol{X} \in \mathbb{R}^{\mathrm{N}\times\mathrm{N}}$ with their entries obtained as

$$R_{ij} = \sum_{(m,n)\in\mathcal{L}_i\cap\mathcal{L}_j} 2r_{mn}, \quad X_{ij} = \sum_{(m,n)\in\mathcal{L}_i\cap\mathcal{L}_j} 2x_{mn}, \tag{6.4}$$

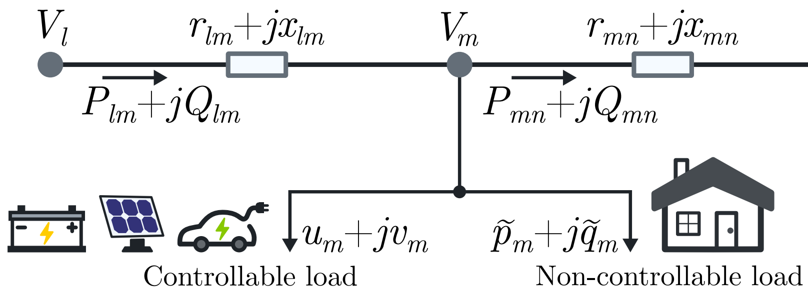

Figure 6.2: Distribution network notation, with arrows indicating direction of positive power flow. Battery energy storage, solar PV and EVs are examples of DERs that can be used as controllable resources.

where i and j represent here the row and column number of the matrices. For each node $m \in \mathcal{N}$, define voltage deviation as $E_m := V_0^2 - V_m^2$, where V_0 is the voltage magnitude at node 0 at the reference value of 1 p.u. As in [Lin and Bitar, 2018; Farivar et al., 2013], the LinDistFlow voltage equation is then written for the entire network in matrix format as

$$\boldsymbol{E} = \boldsymbol{R}(\boldsymbol{u} + \widetilde{\boldsymbol{p}}) + \boldsymbol{X}(\boldsymbol{v} + \widetilde{\boldsymbol{q}}), \tag{6.5}$$

where $\boldsymbol{E}$, $\boldsymbol{u}$, $\boldsymbol{v}$, $\widetilde{\boldsymbol{p}}$, $\widetilde{\boldsymbol{q}} \in \mathbb{R}^{\mathrm{N}}$ are column vectors collecting the variables of each node $m \in \mathcal{N}$ (e.g., $\boldsymbol{u} = [u_1, u_2, ..., u_N]'$). Let $\widetilde{\boldsymbol{E}} := \boldsymbol{R}\widetilde{\boldsymbol{p}} + \boldsymbol{X}\widetilde{\boldsymbol{q}}$ be the underlying voltage deviation due to uncontrollable load and rearrange (6.5) as

$$\boldsymbol{E} = \boldsymbol{R}\boldsymbol{u} + \boldsymbol{X}\boldsymbol{v} + \widetilde{\boldsymbol{E}}. \tag{6.6}$$

We define the node-arc incidence matrix $\boldsymbol{D}$ where each row corresponds to a node $m \in \mathcal{N}$ and each column correspond to a line segment $(m, n) \in \mathcal{E}$. Each column $(m, n) \in \mathcal{E}$ in the matrix $\boldsymbol{D}$ has $+1$ in the row m, -1 in the row n and 0 for the other entries [Ahuja et al., 1993]. As such, we also write the real and reactive power balance equations (6.1)-(6.2) in matrix format as:

$$\boldsymbol{D}\boldsymbol{P} + \boldsymbol{u} + \widetilde{\boldsymbol{p}} = 0, \tag{6.7}$$

$$\boldsymbol{D}\boldsymbol{Q} + \boldsymbol{v} + \widetilde{\boldsymbol{q}} = 0, \tag{6.8}$$

where $\boldsymbol{P}$ and $\boldsymbol{Q}$ are the vectors stacking P_{mn} and Q_{mn}, respectively, for every line segment $(m, n) \in \mathcal{E}$.

6.3 Proportional Feedback Control

We now formulate the proportional VVW control for voltage regulation. The classic proportional control law [Åström and Murray, 2020] is used for both real and reactive power, where the linear slope is centered at the reference (nominal voltage). Specifically,

$$u_m(k) = -\alpha_m E_m(k-1), \tag{6.9}$$

$$v_m(k) = -\beta_m E_m(k-1), \tag{6.10}$$

where k is the control iteration index, $\alpha_m \geq 0$ is the gain coefficient for the controllable real power and $\beta_m \geq 0$ is the gain coefficient for the controllable reactive power. Coefficients are non-negative to ensure local controllers counteract voltage deviations. That is, controllers inject power into the grid to counteract voltage drop; and conversely, controllers absorb power from the grid to counteract voltage rise.

We aim to obtain globally optimal values for α_m and β_m for every $m \in \mathcal{N}$. It is worth mentioning that, as opposed to the previous chapter, the ratio of real to reactive power control is implicitly given here when obtaining globally optimal values for α_m and β_m. In this chapter we design a specific coefficient for real power control and a specific coefficient for reactive power control. The global optimisation problem prioritises real or reactive power depending on the grid impedance, location of DER, operating state of the grid, etc.

Recall that $E_m = V_0^2 - V_m^2$ is the voltage deviation and computed by measuring the local voltage V_m. Therefore, with given α_m and β_m values from an optimisation problem, the controllable real and reactive power in (6.9)-(6.10) are locally, autonomously, and quickly computed for voltage regulation.

Note that we formulate the general VVW problem where both controllable real and reactive power are considered. A volt-var control approach considering only controllable reactive power can easily be obtained from this mathematical framework by making $\alpha_m = 0$, $\forall m \in \mathcal{N}$.

6.3.1 System-Wide Equations: Network with Feedback Control

Define a diagonal matrix $\boldsymbol{A} \in \mathbb{R}^{\mathrm{N}\times\mathrm{N}}$ in which each diagonal entry is the gain of the respective node as $\boldsymbol{A} := \mathrm{diag}(-\alpha_1, ..., -\alpha_N)$. Similarly, define $\boldsymbol{B} := \mathrm{diag}(-\beta_1, ..., -\beta_N)$, where $\boldsymbol{B} \in \mathbb{R}^{\mathrm{N}\times\mathrm{N}}$. Finally, we write the local control law in (6.9)-(6.10) for the entire network as:

$$\boldsymbol{u}(k) = \boldsymbol{A}\boldsymbol{E}(k-1), \tag{6.11}$$

$$\boldsymbol{v}(k) = \boldsymbol{B}\boldsymbol{E}(k-1). \tag{6.12}$$

Combining the linear network model (6.6) with the control law (6.11)-(6.12), results in

$$\boldsymbol{E}(k) = (\boldsymbol{R}\boldsymbol{A} + \boldsymbol{X}\boldsymbol{B})\boldsymbol{E}(k-1) + \widetilde{\boldsymbol{E}}. \tag{6.13}$$

Rearrange (6.13) as

$$\boldsymbol{E}(k) = \boldsymbol{H}\boldsymbol{G}\boldsymbol{E}(k-1) + \widetilde{\boldsymbol{E}}, \tag{6.14}$$

where

$$\boldsymbol{H} := [\boldsymbol{R}\ \boldsymbol{X}], \quad \boldsymbol{G} := \begin{bmatrix} \boldsymbol{A} \\ \boldsymbol{B} \end{bmatrix}, \tag{6.15}$$

with $\boldsymbol{H} \in \mathbb{R}^{N\times 2N}$ and $\boldsymbol{G} \in \mathbb{R}^{2N\times N}$. Finally, we write the system model with control in the state space format as

$$\boldsymbol{E}(k+1) = \boldsymbol{H}\boldsymbol{G}\boldsymbol{E}(k) + \widetilde{\boldsymbol{E}}. \tag{6.16}$$

As in [Baker et al., 2018; Cavraro and Carli, 2018; Singhal et al., 2019], during the fast actuation of electronic power inverters, we consider that the non-controllable load (and thus $\widetilde{\boldsymbol{E}}$) is practically constant. The system in (6.16) achieves asymptotic stability and convergence to steady-state voltages when

$$\rho(\boldsymbol{H}\boldsymbol{G}) < 1, \tag{6.17}$$

where $\rho(\cdot)$ is the spectral radius defined as the maximum absolute eigenvalue of the matrix. For any value of $\boldsymbol{G}$, in which $\rho(\boldsymbol{H}\boldsymbol{G}) < 1$, the linear system (6.16) is proved to converge to steady-state voltages [Singhal et al., 2019; Cavraro and Carli, 2018; Baker et al., 2018]. Since (6.17) holds, the system (6.16) converges to the steady-state equation

$$\boldsymbol{E} = \boldsymbol{H}\boldsymbol{G}\boldsymbol{E} + \widetilde{\boldsymbol{E}}, \tag{6.18}$$

and the control equations (6.11)-(6.12) converges to

$$\boldsymbol{u} = \boldsymbol{A}\boldsymbol{E}, \tag{6.19}$$

$$v = BE. \tag{6.20}$$

In the following section, we design gain parameters with the proposed optimisation problem.

6.4 Problem Formulation

We formulate a global optimisation problem to design proportional gain coefficients of all controllable DERs on the grid. The coefficients are designed to minimise resistive power losses of the entire distribution network, while still providing voltage regulation and stability. The resistive power loss in a line segment $(m, n) \in \mathcal{E}$ is computed as $r_{mn} I_{mn}^2$, where I_{mn} is the current magnitude. We substitute the current magnitude using the complex power equation and formulate the optimisation problem as

$$\begin{aligned} \min_{\boldsymbol{A},\boldsymbol{B}} \quad & \sum_{(m,n)\in\mathcal{E}} r_{mn} \frac{(P_{mn}^2 + Q_{mn}^2)}{V_m^2} \\ \text{s.t.} \quad & (6.6), (6.7), (6.8), (6.17), (6.19), (6.20), \\ & \boldsymbol{A} \leq 0, \\ & \boldsymbol{B} \leq 0. \end{aligned} \tag{6.21}$$

The constraints of optimisation problem (6.21) are: linear network model (6.6)-(6.8), system stability (6.17), steady-state proportional control law for real and reactive power (6.19) and (6.20) and non-negative proportional gains. Coefficients $\boldsymbol{A}, \boldsymbol{B}$ are the only decision variables of interest. Other unknowns of (6.21) are $\boldsymbol{E}, \boldsymbol{P}, \boldsymbol{Q}, \boldsymbol{u}, \boldsymbol{v}$. The optimisation problem seeks to minimise resistive power losses in all line segments. Since high power loss is usually caused by periods of peak power demand/export, this objective function also has the effect of flattening the power curve, reducing power peaks and thus preventing congestion in the distribution network. The objective function of (6.21) and constraints (6.17), (6.19), (6.20) lead to a non-convex optimisation problem. In what follows, we use valid approximations of such equations to formulate a convex optimisation problem.

As in [Baran and Wu, 1989b; Turitsyn et al., 2011; Šulc et al., 2014], we approximate the loss equation in (6.21) by $r_{mn}(P_{mn}^2 + Q_{mn}^2)$ as voltage magnitude has to be kept around the nominal value ($V_m \approx 1$). With this approximation, the cost function becomes quadratic and convex. The non-convex bilinear equality constraints (6.19)-(6.20) are linearised by a Taylor expansion around $\boldsymbol{u} = \boldsymbol{v} = 0$ and $\boldsymbol{E} = \widetilde{\boldsymbol{E}}$. Such linearisation results in $\boldsymbol{u} = \boldsymbol{A}\widetilde{\boldsymbol{E}}$ for the real power and $\boldsymbol{v} = \boldsymbol{B}\widetilde{\boldsymbol{E}}$ for the reactive power. Other options to linearise the bilinear constraints can be formulated based on Taylor expansion around the steady-state values of the previous time step, or to approximate with McCormick relaxations.

As in [Baker et al., 2018], we represent the stability constraint with the Frobenius norm. Matrix norm is an upper bound on the spectral radius and it holds that $\rho(\boldsymbol{HG}) = \rho(\boldsymbol{GH}) \leq \|\boldsymbol{GH}\|_F$. An approximation for the stability constraint is then $\|\boldsymbol{GH}\|_F < 1$. Finally, in order to make it a closed set constraint, the stability constraint is written as $\|\boldsymbol{GH}\|_F \leq 1 - \epsilon$, where $0 < \epsilon \leq 1$ is the stability margin [Baker et al., 2018]. Note that the Frobenius norm boils down to a summation of quadratic terms and thus the stability constraint can be written as a quadratic inequality constraint. Other matrix norms are also possible and are investigated in numerical simulations.

The stability margin represent the distance of the largest gain coefficient from the unstable range of values. For example, for $\epsilon = 0.10$, we have gain coefficients $\boldsymbol{G}$ that keep a distance of at least 10% from the unstable coefficient values. In general, small ϵ results in larger gain coefficients, greater voltage regulation and longer convergence to steady-state. Whereas larger stability margins result in smaller gain coefficients, lower voltage regulation and quicker convergence to steady-state [Farivar et al., 2013].

The optimisation problem is now formulated as:

$$\begin{aligned}
\min_{\boldsymbol{A},\boldsymbol{B}} \quad & \sum_{(m,n)\in\mathcal{E}} r_{mn}(P_{mn}^2 + Q_{mn}^2) \\
\text{s.t.} \quad & (6.6), (6.7), (6.8), \\
& \|\boldsymbol{GH}\|_F \leq 1 - \epsilon, \\
& \boldsymbol{u} = \boldsymbol{A}\widetilde{\boldsymbol{E}}, \\
& \boldsymbol{v} = \boldsymbol{B}\widetilde{\boldsymbol{E}}, \\
& \boldsymbol{A} \leq 0, \\
& \boldsymbol{B} \leq 0.
\end{aligned} \tag{6.22}$$

The optimisation problem (6.22) is formulated with a quadratic objective and a quadratic constraint — problem known as QCQP. The non-linear quadratic objective function and the non-linear quadratic inequality constraint satisfy the convexity conditions, as discussed in (2.2) and (2.3) in Chapter 2. Problem (6.22) is modelled as a convex QCQP as in (2.3) and it has been tested both in MATLAB and Gurobi Optimizer.

Next, we expand (6.22) to a multi-period OPF-PC approach, where the design of proportional gains takes into account a future time horizon with power and energy constraints for controllable DERs.

6.4.1 Time-Horizon OPF-PC

Let $\mathcal{T} = \{1, 2, ..., t, ..., T\}$ be the steady-state discrete time set, where t is the time index and T is the total number of time steps in the horizon. Each $t \in \mathcal{T}$ has a time length $\Delta(t)$, and time lengths can be different for different t.

We model an inverter-based battery storage as the controllable DER. Real and reactive power are restricted by the rated apparent power, and energy charge level is limited by the energy capacity. For a controllable DER at node m, let $\overline{w}_m$ be the rated apparent power and $\overline{s}_m$ the maximum, $\underline{s}_m$ the minimum, and s_m the initial energy charge level. To model the energy charge level of a battery at node m, we first define $\boldsymbol{L}$ by a lower triangular matrix composed of time lengths $\Delta(t)$. Also, define $\boldsymbol{u}_m$ by the vector collecting all steady-state time steps of $u_m(t)$. Specifically,

$$\boldsymbol{L} = \begin{bmatrix} \Delta(1) & 0 & \dots & 0 \\ \Delta(1) & \Delta(2) & \dots & 0 \\ \vdots & \vdots & \ddots & \vdots \\ \Delta(1) & \Delta(2) & \dots & \Delta(T) \end{bmatrix}, \ \boldsymbol{u}_m = \begin{bmatrix} u_m(1) \\ u_m(2) \\ \vdots \\ u_m(T) \end{bmatrix}. \tag{6.23}$$

We then formulate the OPF-PC optimisation, presented in full here for completeness as

$$\begin{aligned}
\min_{\boldsymbol{A},\boldsymbol{B}} \quad & \sum_{t\in\mathcal{T}} \sum_{(m,n)\in\mathcal{E}} r_{mn}\big(P_{mn}^2(t) + Q_{mn}^2(t)\big)\Delta(t) && \text{(6.24a)} \\
\text{s.t.} \quad & \boldsymbol{E}(t) = \boldsymbol{R}\boldsymbol{u}(t) + \boldsymbol{X}\boldsymbol{v}(t) + \widetilde{\boldsymbol{E}}(t), && \text{(6.24b)} \\
& \boldsymbol{D}\boldsymbol{P}(t) + \boldsymbol{u}(t) + \widetilde{\boldsymbol{p}}(t) = 0, && \text{(6.24c)} \\
& \boldsymbol{D}\boldsymbol{Q}(t) + \boldsymbol{v}(t) + \widetilde{\boldsymbol{q}}(t) = 0, && \text{(6.24d)} \\
& \|\boldsymbol{G}(t)\boldsymbol{H}\|_F \le 1 - \epsilon, && \text{(6.24e)} \\
& \boldsymbol{u}(t) = \boldsymbol{A}(t)\widetilde{\boldsymbol{E}}(t), && \text{(6.24f)} \\
& \boldsymbol{v}(t) = \boldsymbol{B}(t)\widetilde{\boldsymbol{E}}(t), && \text{(6.24g)} \\
& \boldsymbol{A}(t) \le 0, && \text{(6.24h)} \\
& \boldsymbol{B}(t) \le 0, && \text{(6.24i)} \\
& u_m^2(t) + v_m^2(t) \le \overline{w}_m^2, \quad \forall m \in \mathcal{N}, && \text{(6.24j)} \\
& +\boldsymbol{L}\boldsymbol{u}_m \le \overline{s}_m - s_m, \quad \forall m \in \mathcal{N}, && \text{(6.24k)} \\
& -\boldsymbol{L}\boldsymbol{u}_m \le s_m - \underline{s}_m, \quad \forall m \in \mathcal{N}, && \text{(6.24l)}
\end{aligned}$$

where constraints (6.24b)-(6.24j) are for all $t \in \mathcal{T}$. The objective function minimises the total power losses on the grid over the time horizon (i.e., total energy loss). Constraints (6.24b)-(6.24i) are the same constraints shown before. Constraint (6.24j) represents the apparent power limitation of inverters. Constraints (6.24k)-(6.24l) represent energy limits of battery storage. Problem (6.24) is convex and implemented as a QCQP.

When a final charge level is desirable at the end of the time horizon, another important constraint to be added in (6.24) is $\sum_{t \in \mathcal{T}} \Delta(t) u_m(t) = \hat{s}_m - s_m$, where $\hat{s}_m$ is the final energy charge level. If the final charge level equals to the initial ($\hat{s}_m = s_m$), then the constraint is simplified as $\sum_{t \in \mathcal{T}} \Delta(t) u_m(t) = 0$, which basically describes that the battery has to charge the same amount of energy that discharges over the day.

Note that nodes without battery storage can simply be modelled as a zero power DER, i.e., $\overline{w}_m = 0$. Constraint (6.24j) can be approximated by a number of linear inequalities to form a convex polygon constraint, where the original circle is inscribed in the regular n-sided polygon [Abadi et al., 2021]. In our numerical simulations, we model (6.24j) as a regular octagon to result in a smaller optimisation problem and quicker solving time. Voltage bounds are deliberately absent in the optimisation problem. Due to the stability constraint and limited amount of controllable power and energy, adding voltage bounds to (6.24) often results in infeasible problem [Abadi et al., 2021; Zhou et al., 2021]. As such, voltage equation (6.24b) can be removed to further simplify and reduce the size of the optimisation problem.

Unlike standard OPF problems, the OPF-PC approach in (6.24) provides proportional gains α_m and β_m for local controllers. Providing gains, rather than power setpoints, enables DERs to compute their own real and reactive power using local voltage feedback. As such, controllable DERs counteract unexpected voltage variations with fast and autonomous response. OPF-PC in (6.24) also provides gains that consider the specific size (power and energy capacity) of each local controller. This setting prevents irregular participation factors of controllable DERs, avoids power saturation and unavailability of local controllers due to fully charged/discharged DERs.

6.5 Receding-Horizon Optimisation

The OPF-PC with time horizon requires forecast of future uncontrollable load ($\widetilde{\boldsymbol{p}}$ and $\widetilde{\boldsymbol{q}}$). We solve problem (6.24) in a receding-horizon fashion to account for model and forecast inaccuracies. With the receding-horizon optimisation (RHO) method, problem (6.24) is solved for a finite time horizon and only the gain coefficients of the first time steps are actually provided to the local controllers. Building on [Attarha et al., 2020], we consider a variable time-discretisation technique, where time steps further in the horizon are averaged

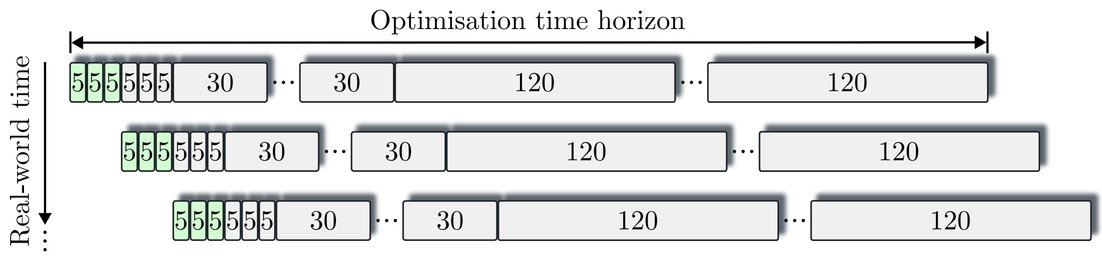

Figure 6.3: RHO with variable time lengths. Optimisation problem is solved every 15 minutes. Gain coefficients of the first three time slots (in green) are actually used.

over a longer time length, and time steps closer to the present time have a finer granularity (i.e., $\Delta(1) \leq \Delta(T)$). Since time steps further in the horizon are less precise and less relevant than immediate steps, such a technique significantly reduces the size of the problem and solving time, with negligible impact on performance [Attarha et al., 2020].

Fig. 6.3 illustrates the RHO method with variable time-discretisation to solve OPF-PC in (6.24). In our numerical simulations, the time horizon is 24 hours: the first six time steps have a 5-min time length ($\Delta(1) = ... = \Delta(6) = 5/60$ h), the following seven time steps have a 30-min time length ($\Delta(7) = ... = \Delta(13) = 30/60$ h), and the last time steps have a 2-hour time length ($\Delta(14) = ... = \Delta(23) = 120/60$ h). Problem (6.24) is solved every 15 minutes and gain coefficients of the first three 5-min time steps is actually provided to the local controllers, as illustrated in Fig. 6.3 in green. Other values for the varying time-discretisation technique are also possible.

Algorithm 1 summarises the OPF-PC approach with the RHO method. Similar to an adaptive control, local controllers have their gain coefficients updated every 5 minutes with globally optimal α_m and β_m gains. Local controllers compute their power actions locally in real time as in (6.9)-(6.10) approximately every 100 ms [Baker et al., 2018; Maharjan et al., 2021].

The OPF-PC approach with the RHO method is built to handle networks with high penetration of renewable sources and DERs, where variability and uncertainty is higher. OPF-PC reruns every 15 minutes with newly measured and updated demand forecast data, reducing uncertainties and improving accuracy of forecast data. Local proportional controllers acting in real time also address differences between forecast and actual demand, providing further resilience to the overall control approach. Local controllers measure the grid voltage every 100 ms and actuate real and reactive power to counter-act any deviations on the grid.

It is worth mentioning that local controllers achieve steady-state voltages within a few seconds. Hence the updating of gain coefficients every 5 minutes

Algorithm 1: OPF-PC approach with RHO

Get grid matrices $\boldsymbol{R}$, $\boldsymbol{X}$ and $\boldsymbol{D}$;
Get DER values $\overline{w}_m$, $\overline{s}_m$, $\underline{s}_m$ for all $m \in \mathcal{N}$;
Define stability margin ϵ;
for *every 15 minutes* **do**
  Measure and forecast $\widetilde{\boldsymbol{p}}$ and $\widetilde{\boldsymbol{q}}$;
  Compute $\widetilde{\boldsymbol{E}}$;
  Get updated DER charge level s_m for all $m \in \mathcal{N}$;
  Solve convex optimisation problem (6.24);
  Obtain gain matrices $\boldsymbol{A}(t), \boldsymbol{B}(t)$ for $t \in \{1, 2, 3\}$;
  for *every 5 minutes* $(t \in \{1, 2, 3\})$ **do**
    Update α_m and β_m of every local controller;
  end
end

takes effect well after the real-time control of local inverters has achieved asymptotic stability.

6.6 Benchmark Approaches

We present two different approaches from the literature to design gain coefficients of proportional controllers. Similar to the design of gain coefficients in Chapter 5, the first benchmark approach computes gain coefficients directly by taking $\boldsymbol{A} = \boldsymbol{B} = -g\boldsymbol{I}$, where $\boldsymbol{I}$ is the N $\times$ N identity matrix and g is the gain coefficient for every controller [Cavraro and Carli, 2018]. From (6.17) and with the addition of the stability margin ϵ, the gain coefficient is computed directly as

$$g = \frac{1-\epsilon}{\rho(\boldsymbol{R}+\boldsymbol{X})}, \tag{6.25}$$

where $0 < \epsilon \leq 1$ provides asymptotic stability and convergence to steady-state voltages for the system (6.16). As an example, a stability margin of 10% ($\epsilon = 0.1$) is equivalent to a gain coefficient of 90% of the critical ($g = 0.9\overline{g}$) as presented in Chapter 5. Note that (6.25), termed Direct approach, provides coefficients that neglect location, size and capacity of controllable DERs.

The second benchmark approach, termed here as Opt-Bench, is an optimisation-based approach to design gain coefficients. Rearranging and approximating the steady-state voltage equation (6.18) as in [Baker et al., 2018], we get

$$E = (I - HG)^{-1}\widetilde{E} \approx (I + HG)\widetilde{E}. \tag{6.26}$$

Rearrange the approximation as

$$E \approx (I + RA + XB)\widetilde{E}. \tag{6.27}$$

An optimisation problem is used to obtain gain coefficients to minimise the maximum voltage deviation in the network ($\|E\|_\infty$), while keeping the gains in the stable range [Baker et al., 2018]. Specifically,

$$\begin{aligned}
\min_{A,B} \quad & \|E\|_\infty && (6.28a)\\
\text{s.t.} \quad & E = (I + RA + XB)\widetilde{E}, && (6.28b)\\
& \|GH\|_F \leq 1 - \epsilon, && (6.28c)\\
& A \leq 0, && (6.28d)\\
& B \leq 0. && (6.28e)
\end{aligned}$$

The constraints include the steady-state voltage approximate equation (6.28b), the stability constraint (6.28c), and non-negative gain coefficients (6.28d)-(6.28e). The unknowns of optimisation problem (6.28) are A, B, E, but gain coefficients are the only decision variables of interest. Problem (6.28) is convex and the objective function can be formulated as a number of linear inequality constraints. Both benchmark approaches provide gain coefficients that do not encapsulate DER limitation.

6.7 Numerical Simulations

Two different test feeders based on real distribution networks are implemented for numerical simulations in this chapter. We first consider an 8-node network based on a Belgian residential low-voltage feeder [Zeraati et al., 2018; Mediwaththe and Blackhall, 2021]. The slack bus is fixed with constant single-phase nominal voltage of 230 V (1 p.u.). We populate the nodes with residential systems with solar PV from a real-world, time-varying and de-identified data from the NextGen dataset [Shaw et al., 2019]. Similar to Chapter 5, two residential systems are connected to every node downstream of the substation bus, with a total of 14 different users on the network.

For power flow calculations, loads are modelled as constant power loads and reactive power demand is obtained by considering a power factor of 0.95. Half of the residential systems have a participating controller. Stability margin is selected as 10 per cent ($\epsilon = 0.1$), which resulted in a constant gain coefficient of $g = 0.45$ VA/V^2 for the Direct approach in (6.25). The optimisation-based approaches provide tailored gain coefficients for each DER and for each 5-min time step, according to the operating state of the network.

All numerical results for the OPF-PC approach are obtained with the multi-period OPF-PC as in (6.24), running in the receding-horizon fashion described in Section 6.5 and Algorithm 1. We carry out simulations on MATLAB R2022a and solve optimisation problems with Gurobi Optimizer V10.0.1, using a MacBook Air with Apple M1 2020 chip, 16 GB Ram. Numerical simulations are run with the full AC non-linear power flow model [Garcia et al., 2000]. That is, the proposed approach is formulated with the linear model but tested with the full non-linear network model.

6.7.1 Dynamic Performance

Similar to [Arnold et al., 2016] we initially consider unrestricted controllable DERs to fully assess the dynamic performance of control approaches with abundant controllable power.

Fig. 6.4 illustrates the dynamic performance of each approach for an extreme voltage deviation scenario. This extreme scenario represents a case where the linear model and approximations are significantly far from exact values. Both OPF-PC plots in Fig. 6.4 have the same gain coefficients, but they differ in their initial power values. Except for the OPF-PC in black line, all local controllers initialise with $u_m(k) = v_m(k) = 0$ for $k = 0$. The initial values of the OPF-PC in black line are the steady-state values of the previous time step. We observe in Fig. 6.4 that proportional controllers converge to steady-state voltages within 50 iterations and provide significant voltage regulation on the grid: from 1.13 p.u. to 1.07 p.u. When the initial controllable power is the steady-state of the previous time step (OPF-PC in black line), we observe that voltage converges to steady state almost immediately. Note that all approaches resulted in similar steady-state voltages, as the same stability margin of 10% was selected. For this numerical simulation with unrestricted controllable DERs, the stability criterion is the only constraint limiting the increase of proportional gains and consequently reducing voltage deviation.

In Fig. 6.4, we consider that the demand condition is constant during the fast control actuation of local electronic inverters, as in [Baker et al., 2018; Cavraro and Carli, 2018; Singhal et al., 2019]. A significant and sudden change of network condition may impact the performance of local controllers and can be further investigated in future work.

Fig. 6.5 illustrates the spectral radius and different norms of $(\boldsymbol{GH})$ as the proportional gains are updated over a day by OPF-PC approach. Observe

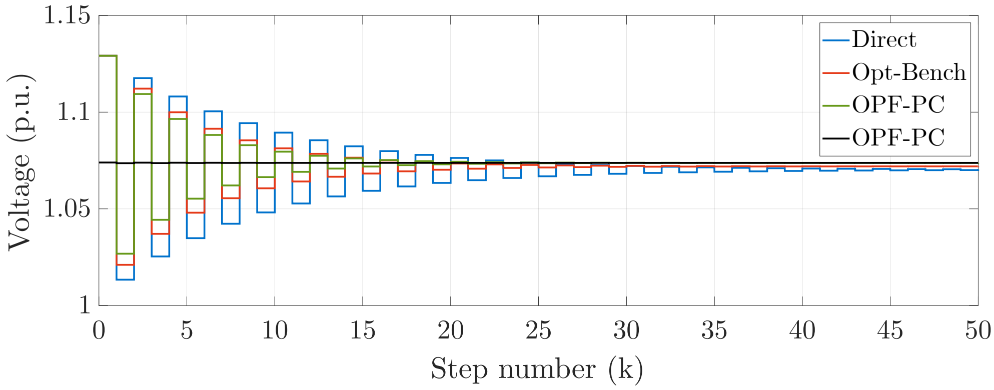

Figure 6.4: Dynamic voltage behaviour at node 7 for a voltage rise case.

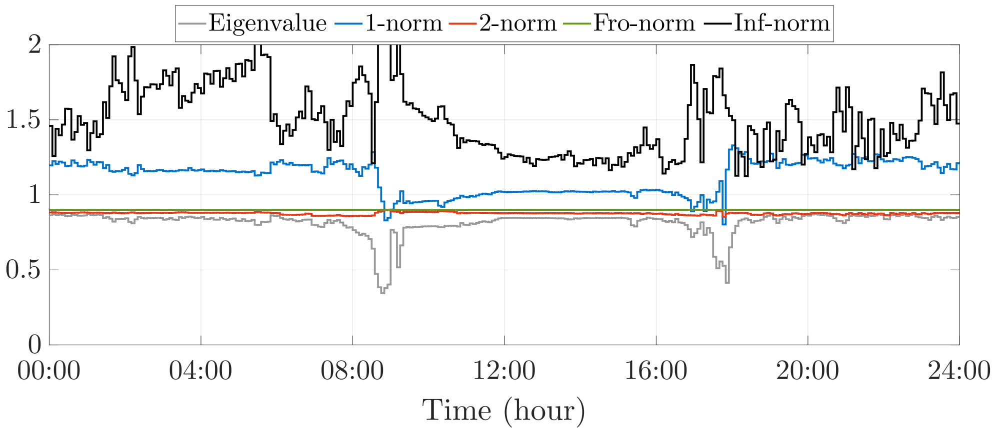

Figure 6.5: Spectral radius and different norms of $(\boldsymbol{GH})$ for the OPF-PC approach over a day.

that the Frobenius norm in green line is at 0.90 throughout the day and is always greater than or equal to the spectral radius in grey line. The spectral radius of $(\boldsymbol{GH})$ represents the dynamics and convergence rate of the system and is clearly less than 1, indicating stability throughout the day. Fig. 6.5 also presents the 1-norm, computed as the maximum absolute column sum of the matrix; Inf-norm, computed as the maximum absolute row sum of the matrix; and 2-norm of matrix $(\boldsymbol{GH})$. The closer the norms are to the spectral radius the closer is the estimate of the actual dynamics of the system and the more precise and less conservative the stability constraint can be. The 2-norm and Frobenius norm are closer to the actual spectral radius. Frobenius norm is simpler to include in optimisation problems and results in a convex constraint. The 1-norm and Inf-norm are also simple to compute and include in optimisation problems. However, they both are significantly larger than the actual spectral radius and can result in excessively conservative gain values.

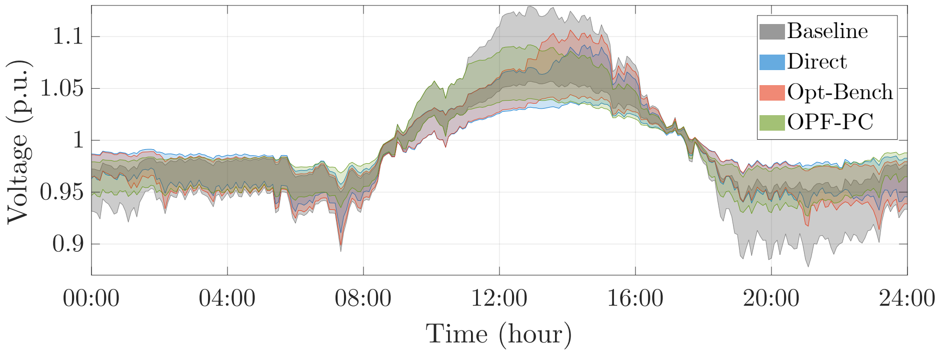

(a)

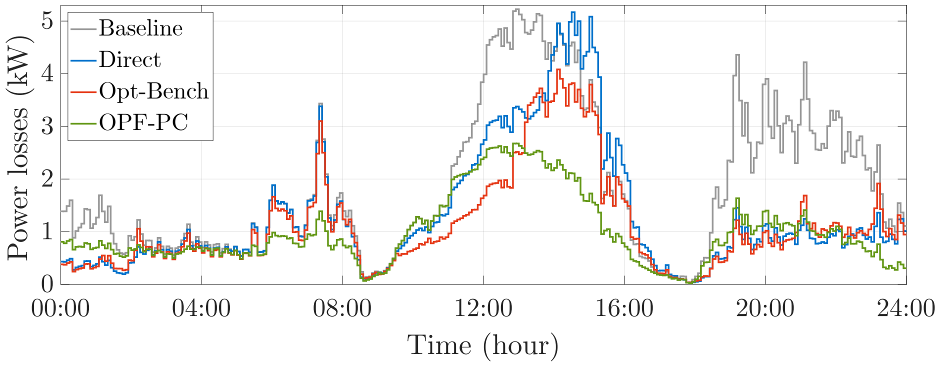

(b)

Figure 6.6: Steady-state results: (a) Voltage magnitude across the grid and (b) total resistive power losses in the network.

6.7.2 Steady-State Numerical Results

In what follows, we consider that controllable DERs are similar to a commercial home battery storage. Let the rated apparent power be 5 kVA ($\overline{w}_m = 5$), energy capacity be 10 kWh ($\overline{s}_m = 10$ and $\underline{s}_m = 0$) and initial charge level be 3 kWh ($s_m = 3$).

Fig. 6.6 illustrates steady-state results for a day with large voltage deviations due to high peak demand and PV generation. The range of the voltage magnitude across the network is presented in Fig. 6.6(a) and the total resistive power loss in Fig. 6.6(b). The Baseline simulations represent the no-control case. In Fig. 6.6(a), we observe that grid voltage deviation is significantly reduced when OPF-PC is employed, keeping the entire network within the 0.90 and 1.10 p.u. range. In Fig. 6.6(b), the total losses is also considerably reduced when employing the proposed approach, particularly during the critical periods of peak demand and solar PV generation.

Fig. 6.7 illustrates the steady-state controllable real (solid lines) and reactive power (dashed lines) and the energy charge level of the DER located at the

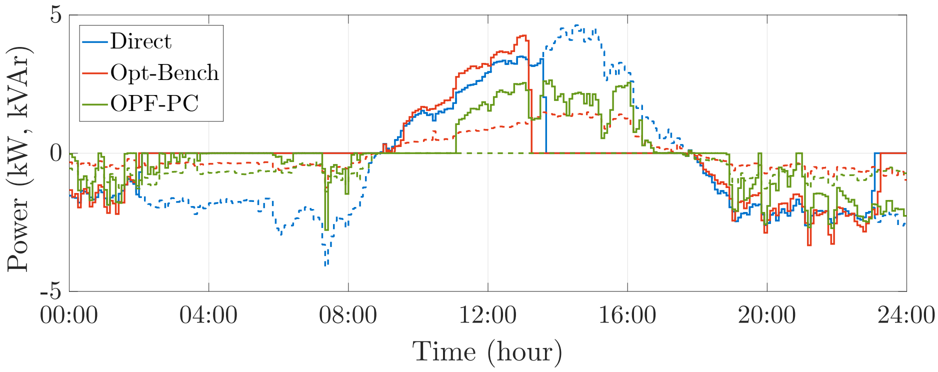

(a)

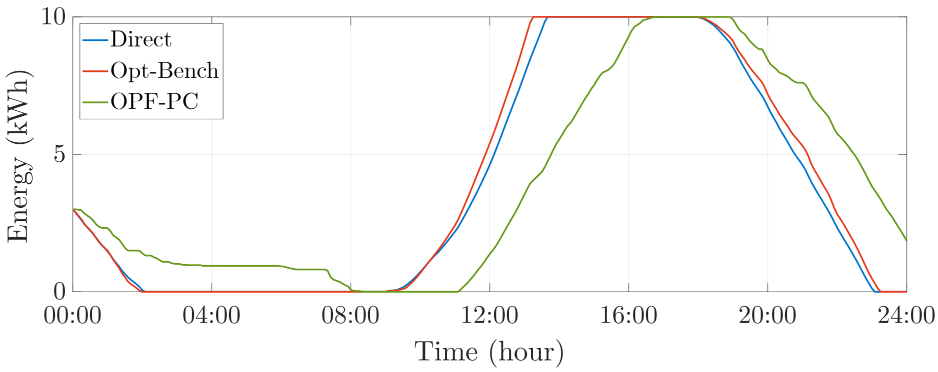

(b)

Figure 6.7: Controllable DER at node 7: (a) real power (u_m, solid lines) and reactive power (v_m, dashed lines); and (b) energy charge level.

end of the feeder (node 7). As the Direct and Opt-Bench approaches do not take into account DER limitation to design the proportional gain coefficients, the controllable real power is often interrupted due to fully charged/discharged energy levels. With real power unavailable during the critical periods, only reactive power is left to perform voltage regulation. The OPF-PC approach encapsulates DER power and energy limits into proportional gains and results in real power actuation only during critical times. Observe that OPF-PC results in zero α_m and β_m gains (thus zero power) during the transition between demand and reverse power flow, when PV generation matches power consumption and indeed no voltage regulation is needed. In addition, with the OPF-PC, the gains for reactive power control are zero during reverse power flow, resulting in lower grid power losses.

Table 6.1 presents numerical simulations for other two distinct days of the year with different power consumption and PV generation profiles. The results are summarised by four important performance indices: maximum and minimum voltage on the network during that day (Max volt and Min volt), the

Table 6.1: Summary of numerical simulations on the 8-node feeder.

Index	**Baseline**	**Direct**	**Opt-Bench**	**OPF-PC**
Max volt (p.u.)	1.042	1.024	1.023	1.024
Min volt (p.u.)	0.886	0.904	0.893	0.921
Ene loss (kWh)	24.3	22.2	20.5	17.7
S sub (kVA)	44.9	44.3	42.7	30.7
Max volt (p.u.)	1.137	1.111	1.125	1.099
Min volt (p.u.)	0.932	0.962	0.964	0.963
Ene loss (kWh)	30.6	27.8	21.4	18.5
S sub (kVA)	53.3	57.7	53.9	39.5

total energy loss on the network for that day (Ene loss) and the peak apparent power at the substation during that day (S sub). Observe that without controlling DERs (Baseline), voltage magnitude goes well beyond 1.10 p.u. and 0.90 p.u. All approaches managed to reduce voltage deviation when compared to the Baseline, with the proposed approach providing greater voltage regulation on the network. OPF-PC also provided proportional gain coefficients that resulted in local controllers significantly reducing the total energy losses and peak power demand on the network. The considerable reduction in peak power from the substation can prevent overloading transformers and lines and avoid expensive upgrades on the network [NREL, 2019b].

We also run numerical simulations on a 42-node distribution feeder based on a medium-voltage network from Southern California Edison [Zhou et al., 2021]. We populate the network with de-identified customer data from the real-world, time-varying NextGen dataset [Shaw et al., 2019], resulting in 5530 customers on the feeder. Half of the customers have a controllable DER with the same size as described before and stability margin is selected as 10 per cent ($\epsilon = 0.1$).

Table 6.2 summarises numerical simulations on the 42-node feeder for two distinct days of the year with different power consumption and PV generation profiles. Observe that all approaches brought the voltage closer to the nominal when comparing to the Baseline, despite milder voltage deviations on the network. The voltage slightly closer to the nominal for the benchmark approaches on the second day is due to unnecessary control of reactive power that results in excessive grid power losses and high power peaks, particularly during solar PV exports. OPF-PC have shown strong reduction in grid power losses and peak power from substation in all cases. Minimising grid power losses, as in OPF-PC, have clearly contributed to flatten peak power

Table 6.2: Summary of numerical simulations on the 42-node feeder.

Index	Baseline	Direct	Opt-Bench	OPF-PC
Max volt (p.u.)	1.004	1.004	1.003	1.004
Min volt (p.u.)	0.930	0.952	0.957	0.958
Ene loss (MWh)	3.52	2.83	2.79	2.63
S sub (MVA)	12.84	11.77	11.72	9.79
Max volt (p.u.)	1.039	1.028	1.025	1.034
Min volt (p.u.)	0.969	0.980	0.982	0.979
Ene loss (MWh)	5.96	5.32	5.68	4.50
S sub (MVA)	19.69	18.85	19.44	17.24

demand/export and to prevent congestion in distribution networks.

Table 6.3 presents the number of variables and constraints in the optimisation problem of both optimisation-based approaches for both test feeders. The solving time to output gain coefficients for the next 15 min is also presented in Table 6.3. Note that the Direct approach is not optimisation-based and thus presents negligible central computation requirement. Mainly due to the future time-horizon capability, the proposed approach presents larger problem size and computational time. Even with the conventional personal computer used for numerical simulations in this chapter, the OPF-PC computation time is much smaller than the updating period of gain coefficients. That is, for each run the OPF-PC has a 15 minute time-window available to solve, and it only took 4.4 seconds to solve for the 42-node network.

It is important to note that non-convex optimisation problems and the number of integer binary variables pose a great challenge to solving efficiency and scalability of control approaches to larger (more nodes) networks [Chen et al., 2023]. The proposed OPF-PC approach is formulated as a convex optimisation problem with no integer binary variables. These characteristic improve solving efficiency and scalability, making the OPF-PC approach particularly promising for larger networks with high integration of DERs.

6.8 Conclusion

In this chapter, we propose a two-layer control approach for controlling real and reactive power of DERs. The global OPF-based optimisation computes coefficients of local proportional VVW controllers to provide voltage regulation in distribution networks. The gain coefficients are designed to reduce

Table 6.3: Problem size and computational time.

Approach	Network	# Variables	# Constraints	Time (s)
Opt-Bench	8 nodes	22	22	0.03
	42 nodes	124	156	0.07
OPF-PC	8 nodes	966	2277	0.34
	42 nodes	5658	13225	4.42

total grid power losses, while considering DER constraints and keeping overall system stability. OPF-PC is solved in a receding-horizon fashion and gains are provided regularly to local controllers, which then respond fast and autonomously to local voltage variations.

Numerical simulations with the full AC non-linear power flow model have shown convergence to steady-state voltages and greater performance when local VVW controllers are tuned by the OPF-PC approach. With longer yet viable computational time, the OPF-PC approach results in substantial grid voltage regulation and strong reduction of grid power losses and peak demand compared to the state-of-the-art.

Chapter 7

Final Remarks and Future Work

The massive uptake of distributed solar PV in distribution networks has created technical challenges for grid operators. Other DERs, such as the residential battery storage and plug-in EVs, are also set for gigantic growth in the years to come and can pose their own problems on distribution networks. When adequately controlled, however, DERs provide not only financial savings for customers but also grid services such as voltage regulation and losses and peak demand reduction. In this context, better approaches to control these highly variable and heterogeneous DERs are needed.

In this thesis, we propose several optimisation and control approaches to coordinate these distributed resources and improve network operation. In Chapter 3, four local QP optimisation are presented to charge and discharge residential battery storage to improve voltages and customer savings. The optimisation problems are network-agnostic and only consider real power of elements in the residential system. In Chapter 4, a network-cognisant formulation for a local QP optimisation is proposed to control both real and reactive power of residential batteries. Local measurements of the grid voltage are also included in the feedback control and gain coefficients are designed based on the DER capability.

In Chapter 5, gain coefficients are designed based on a stability criterion and a novel formulation for the local VVW control is proposed. Here, parameters are locally designed by an optimisation problem. In Chapter 6, a system-wide optimisation problem is proposed to provide globally optimal gain coefficients for local proportional controllers. This optimisation problem designs gain coefficients that not only consider the stability criterion and DER capabilities, but also encapsulate present and future operating states of the entire distribution network.

A few important takeaways of this thesis can be summarised as follows:

- Network-cognisant control can provide greater benefits. Knowing the impedance characteristic of the network unlocks the physical relationship between power and voltage deviation/regulation, as well as power losses on the network. With such an information, control approaches precisely incorporate the efficacy of each real and reactive power for voltage regulation, and how they reduce grid power losses.

- Voltage magnitude measurements can provide greater benefits. Unlike using only grid power as proxy for voltage regulation, as in Chapter 3, directly measuring grid voltage magnitude and properly actuating real and reactive power to counteract voltage deviations results in more effective voltage regulation. With proper design of gain coefficients, voltage feedback control responds extremely quickly to grid state variations with practically no voltage oscillations (interactions between inverters).

- Two-layer control approach can provide greater benefits. A central-local combination brings advantages of both worlds: the constrained and optimal solution of global optimisation problems and the fast and autonomous response of local controllers. While local controllers on the bottom layer respond quickly and effectively to fast grid voltage variations, the system-wide optimisation on the top layer sends to local controllers holistic and network-cognisant parameters at a slower timescale. This timescale decomposition allows the large-scale optimisation problem to be solved as a online planning tool, rather than a real-time controller.

The contributions of this thesis are mainly within the local/autonomous realm of optimisation and control of DERs; and a substantial effort is also placed in a two-layer control approach, where we combine local control with global optimisation in Chapter 6. The author of this thesis hopes the original approaches proposed in this PhD program contribute to this important field of knowledge and, ultimately, to the transition to a renewable and sustainable electricity grid.

7.1 Future Work

Related to the scope of this thesis, there are, of course, many other aspects and topics that can be investigated to contribute to optimisation and control of DERs in distribution networks. In this section, we discuss a few topics that could be interesting to pursue in the future.

As briefly mentioned in Chapter 4, the assessment on how different optimisation and control approaches impact battery degradation could be a topic for future investigation. Such investigation could also analyse the trade-off between battery model detail and solving efficiency/scalability of optimisation problems, outlining the most appropriate model for each application.

Another topic for future work would be how to systematically and analytically tune weights in a multi-objective optimisation problem to balance grid-customer benefits. Or how to specifically translate grid services and sustainable objectives into economic terms such that the optimisation can simply minimise a financial objective.

Another future research option is the investigation on the effect of mesh distribution networks on optimisation and control of DERs. Or, more broadly, if specific network topologies can give specific insights and contributions to optimisation and control of DERs. The author of this thesis also envisages that the combination of system-wide optimisation-based approaches with local and autonomous control (two-layer or multi-layer control) can provide greater benefits and should be further considered in future works.

The optimisation and control proposed in this thesis, as well as in many papers in the literature, directly include grid voltage magnitude in their approaches. Voltage magnitude must be maintained close to the nominal value and thus directly represent operational goals and constraints. The commonly disregarded phase angle of the voltage phasor at a node relative to other nodes on the network can also encapsulate information of the grid operating state [Ochoa and Wilson, 2010; Pesente et al., 2018].

There is virtually no specific operational constraints or objectives regarding phase angles in distribution networks. The phase angle deviation among voltage phasors at different nodes on the grid works as an indicator for thermal limits, reverse power flow, and the network loading conditions in general. Although these grid conditions are also captured by current (or power) measurements on the network, voltage phasors are associated with nodes, as opposed to line branches, and can potentially be communicated with less privacy concerns. Voltage phase angles, measured by phasor measurement units (PMUs), can also be used to estimate the state of the grid and provide an alternative in cases where line measurement devices cannot easily be deployed [Ochoa and Wilson, 2010; Wang et al., 2013, 2015a; von Meier et al., 2014, 2017; von Meier et al., 2020; Sankur et al., 2020].

In this context, the inclusion of voltage phase angles in optimisation and control of DERs in distribution networks could be another topic for future work.

Bibliography

ABADI, S.; MAHMOODI, M.; SCOTT, P.; BLACKHALL, L.; AND THIEBAUX, S., 2019. Active management of LV residential networks under high PV penetration. In *2019 IEEE Milan PowerTech*, 1–6. Milan, Italy. (cited on page 55)

ABADI, S. M. N. R.; ATTARHA, A.; SCOTT, P.; AND THIÉBAUX, S., 2021. Affinely adjustable robust volt/var control for distribution systems with high PV penetration. *IEEE Transactions on Power Systems*, 36, 4 (2021), 3238–3247. (cited on pages 48, 89, 90, and 98)

AEMO, 2019. *Maintaining Power System Security with High Penetrations of Wind and Solar Generation – International insights for Australia*. Available: https://www.aemo.com.au/-/media/Files/Electricity/NEM/Security_and_Reliability/Future-Energy-Systems/2019/AEMO-RIS-International-Review-Oct-19.pdf, Accessed 30 May 2023. (cited on page 1)

AEMO, 2020a. *Renewable Integration Study Stage 1 Appendix A: High Penetrations of Distributed Solar PV*. Available: https://aemo.com.au/-/media/files/major-publications/ris/2020/ris-stage-1-appendix-a.pdf?la=en, Accessed 30 May 2023. (cited on pages 1, 2, and 41)

AEMO, 2020b. *Renewable Integration Study: Stage 1 report*. Available: https://aemo.com.au/-/media/files/major-publications/ris/2020/renewable-integration-study-stage-1.pdf?la=en, Accessed 30 May 2023. (cited on pages 1 and 70)

AHMADI, H.; MARTI, J. R.; AND VON MEIER, A., 2016. A linear power flow formulation for three-phase distribution systems. *IEEE Transactions on Power Systems*, 31 (2016), 5012 – 5021. (cited on page 16)

AHUJA, R. K.; MAGNANTI, T. L.; AND ORLIN, J. B., 1993. *Network Flows: Theory, Algorithms, and Applications*. Prentice Hall, Upper Saddle River, New Jersey 07458. (cited on page 92)

ALONSO, A. M. S.; ARENAS, L. D. O.; BRANDAO, D. I.; TEDESCHI, E.; AND MARAFAO, F. P., 2022. Integrated local and coordinated overvoltage control to increase energy feed-in and expand DER participation in low-voltage networks. *IEEE Transactions on Sustainable Energy*, 13, 2 (2022), 1049–1061. (cited on pages 11 and 89)

Annaswamy, A. M.; Johansson, K. H.; and Pappas, G. J., 2023. Control for societal-scale challenges: Road map 2030. Technical report, IEEE Control Systems Society Publication. Available: https://ieeecss.org/post/control-societal-scale-challenges-roadmap-2030, Accessed 30 May 2023. (cited on pages 1, 3, 5, and 89)

Antoniadou-Plytaria, K. E.; Kouveliotis-Lysikatos, I. N.; Georgilakis, P. S.; and Hatziargyriou, N. D., 2017. Distributed and decentralized voltage control of smart distribution networks: Models, methods, and future research. *IEEE Transactions on Smart Grid*, 8, 6 (2017), 2999–3008. (cited on pages 4, 5, 11, 42, 70, and 89)

Arnold, D. B.; Sankur, M.; Dobbe, R.; Brady, K.; Callaway, D. S.; and von Meier, A., 2016. Optimal dispatch of reactive power for voltage regulation and balancing in unbalanced distribution systems. In *2016 IEEE Power and Energy Society General Meeting (PESGM)*, 1–5. Boston, MA, USA. (cited on pages 5, 12, 17, 27, 42, 45, 56, 70, 79, 89, and 102)

Arnold, D. B.; Sankur, M. D.; Negrete-Pincetic, M.; and Callaway, D. S., 2018. Model-free optimal coordination of distributed energy resources for provisioning transmission-level services. *IEEE Transactions on Power Systems*, 33, 1 (2018), 817–828. (cited on page 2)

Attarha, A., 2022. *Network-Secure Consumer Bidding in Energy and Reserve Markets*. Ph.D. thesis, The Australian National University (ANU). (cited on page 4)

Attarha, A.; Scott, P.; and Thiebaux, S., 2020. Network-aware co-optimisation of residential DER in energy and FCAS markets. In *21st Power Systems Computation Conference (PSCC)*, 1–8. Porto, Portugal. (cited on pages 98 and 99)

AusNet Services, 2021. *Model standing offer for basic connection services: Basic micro Embedded Generation (EG) – inverter energy system*. Available: https://www.aer.gov.au/system/files/AusNet%20Services%20-%20Revised%20Regulatory%20Proposal%20-%202021-26%20-%20Model%20Standing%20Offer%20for%20Basic%20Connection%20Services%20-%20December%202020.pdf, Accessed 30 May 2023. (cited on page 54)

Baker, K.; Bernstein, A.; Dall'Anese, E.; and Zhao, C., 2018. Network-cognizant voltage droop control for distribution grids. *IEEE Transactions on*

Power Systems, 33, 2 (2018), 2098–2108. (cited on pages 55, 64, 70, 77, 78, 79, 89, 90, 94, 96, 99, 100, 101, and 102)

Baran, M. and Wu, F. F., 1989a. Optimal sizing of capacitors placed on a radial distribution system. *IEEE Transactions on Power Delivery*, 4, 1 (1989), 735–743. (cited on pages 12, 44, 46, 71, 72, and 91)

Baran, M. E. and Wu, F. F., 1989b. Network reconfiguration in distribution systems for loss reduction and load balancing. *IEEE Transactions on Power Delivery*, 4, 2 (1989), 1401–1407. doi:10.1109/61.25627. (cited on pages 45, 51, 52, and 95)

Bertsekas, D. P., 1999. *Nonlinear Programming*. Athena Scientific, Belmont, Massachusetts. (cited on page 13)

Borrelli, F.; Bemporad, A.; and Morari, M., 2017. *Predictive Control for linear and hybrid systems*. Cambridge University Press, University Printing House, Cambridge CB2 8BS, United Kingdom. (cited on pages 11, 13, 14, 15, 44, and 91)

Boyd, S. and Vandenberghe, L., 2004. *Convex Optimization*. Cambridge University Press, The Edinburgh Building, Cambridge, CB2 8RU, UK. (cited on pages 11, 13, 14, and 15)

Callaway, D. S. and Hiskens, I. A., 2011. Achieving controllability of electric loads. *Proceedings of the IEEE*, 99, 1 (2011), 184–199. doi:10.1109/JPROC.2010.2081652. (cited on page 1)

Carvalho, W. C. and Pesente, J. R., 2014. Three-phase power flow calculation using the current injection method to assess the effect of unbalanced loads. In *XI SESEP - Eleventh Seminar of the Paraguayan Electric Sector*, 1–8. Asuncion, Paraguay. (cited on page 17)

Cavraro, G. and Carli, R., 2018. Local and distributed voltage control algorithms in distribution networks. *IEEE Transactions on Power Systems*, 33, 2 (2018), 1420–1430. (cited on pages 5, 13, 42, 54, 55, 70, 77, 89, 94, 100, and 102)

Chakraborty, S.; Hoke, A.; and Lundstrom, B., 2015. Evaluation of multiple inverter volt-VAR control interactions with realistic grid impedances. In *Proc. 2015 IEEE Power & Energy Society General Meeting*, 1–5. Denver, CO, USA. (cited on page 55)

Chen, Y.; Pan, F.; Qiu, F.; Xavier, A. S.; Zheng, T.; Marwali, M.; Knueven, B.; Guan, Y.; Luh, P. B.; Wu, L.; Yan, B.; Bragin, M. A.; Zhong, H.; Giacomoni, A.; Baldick, R.; Gisin, B.; Gu, Q.; Philbrick, R.; and Li, F., 2023. Security-constrained unit commitment for electricity market: Modeling, solution methods, and future challenges. *IEEE Transactions on Power Systems*, 38, 5 (2023), 4668–4681. doi:10.1109/TPWRS.2022.3213001. (cited on pages 10, 24, and 107)

Collins, L. and Ward, J., 2015. Real and reactive power control of distributed PV inverters for overvoltage prevention and increased renewable generation hosting capacity. *Renewable Energy*, 81 (2015), 464 – 471. (cited on pages 1 and 21)

De Brabandere, K.; Woyte, A.; Belmans, R.; and Nijs, J., 2004. Prevention of inverter voltage tripping in high density PV grids. In *19th European PV Solar Energy Conference and Exhibition*, 1–4. Paris, France. (cited on page 22)

de Carvalho, W.; Attarha, A.; and Pota, H. R., 2022. Local volt-var-watt control for voltage regulation in distribution networks. In *2022 IEEE PES 14th Asia-Pacific Power and Energy Engineering Conference (APPEEC)*, 1–6. doi:10.1109/APPEEC53445.2022.10072192. 14th IEEE APPEEC, Melbourne, Australia. (cited on pages 7 and 67)

de Carvalho, W.; Attarha, A.; and Pota, H. R., 2024. Optimization-based proportional control for voltage regulation with DERs in distribution networks. *Manuscript in preparation*, (2024), 1–10. (cited on pages 7 and 85)

de Carvalho, W. C., 2019. *Fuzzy logic and energy storage system for wind power smoothing*. University of Sao Paulo (USP). (cited on page 3)

de Carvalho, W. C.; Ratnam, E. L.; Blackhall, L.; and von Meier, A., 2023. Optimization-based operation of distribution grids with residential battery storage: Assessing utility and customer benefits. *IEEE Transactions on Power Systems*, 38, 1 (2023), 218–228. doi:10.1109/TPWRS.2022.3163371. (cited on pages 7, 37, and 70)

de Carvalho, W. C.; Ratnam, E. L.; Blackhall, L.; von Meier, A.; and Murray, A., 2020. Over-voltage disconnection of DER inverters: Assessing customer savings. *IFAC-PapersOnLine*, 53, 2 (2020), 13230–13235. 21th IFAC World Congress, Berlin, Germany. (cited on pages 1, 7, and 19)

Dobbe, R.; Sondermeijer, O.; Fridovich-Keil, D.; Arnold, D.; Callaway, D.; and Tomlin, C., 2020. Toward distributed energy services: Decentralizing optimal power flow with machine learning. *IEEE Transactions on Smart Grid*, 11, 2 (2020), 1296–1306. (cited on pages 11, 17, and 27)

ENEA; CitiPower; and Powercor, 2020. *Future grid for distributed energy*. Available: https://www.enea-consulting.com/static/03d62d08075b419fdb97677453e89360/enea-future-grid-for-distributed-energy.pdf, Accessed 30 May 2023. (cited on pages 1, 2, 70, and 89)

EPRI, 2016. *Common Functions for Smart Inverters: 4th Edition*. Available: https://www.epri.com/#/pages/product/3002008217/, Accessed 30 May 2023. (cited on pages 1 and 23)

Evoenergy, 2019. *Schedule of electricity network charges 2019/20*. Available: https://www.evoenergy.com.au/residents/pricing-and-tariffs/electricity-network-pricing, Accessed 29 May 2020. (cited on page 29)

Evoenergy, 2020. *Schedule of electricity network charges 2020/21*. Available: https://www.evoenergy.com.au/residents/pricing-and-tariffs/electricity-network-pricing, Accessed 28 Mar 2022. (cited on page 57)

Farivar, M.; Chen, L.; and Low, S., 2013. Equilibrium and dynamics of local voltage control in distribution systems. In *52nd IEEE Conference on Decision and Control*, 4329–4334. (cited on pages 13, 44, 89, 91, 92, and 96)

Farivar, M.; Neal, R.; Clarke, C.; and Low, S., 2012. Optimal inverter var control in distribution systems with high pv penetration. In *2012 IEEE Power and Energy Society General Meeting*, 1–7. doi:10.1109/PESGM.2012.6345736. (cited on page 44)

Franco, J. F.; Ochoa, L. F.; and Romero, R., 2018. AC OPF for smart distribution networks: An efficient and robust quadratic approach. *IEEE Transactions on Smart Grid*, 9, 5 (2018), 4613–4623. (cited on page 16)

Garcia, P. A. N.; Pereira, J. L. R.; Carneiro, S.; da Costa, V. M.; and Martins, N., 2000. Three-phase power flow calculations using the current injection method. *IEEE Transactions on Power Systems*, 15, 2 (2000), 508–514. (cited on pages 17, 57, 79, and 102)

Hashemi, S. and Østergaard, J., 2018. Efficient control of energy storage for increasing the PV hosting capacity of LV grids. *IEEE Transactions on Smart Grid*, 9, 3 (2018), 2295–2303. (cited on pages 41, 54, and 70)

Hashmi, M. U.; Deka, D.; Bušić, A.; Pereira, L.; and Backhaus, S., 2020. Arbitrage with power factor correction using energy storage. *IEEE Transactions on Power Systems*, 35, 4 (2020), 2693–2703. (cited on pages 41, 48, and 54)

IEA, 2022. *Unlocking the Potential of Distributed Energy Resources: Power system opportunities and best practices*. Available: https://www.iea.org/reports/unlocking-the-potential-of-distributed-energy-resources, Accessed 30 May 2023. (cited on pages 13 and 89)

IEEE, 2018. IEEE standard for interconnection and interoperability of distributed energy resources with associated electric power systems interfaces. *IEEE Std 1547-2018 (Rev. of IEEE Std 1547-2003)*, (2018), 1–138. (cited on pages 13, 54, and 55)

Islam, S. A. U.; Ratnam, E. L.; Goel, A.; and Bernstein, D. S., 2019. Phasor-based adaptive control of a test-feeder distribution network: Application of retrospective cost adaptive control to the IEEE 13-node test feeder. *IEEE Control Systems Magazine*, 39, 4 (2019), 56–74. (cited on pages 17 and 27)

Jahangiri, P. and Aliprantis, D. C., 2013. Distributed volt/var control by PV inverters. *IEEE Transactions on Power Systems*, 28, 3 (2013), 3429–3439. (cited on pages 2 and 55)

Jayasekara, N.; Wolfs, P.; and Masoum, M. A., 2014. An optimal management strategy for distributed storages in distribution networks with high penetrations of PV. *Electrical Power Systems Research*, 116 (2014), 147 – 157. (cited on pages 1, 10, 21, and 26)

Joo, J.; Chava, M.; Sankur, M.; Arnold, D.; and Stewart, E., 2017. Model predictive control of flexible demand for voltage support in unbalanced distribution systems. In *2017 IEEE Power Energy Society General Meeting*, 1–5. Chicago, IL, USA. (cited on pages 12, 17, 27, 42, and 89)

Kabir, M. N.; Mishra, Y.; Ledwich, G.; Dong, Z. Y.; and Wong, K. P., 2014. Coordinated control of grid-connected photovoltaic reactive power and battery energy storage systems to improve the voltage profile of a residential distribution feeder. *IEEE Transactions on Industrial Informatics*, 10, 2 (2014), 967–977. (cited on page 11)

Kersting, W. H., 2001. Radial distribution test feeders. In *2001 IEEE Power Engineering Society Winter Meeting. Conference Proceedings*, 908–912 vol.2. Columbus, OH, USA. (cited on pages 17, 27, 56, and 57)

Kotsalos, K.; Miranda, I.; Silva, N.; and Leite, H., 2019. A horizon optimization control framework for the coordinated operation of multiple distributed energy resources in low voltage distribution networks. *Energies*, 12, 6 (2019). (cited on page 11)

LIN, W. AND BITAR, E., 2018. Decentralized stochastic control of distributed energy resources. *IEEE Transactions on Power Systems*, 33, 1 (2018), 888–900. (cited on pages 45, 46, 72, 73, 91, and 92)

MAHARJAN, S.; KHAMBADKONE, A. M.; AND PENG, J. C.-H., 2021. Robust constrained model predictive voltage control in active distribution networks. *IEEE Transactions on Sustainable Energy*, 12, 1 (2021), 400–411. doi:10.1109/TSTE.2020.3001115. (cited on pages 5, 55, 79, 89, and 99)

MAHMUD, N. AND ZAHEDI, A., 2016. Review of control strategies for voltage regulation of the smart distribution network with high penetration of renewable distributed generation. *Renewable and Sustainable Energy Reviews*, 64 (2016), 582–595. (cited on pages 3 and 70)

MARRA, F.; YANG, G.; TRAEHOLT, C.; OSTERGAARD, J.; AND LARSEN, E., 2014. A decentralized storage strategy for residential feeders with photovoltaics. *IEEE Transactions on Smart Grid*, 5, 2 (March 2014), 974–981. (cited on pages 1, 2, 11, and 21)

MARTINS, M. A. I.; RHODE, L. B.; AND ALMEIDA, A. B. D., 2022. A novel battery wear model for energy management in microgrids. *IEEE Access*, 10 (2022), 30405–30413. doi:10.1109/ACCESS.2022.3160239. (cited on pages 24 and 29)

MEDIWATHTHE, C. P. AND BLACKHALL, L., 2021. Network-aware demand-side management framework with a community energy storage system considering voltage constraints. *IEEE Transactions on Power Systems*, 36, 2 (2021), 1229–1238. (cited on pages 17, 71, 79, and 101)

MEDIWATHTHE, C. P.; SHAW, M.; HALGAMUGE, S.; SMITH, D. B.; AND SCOTT, P., 2020. An incentive-compatible energy trading framework for neighborhood area networks with shared energy storage. *IEEE Transactions on Sustainable Energy*, 11, 1 (2020), 467–476. (cited on page 16)

MOLZAHN, D. K.; DÖRFLER, F.; SANDBERG, H.; LOW, S. H.; CHAKRABARTI, S.; BALDICK, R.; AND LAVAEI, J., 2017. A survey of distributed optimization and control algorithms for electric power systems. *IEEE Transactions on Smart Grid*, 8, 6 (2017), 2941–2962. (cited on page 42)

MURRAY, W.; ADONIS, M.; AND RAJI, A., 2021. Voltage control in future electrical distribution networks. *Renewable and Sustainable Energy Reviews*, 146 (2021), 111100. doi:https://doi.org/10.1016/j.rser.2021.111100. (cited on pages 1, 2, 5, 11, and 13)

Nazir, N. and Almassalkhi, M., 2021. Voltage positioning using co-optimization of controllable grid assets in radial networks. *IEEE Transactions on Power Systems*, 36, 4 (2021), 2761–2770. (cited on page 89)

Niazazari, I. and Livani, H., 2017. Disruptive event classification using PMU data in distribution networks. In *2017 IEEE Power Energy Society General Meeting*, 1–5. (cited on pages 17 and 27)

NREL, 2019a. *Cost Projections for Utility-Scale Battery Storage*. Available: https://www.nrel.gov/docs/fy19osti/73222.pdf, Accessed 30 May 2023. (cited on pages 2 and 89)

NREL, 2019b. *An Overview of Distributed Energy Resource (DER) Interconnection: Current Practices and Emerging Solutions*. Available: https://www.nrel.gov/docs/fy19osti/72102.pdf, Accessed 30 May 2023. (cited on pages 5, 89, and 106)

Ochoa, L. F. and Wilson, D. H., 2010. Angle constraint active management of distribution networks with wind power. In *2010 IEEE PES Innovative Smart Grid Technologies Conference Europe (ISGT Europe)*, 1–5. Gothenberg, Sweden. (cited on page 111)

Palmintier, B.; Broderick, R.; Mather, B.; Coddington, M.; Baker, K.; Ding, F.; Reno, M.; Lave, M.; and Bharatkumar, A., 2016. On the path to sunshot: Emerging issues and challenges in integrating solar with the distribution system. Technical Report NREL/TP-5D00-65331, National Renewable Energy Laboratory (NREL), Golden, CO. (cited on page 41)

Pesente, J. R.; Otto, R. B.; and Ramos, R. A., 2018. A study on the use of synchrophasors in a special protection scheme of the Itaipu 60Hz power plant. In *2018 IEEE Power Energy Society General Meeting (PESGM)*, 1–5. (cited on page 111)

Petrou, K.; Ochoa, L. F.; Procopiou, A. T.; Theunissen, J.; Bridge, J.; Langstaff, T.; and Lintern, K., 2018. Limitations of residential storage in PV-rich distribution networks: An Australian case study. In *2018 IEEE Power & Energy Society General Meeting (PESGM)*, 1–5. (cited on page 41)

Porteous, C.; Godfrey, B.; and Finkel, A., 2018. *Taking charge: the energy storage opportunity for Australia*. Available: https://www.chiefscientist.gov.au/sites/default/files/Energy-storage-paper.pdf, Accessed 30 May 2023. (cited on pages 2 and 21)

Poudel, S.; Mukherjee, M.; Sadnan, R.; and Reiman, A. P., 2023. Fairness-aware distributed energy coordination for voltage regulation in power distribution systems. *IEEE Transactions on Sustainable Energy*, (2023), 1–14. doi:10.1109/TSTE.2023.3252944. (cited on pages 19 and 33)

Procopiou, A. T.; Liu, M. Z.; Nacmanson, W.; and Ochoa, L., 2020. Advanced planning of PV-rich distribution networks – deliverable 4: Non-traditional solutions. Technical report, The University of Melbourne. (cited on page 41)

Procopiou, A. T.; Petrou, K.; Ochoa, L. F.; Langstaff, T.; and Theunissen, J., 2019. Adaptive decentralized control of residential storage in PV-rich MV–LV networks. *IEEE Transactions on Power Systems*, 34, 3 (2019), 2378–2389. (cited on pages 42 and 89)

Ranaweera, I. and Midtgard, O., 2016. Optimization of operational cost for a grid-supporting PV system with battery storage. *Renewable Energy*, 88 (2016), 262 – 272. (cited on pages 1, 10, and 21)

Ranaweera, I.; Midtgard, O.-M.; and Korpas, M., 2017. Distributed control scheme for residential battery energy storage units coupled with PV systems. *Renewable Energy*, 113 (2017), 1099 – 1110. (cited on pages 11 and 41)

Ratnam, E. L. and Weller, S. R., 2018. Receding horizon optimization-based approaches to managing supply voltages and power flows in a distribution grid with battery storage co-located with solar PV. *Applied Energy*, 210 (2018), 1017 – 1026. (cited on page 10)

Ratnam, E. L.; Weller, S. R.; and Kellett, C. M., 2015a. An optimization-based approach to scheduling residential battery storage with solar PV: Assessing customer benefit. *Renewable Energy*, 75 (2015), 123 – 134. (cited on pages 10 and 27)

Ratnam, E. L.; Weller, S. R.; and Kellett, C. M., 2015b. Scheduling residential battery storage with solar PV: Assessing the benefits of net metering. *Applied Energy*, 155 (2015), 881 – 891. (cited on pages 10, 48, and 54)

Ratnam, E. L.; Weller, S. R.; and Kellett, C. M., 2016. Central versus localized optimization-based approaches to power management in distribution networks with residential battery storage. *International Journal of Electrical Power and Energy Systems*, 80 (2016), 396 – 406. (cited on pages 10, 22, 24, 26, 28, 42, and 57)

Reniers, J. M.; Mulder, G.; Ober-Blobaum, S.; and Howey, D. A., 2018. Improving optimal control of grid-connected lithium-ion batteries through more accurate battery and degradation modelling. *Journal of Power Sources*, 379 (2018), 91 – 102. (cited on page 24)

Robbins, B. A. and Dominguez-Garcia, A. D., 2016. Optimal reactive power dispatch for voltage regulation in unbalanced distribution systems. *IEEE Transactions on Power Systems*, 31, 4 (2016), 2903–2913. (cited on pages 16 and 89)

Sankur, M. D.; Dobbe, R.; Stewart, E.; Callaway, D. S.; and Arnold, D. B., 2016. A linearized power flow model for optimization in unbalanced distribution systems. *ArXiv e-prints*, 1606.04492v1 (June 2016), 1–6. (cited on pages 12, 42, and 45)

Sankur, M. D.; Dobbe, R.; von Meier, A.; and Arnold, D. B., 2020. Model-free optimal voltage phasor regulation in unbalanced distribution systems. *IEEE Transactions on Smart Grid*, 11, 1 (2020), 884–894. (cited on page 111)

Sankur, M. D.; Dobbe, R.; von Meier, A.; Stewart, E. M.; and Arnold, D. B., 2018. Optimal voltage phasor regulation for switching actions in unbalanced distribution systems. *ArXiv e-prints*, 1804.02080v4 (April 2018), 1–11. (cited on pages 42, 45, and 56)

Sayeef, S.; Heslop, S.; Cornforth, D.; Moore, T.; Percy, S.; Ward, J. K.; Berry, A.; and Rowe, D., 2012. *Solar intermittency: Australia's clean energy challenge. Characterising the effect of high penetration solar intermittency on Australian electricity networks*. CSIRO Technical Report, Available: https://doi.org/10.4225/08/584c43986a4c0, Accessed 30 May 2023. (cited on pages 21, 23, and 28)

Schoene, J.; Zheglov, V.; Humayun, M.; Poudel, B.; Kamel, M.; Gebeyehu, A.; Garcia, M.; Robles, S.; and Son, H., 2017. Investigation of oscillations caused by voltage control from smart PV on a secondary system. In *Proc. 2017 IEEE Power & Energy Society General Meeting*, 1–5. (cited on page 55)

Scott, P., 2016. *Distributed Coordination and Optimisation of Network-Aware Electricity Prosumers*. Ph.D. thesis, The Australian National University (ANU). (cited on page 70)

Shahsavari, A.; Sadeghi-Mobarakeh, A.; Stewart, E.; and Mohsenian-Rad, H., 2016. Distribution grid reliability analysis considering regulation down load resources via micro-PMU data. In *2016 IEEE International Conference on Smart Grid Communications (SmartGridComm)*, 472–477. (cited on page 2)

Shaw, M.; Sturmberg, B.; Guo, L.; Gao, X.; Ratnam, E.; and Blackhall, L., 2019. The NextGen energy storage trial in the ACT, Australia. In *Proceedings of the Tenth ACM International Conference on Future Energy Systems*, 439–442. Phoenix, AZ, USA. (cited on pages 17, 22, 28, 29, 43, 56, 57, 71, 79, 101, and 106)

Singhal, A.; Ajjarapu, V.; Fuller, J.; and Hansen, J., 2019. Real-time local Volt/Var control under external disturbances with high PV penetration. *IEEE Transactions on Smart Grid*, 10, 4 (2019), 3849–3859. (cited on pages 5, 55, 64, 70, 77, 89, 94, and 102)

Smith, J. W.; Sunderman, W.; Dugan, R.; and Seal, B., 2011. Smart inverter volt/var control functions for high penetration of PV on distribution systems. In *2011 IEEE/PES Power Systems Conference and Exposition*, 1–6. (cited on pages 41 and 54)

Spanias, C.; Aristidou, P.; and Michaelides, M., 2019. Demand-side volt/-var/watt regulation for effective voltage control in distribution grids. In *2019 IEEE PES Innovative Smart Grid Technologies Europe (ISGT-Europe)*, 1–5. (cited on page 70)

Swartz, J.; Wais, B.; Ratnam, E.; and von Meier, A., 2021. Visual tool for assessing stability of DER configurations on three-phase radial networks. In *2021 IEEE Madrid PowerTech*, 1–6. Madrid, Spain. (cited on page 55)

Tesla, 2024. *Tesla Powerwall 2 Datasheet - North America*. Available: https://digitalassets.tesla.com/tesla-contents/image/upload/powerwall-2-ac-datasheet-en-na_001, Accessed 28 Jan 2024. (cited on page 35)

The MathWorks, Inc., 2023a. *MATLAB Documentation: fmincon – Find minimum of constrained nonlinear multivariable function*. Available: https://www.mathworks.com/help/optim/ug/fmincon.html, Accessed 30 May 2023. (cited on page 16)

The MathWorks, Inc., 2023b. *MATLAB Documentation: Linear or Quadratic Objective with Quadratic Constraints*. Available: https://www.mathworks.com/help/optim/ug/linear-or-quadratic-problem-with-quadratic-constraints.html, Accessed 30 May 2023. (cited on page 16)

The MathWorks, Inc., 2023c. *MATLAB Documentation: linprog – Solve linear programming problems*. Available: https://www.mathworks.com/help/optim/ug/linprog.html, Accessed 30 May 2023. (cited on page 16)

The MathWorks, Inc., 2023d. *MATLAB Documentation: quadprog – Quadratic programming*. Available: https://www.mathworks.com/help/optim/ug/quadprog.html, Accessed 30 May 2023. (cited on page 16)

Tonkoski, R.; Turcotte, D.; and EL-Fouly, T. H. M., 2012. Impact of high PV penetration on voltage profiles in residential neighborhoods. *IEEE Transactions on Sustainable Energy*, 3, 3 (July 2012), 518–527. (cited on pages 21 and 28)

Torbaghan, S. S.; Suryanarayana, G.; Höschle, H.; D'hulst, R.; Geth, F.; Caerts, C.; and Van Hertem, D., 2020. Optimal flexibility dispatch problem using second-order cone relaxation of AC power flows. *IEEE Transactions on Power Systems*, 35, 1 (2020), 98–108. (cited on page 89)

Turitsyn, K.; Sulc, P.; Backhaus, S.; and Chertkov, M., 2010a. Local control of reactive power by distributed photovoltaic generators. In *2010 First IEEE International Conference on Smart Grid Communications*, 79–84. doi:10.1109/SMARTGRID.2010.5622021. (cited on pages 44, 51, and 52)

Turitsyn, K.; Sulc, P.; Backhaus, S.; and Chertkov, M., 2011. Options for control of reactive power by distributed photovoltaic generators. *Proceedings of the IEEE*, 99, 6 (2011), 1063–1073. (cited on page 95)

Turitsyn, K.; Šulc, P.; Backhaus, S.; and Chertkov, M., 2010b. Distributed control of reactive power flow in a radial distribution circuit with high photovoltaic penetration. In *IEEE PES General Meeting*, 1–6. doi:10.1109/PES.2010.5589663. (cited on pages 5, 11, 44, 75, and 77)

Ueda, Y.; Kurokawa, K.; Tanabe, T.; Kitamura, K.; and Sugihara, H., 2008. Analysis results of output power loss due to the grid voltage rise in grid-connected photovoltaic power generation systems. *IEEE Transactions on Industrial Electronics*, 55, 7 (July 2008), 2744–2751. (cited on page 22)

Victorian DNSP, 2019. *Victorian Distribution Network Service Provider (DNSP) basic micro EG connections power quality response mode settings*. Available: https://www.solarquotes.com.au/blog/wp-content/uploads/2019/11/vic-rules.pdf, Accessed 30 May 2023. (cited on page 54)

von Appen, J.; Stetz, T.; Braun, M.; and Schmiegel, A., 2014. Local voltage control strategies for PV storage systems in distribution grids. *IEEE Transactions on Smart Grid*, 5, 2 (March 2014), 1002–1009. (cited on pages 10, 21, and 42) von Meier, A.; Culler, D.; McEachern, A.; and Arghandeh, R., 2014. Micro-synchrophasors for distribution systems. In *2014 IEEE PES Innovative Smart Grid Technologies Conference, ISGT 2014*, 1–5. (cited on page 111)

von Meier, A.; Ratnam, E. L.; Brady, K.; Moffat, K.; and Swartz, J., 2020. Phasor-based control for scalable integration of variable energy resources. *Energies*, 13, 1 (2020). (cited on pages 3, 41, 70, 78, and 111)

von Meier, A.; Stewart, E.; McEachern, A.; Andersen, M.; and Mehrmanesh, L., 2017. Precision micro-synchrophasors for distribution systems: A summary of applications. *IEEE Transactions on Smart Grid*, 8, 6 (2017), 2926–2936. (cited on page 111)

Vonsien, S. and Madlener, R., 2020. Li-ion battery storage in private households with PV systems: Analyzing the economic impacts of battery aging and pooling. *Journal of Energy Storage*, 29 (2020), 101407. doi:https://doi.org/10.1016/j.est.2020.101407. (cited on pages 29 and 35)

Wang, D.; Takoudis, C.; Wilson, D.; and Murphy, G., 2015a. Quantifying benefit of angle constraint active manaement on 33 kV distribution network. In *23 International Conference on Electricity Distribution*. Lyon, France. (cited on page 111)

Wang, D.; Wilson, D.; Venkata, S. S.; and Murphy, G., 2013. PMU-based angle constraint active management on 33 kV distribution network. In *22 International Conference on Electricity Distribution*. Stockholm, Sweden. (cited on page 111)

Wang, Y.; Tan, K. T.; Peng, X. Y.; and So, P. L., 2016. Coordinated control of distributed energy-storage systems for voltage regulation in distribution networks. *IEEE Transactions on Power Delivery*, 31, 3 (2016), 1132–1141. (cited on pages 2 and 42)

Wang, Y.; Zhang, P.; Li, W.; Xiao, W.; and Abdollahi, A., 2012. Online overvoltage prevention control of photovoltaic generators in microgrids. *IEEE Transactions on Smart Grids*, 3, 4 (Dec 2012), 2071–2078. (cited on pages 21 and 23)

Wang, Z.; Lihan Qin; Gu, C.; and Li, F., 2015b. Distributed storage capacity reservations for residential PV generation utilization and LV network operation. In *2015 IEEE Power and Energy Society General Meeting*. Denver, CO, USA. (cited on page 21)

Yao, E.; Samadi, P.; Wong, V. W. S.; and Schober, R., 2016. Residential demand side management under high penetration of rooftop photovoltaic units. *IEEE Transactions on Smart Grid*, 7, 3 (2016), 1597–1608. doi:10.1109/TSG.2015.2472523. (cited on pages 42 and 47)

Zeraati, M.; Hamedani Golshan, M. E.; and Guerrero, J. M., 2018. Distributed control of battery energy storage systems for voltage regulation in distribution networks with high PV penetration. *IEEE Transactions on Smart Grid*, 9, 4 (July 2018), 3582–3593. (cited on pages 17, 42, 71, 79, 89, and 101)

Zhang, Y.; Meng, K.; Luo, F.; Yang, H.; Zhu, J.; and Dong, Z. Y., 2020. Multi-agent-based voltage regulation scheme for high photovoltaic penetrated active distribution networks using battery energy storage systems. *IEEE Access*, 8 (2020), 7323–7333. (cited on page 11)

Zhou, X.; Farivar, M.; Liu, Z.; Chen, L.; and Low, S. H., 2021. Reverse and forward engineering of local voltage control in distribution networks. *IEEE Transactions on Automatic Control*, 66, 3 (2021), 1116–1128. (cited on pages 17, 89, 98, and 106)

Zhu, H. and Liu, H. J., 2016. Fast local voltage control under limited reactive power: Optimality and stability analysis. *IEEE Transactions on Power Systems*, 31, 5 (2016), 3794–3803. (cited on page 89)

Åström, K. J. and Murray, R. M., 2020. *Feedback Systems: An Introduction for Scientists and Engineers*. Princeton University Press. (cited on pages 65 and 93)

Šulc, P.; Backhaus, S.; and Chertkov, M., 2014. Optimal distributed control of reactive power via the alternating direction method of multipliers. *IEEE Transactions on Energy Conversion*, 29, 4 (2014), 968–977. (cited on page 95)